Final Report

to

Dr. Donald J. Silversmith
Air Force Office of Scientific Research

Development of III-Nitride Materials for IR Applications

AFOSR Program #FA9550-04-1-0229

James S. Speck

Materials Department
University of California
Santa Barbara, CA 93106

1

REPORT DOCUMENTATION PAGE

1. REPORT DATE *(DD-MM-YYYY)*	2. REPORT TYPE	3. DATES COVERED *(From - To)*

4. TITLE AND SUBTITLE	5a. CONTRACT NUMBER
	5b. GRANT NUMBER
	5c. PROGRAM ELEMENT NUMBER

6. AUTHOR(S)	5d. PROJECT NUMBER
	5e. TASK NUMBER
	5f. WORK UNIT NUMBER

7. PERFORMING ORGANIZATION NAME(S) AND ADDRESS(ES)	8. PERFORMING ORGANIZATION REPORT NUMBER

9. SPONSORING/MONITORING AGENCY NAME(S) AND ADDRESS(ES)	10. SPONSOR/MONITOR'S ACRONYM(S)
	11. SPONSOR/MONITOR'S REPORT NUMBER(S)

12. DISTRIBUTION/AVAILABILITY STATEMENT

13. SUPPLEMENTARY NOTES

14. ABSTRACT

15. SUBJECT TERMS

16. SECURITY CLASSIFICATION OF:			17. LIMITATION OF ABSTRACT	18. NUMBER OF PAGES	19a. NAME OF RESPONSIBLE PERSON
a. REPORT	b. ABSTRACT	c. THIS PAGE			
					19b. TELEPHONE NUMBER *(Include area code)*

INSTRUCTIONS FOR COMPLETING SF 298

1. REPORT DATE. Full publication date, including day, month, if available. Must cite at least the year and be Year 2000 compliant, e.g. 30-06-1998; xx-06-1998; xx-xx-1998.

2. REPORT TYPE. State the type of report, such as final, technical, interim, memorandum, master's thesis, progress, quarterly, research, special, group study, etc.

3. DATES COVERED. Indicate the time during which the work was performed and the report was written, e.g., Jun 1997 - Jun 1998; 1-10 Jun 1996; May - Nov 1998; Nov 1998.

4. TITLE. Enter title and subtitle with volume number and part number, if applicable. On classified documents, enter the title classification in parentheses.

5a. CONTRACT NUMBER. Enter all contract numbers as they appear in the report, e.g. F33615-86-C-5169.

5b. GRANT NUMBER. Enter all grant numbers as they appear in the report, e.g. AFOSR-82-1234.

5c. PROGRAM ELEMENT NUMBER. Enter all program element numbers as they appear in the report, e.g. 61101A.

5d. PROJECT NUMBER. Enter all project numbers as they appear in the report, e.g. 1F665702D1257; ILIR.

5e. TASK NUMBER. Enter all task numbers as they appear in the report, e.g. 05; RF0330201; T4112.

5f. WORK UNIT NUMBER. Enter all work unit numbers as they appear in the report, e.g. 001; AFAPL30480105.

6. AUTHOR(S). Enter name(s) of person(s) responsible for writing the report, performing the research, or credited with the content of the report. The form of entry is the last name, first name, middle initial, and additional qualifiers separated by commas, e.g. Smith, Richard, J, Jr.

7. PERFORMING ORGANIZATION NAME(S) AND ADDRESS(ES). Self-explanatory.

8. PERFORMING ORGANIZATION REPORT NUMBER. Enter all unique alphanumeric report numbers assigned by the performing organization, e.g. BRL-1234; AFWL-TR-85-4017-Vol-21-PT-2.

9. SPONSORING/MONITORING AGENCY NAME(S) AND ADDRESS(ES). Enter the name and address of the organization(s) financially responsible for and monitoring the work.

10. SPONSOR/MONITOR'S ACRONYM(S). Enter, if available, e.g. BRL, ARDEC, NADC.

11. SPONSOR/MONITOR'S REPORT NUMBER(S). Enter report number as assigned by the sponsoring/ monitoring agency, if available, e.g. BRL-TR-829; -215.

12. DISTRIBUTION/AVAILABILITY STATEMENT. Use agency-mandated availability statements to indicate the public availability or distribution limitations of the report. If additional limitations/ restrictions or special markings are indicated, follow agency authorization procedures, e.g. RD/FRD, PROPIN, ITAR, etc. Include copyright information.

13. SUPPLEMENTARY NOTES. Enter information not included elsewhere such as: prepared in cooperation with; translation of; report supersedes; old edition number, etc.

14. ABSTRACT. A brief (approximately 200 words) factual summary of the most significant information.

15. SUBJECT TERMS. Key words or phrases identifying major concepts in the report.

16. SECURITY CLASSIFICATION. Enter security classification in accordance with security classification regulations, e.g. U, C, S, etc. If this form contains classified information, stamp classification level on the top and bottom of this page.

17. LIMITATION OF ABSTRACT. This block must be completed to assign a distribution limitation to the abstract. Enter UU (Unclassified Unlimited) or SAR (Same as Report). An entry in this block is necessary if the abstract is to be limited.

Objectives

The AFOSR program, which was recently completed under an approved no-cost extension through November 1, 2007, focused on three new areas for the III-nitrides: (i) the growth and optical properties of GaN QDs – with particular application to intersubband transitions; (ii) basic studies of the molecular beam epitaxy (MBE) growth of GaN; and (iii) development of the new narrow bandgap material InN. The research in each of these three areas has excelled, as highlighted below.

GaN Quantum Dots

In the past three years, under support from AFOSR, the UCSB group has unveiled the growth mechanisms of GaN quantum dots by plasma-assisted MBE (PAMBE) on partially relaxed AlN templates. In conjunction with these detailed growth studies, we demonstrated the interplay between growth conditions, GaN wetting layer thickness, and GaN QD size, density and luminescence properties.

Using a combination of *in situ* reflection high-energy electron diffraction and line-of-sight quadrupole mass spectrometry during rf-plasma assisted molecular beam epitaxy (PA-MBE) we were able to elucidate the detailed mechanisms of the growth of GaN QDs. We found that the Ga-adsorbate coverage of 1.0 ML (monolayer) was critical in the mediation of a fundamental change in the GaN Stranski-Krastanov (SK) growth mode on AlN. For Ga-adsorbate coverage less than 1.0 ML, the SK transition occurred during GaN growth. For larger Ga-adsorbate coverages, the SK transition occurred after the desorption of the Ga coverage in excess of 1.0 ML. Also, we performed variable GaN coverage growth experiments followed by desorption of the Ga adsorbate and subsequent GaN thermal decomposition to determine that the critical GaN coverage for the SK transition was less than 2.0 ML under Ga-droplet PA-MBE growth conditions. This work, which was a culmination of our basic growth studies of GaN QDs was recently published [**Appendix I:** J. Brown et al., J. Appl. Phys. **99**, 124909 (2006).]

The work of GaN QDs was brought together in a key final paper. In this work, we reported on the Ga-flux dependence of GaN growth mode, morphology, and optical properties of Stranski-Krastanov (S-K) quantum dots in AlN (0001). We correlated reflection high-energy electron diffraction (RHEED) specular intensity transients during rf-plasma assisted molecular beam epitaxy to S-K island dimensions measured by atomic force microscopy. Single layer quantum dots with controlled size and density were characterized via room temperature photoluminescence (PL) with a pulsed 193 nm excitation source. We used a self-consistent one-dimensional Schrödinger-Poisson calculation to distinguish the contribution of wetting layer quantum wells (1-4 ML) from quantum dots in the PL spectra [**Appendix II:** J. Brown et al. Jpn. J. Appl. Phys. Part 2, L669 (2006).]

GaN: Basic MBE Growth Studies

In the final year of the program, we extended the strong efforts of understanding the critical issues of high–quality GaN growth by PAMBE. As the improvement of GaN material properties depends crucially on the Ga surface adlayer present under Ga–rich growth conditions, we placed special emphasis on in situ investigations of this adlayer by quadrupole mass spectrometry (QMS) and in situ reflection high energy electron diffraction (RHEED). Essentially, we have shown by QMS and RHEED desorption transient measurements that the Ga

adlayer followed a layer–by–layer adsorption and desorption behavior and exhibited a maximum steady–state coverage of 2.4 monolayers (ML) on (0001) GaN and 2.7 ML on (0001) AlN, respectively. In addition, we investigated the temperature dependence of the Ga adlayer desorption transients and determined that the desorption activation energies for the individual monolayers were similar for both (0001) GaN and (0001) AlN surfaces [**Appendix III**: J. Brown et al., J. Appl. Phys. **99**, 074902 (2006); **Appendix IV**: J. Brown et al., J. Vac. Sci. Technol. A **24**, 1979 (2006)].

All these growth studies along the established growth diagrams for the PAMBE growth of GaN have been limited to Ga–rich conditions and temperatures well below thermal decomposition (< 750 °C). To further improve the quality of GaN–based devices grown by PAMBE, we have most recently pursued GaN growth at much higher temperatures. Below we include results from three pre–stage publications (which were all submitted or prepared for submission to Applied Physics Letters – one of the three of these papers has now been accepted for publication).
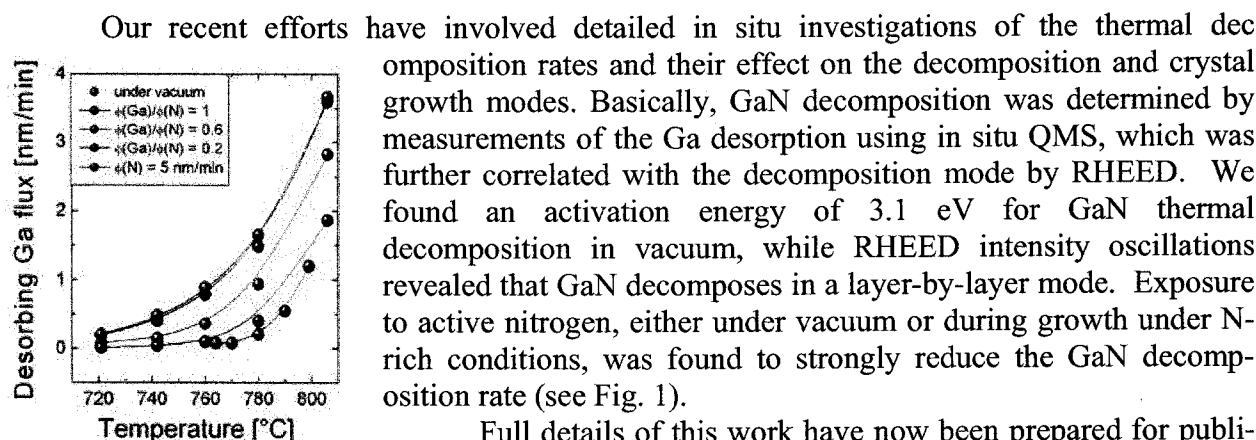
Our recent efforts have involved detailed in situ investigations of the thermal decomposition rates and their effect on the decomposition and crystal growth modes. Basically, GaN decomposition was determined by measurements of the Ga desorption using in situ QMS, which was further correlated with the decomposition mode by RHEED. We found an activation energy of 3.1 eV for GaN thermal decomposition in vacuum, while RHEED intensity oscillations revealed that GaN decomposes in a layer-by-layer mode. Exposure to active nitrogen, either under vacuum or during growth under N-rich conditions, was found to strongly reduce the GaN decomposition rate (see Fig. 1).

Fig. 1: Reduced Ga desorption (i.e. decomposition rate) with N–rich conditions.

Full details of this work have now been prepared for publication (S. Fernandez–Garrido et al., "In-situ GaN decomposition analysis by quadrupole mass spectrometry and reflection high-energy electron diffraction", prepared for submission to J. Appl. Phys. (2007).).
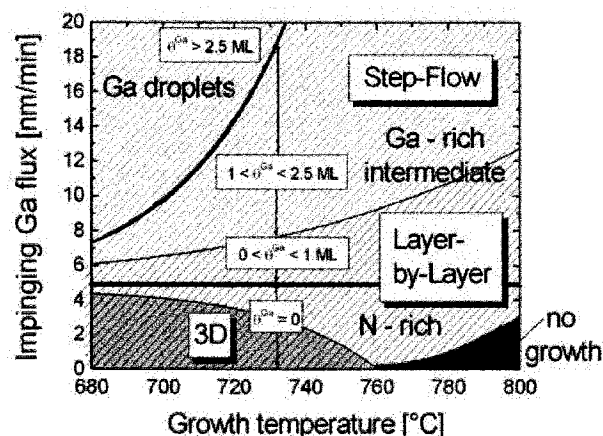

Fig. 2: Growth mode map highlighting the interrelation with the three standard GaN growth regimes (N–rich, Ga–rich intermediate and Ga droplets).

In another work, we have further analyzed the growth modes and their dependencies on Ga adlayer coverage and growth temperature during the homoepitaxial (0001) GaN growth by PAMBE over a very wide range of temperatures. Consequently, we were able to establish a new growth mode map for (0001) GaN growth as a function of Ga/N flux ratio and growth temperature, exhibiting distinct transitions between three–dimensional (3D), layer–by–layer and step–flow growth mode (see Fig. 2). The layer–by–layer to step–flow growth transition under Ga–rich growth was surfactant mediated and related to a Ga adlayer coverage of one monolayer. Under N–rich conditions the transition from 3D to layer–by–layer growth was predominantly thermally activated, facilitating two–dimensional growth at temperatures of thermal decomposition. The precise knowledge of these growth mode transitions allows control of the growth surfaces over a wide range of temperatures, even in regions of thermal decomposition.

Full details of this work have now been published (**Appendix V**: G. Koblmüller et al., "In-situ investigation of growth modes during plasma–assisted molecular beam epitaxy of (0001) GaN", Appl. Phys. Lett. **91**, 161904 (2007)).

With regard to the unexpectedly wide range of Ga and N fluxes yielding layer–by–layer growth of GaN, we have further investigated the sustainability of the two–dimensional (2D) growth regime under N–rich conditions. We have found that at temperatures of GaN thermal decomposition (> 750 °C), superior surface morphologies with roughness of less than 1 nm (rms) can be achieved for thick GaN films (with thicknesses greater than 1 μm) grown under N–rich conditions on MOCVD–GaN templates (see 3×3 μm^2 and 1×1 μm^2 (insetted) AFM images in Fig. 3). TEM studies revealed that no new dislocations were generated, with the total threading dislocation density given by the underlying MOCVD-grown GaN template

Fig. 3: AFM morphology of 1μm–thick GaN grown N–rich at 780 °C.

(5×10^8 cm^{-2}). Room temperature electron mobilities ranging as high as 1125 cm^2/Vs were measured for slightly Si–doped (low-10^{16} cm^{-3}) GaN films, surpassing the commonly insulating nature of GaN grown under N–rich conditions at low temperature. *These mobilities, are the highest ever reported for MOCVD or MBE grown GaN.* Along with the improved electrical transport, the impurity incorporation of oxygen has been reduced as measured by secondary ion mass spectroscopy (SIMS). This work highlights an alternative approach for achieving high–quality (0001) GaN films by PAMBE, circumventing the restrictions to Ga–rich growth at moderately low growth temperatures.
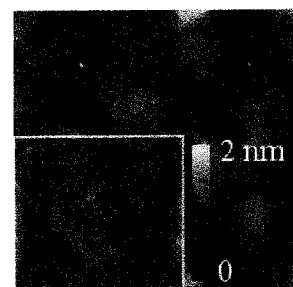
Full details of this work have now been published (**Appendix VI**: G. Koblmüller et al., "High electron mobility GaN grown under N–rich conditions by plasma–assisted molecular beam epitaxy", Appl. Phys. Lett. **91**, 221905 (2007)).

InN: Growth, Properties and Device Applications

Over the past two years we have also developed a significant body of new research on InN. In particular, we have performed extensive growth and property studies of both In-face and N-face InN. We have established detailed growth diagrams for both In-face and N-face materials, giving the dependence of the In/N flux ratio and growth temperature on the surface

4

properties. Based on this excellent growth control, we have realized the lowest bandgap material reported (0.62 eV both in absorption and emission at room temperature); the lowest unintentional electron concentrations ($< 10^{17}$ cm^{-3}); and the highest electron mobilities (3570cm^2/Vs at 300 K). In addition, we have analyzed the multiple carrier transport present in InN and clearly devided two electron species attributed to the bulk layer and a surface accumulation layer. Also, we have demonstrated the importance of InN for its use for terahertz applications. The following six publication have emerged from these results:

Appendix VII: C. Gallinat et al., Appl. Phys. Lett. **89**, 032109 (2006); **Appendix VIII**: G. Koblmüller et al., Appl. Phys. Lett. **89**, 071902 (2006).); **Appendix IX**: T. Fehlberg et al., Jpn. J. Appl. Phys. Part 2 **45**, L1090 (2006).); **Appendix X**: G. Chern et al., Appl. Phys. Lett. **89**, 141115 (2006).); **Appendix XI**: G. Koblmüller et al., J. Appl. Phys. **101**, 083516 (2007).); **Appendix XII**: C. S. Gallinat et al., J. Appl. Phys. **102** 064907 (2007).

We have published 17 papers in archival journals during the course of this program and an several additional manuscripts are in final preparation. This program supported the dissertation work of Dr. Jay Brown and Dr. Chad Gallinat, and Ms. Amorette Getty. Additionally, the program supported the postdoctoral work of Dr. Gregor Koblmüller and the extended visits of Dr. Alexei Romanov (Ioffe Institute).

Additionally, during the course of this program, the PI (Speck) was the recipient of the *Quantum Device Award* from the *International Symposium on Compound Semiconductors* for his work on GaN MBE growth and was named an inaugural *MRS Fellow* from the *Materials Research Society*.

Publications

"Continuous evolution of Ga adlayer coverages during plasma-assisted molecular-beam epitaxy of (0001) GaN,"
G. Kobmuller, J. Brown, R. Averback, H. Riechert, P. Pongratz, J.S. Speck, Appl. Phys. Lett. **86**, 041908 (2005)

"Ga Adlayer Governed Surface Defect Evolution of (0001)GaN Films Grown by Plasma-Assisted Molecular Beam Epitaxy,"
Gregor Kobmuller, Jay Brown, Robert Averbeck, Henning Riechert, Peter Pongratz and James S. Speck, Japn. J. Appl. Phys. **44**, L906 (2005).

"Quantification of Ga surface coverages and their desorption kinetics on GaN (0001) and (000–1) surfaces,"
G. Koblmüller, J. Brown, R. Averbeck, H. Riechert, P. Pongratz, P. M. Petroff, and J. S. Speck, phys. stat. sol. c (2005).

"Buried stressors in nitride semiconductors: Influence on electronic properties,"
A.E. Romanov, P. Waltereit, and J.S. Speck, J. Appl. Phys. **97**, 043708 (2005).

"GaN quantum dot density control by rf-plasma molecular beam epitaxy,"
J. Brown, F. Wu, P.M. Petroff, J.S. Speck, Appl. Phys. Lett. **84**, 690 (2004).

"In situ characterization of GaN quantum dot growth with reflection high-energy electron diffraction and line-of-sight mass spectrometry,"
J. S. Brown, G. Koblmuller, R. Averbeck, H. Riechert, J. S. Speck, *J. Appl. Phys.* **99**, 124909 (2006).

"Optical properties of GaN/AlN(0001) quantum dots grown by plasma-assisted molecular beam epitaxy,"
J. S. Brown, P. M. Petroff, F. Wu, J. S. Speck, *Jpn. J. Appl. Phys.* **45**, L669 (2006).

"Ga-adsorbate on (0001) GaN. *In situ* characterization with quadrupole mass spectroscopy and reflection high-energy electron diffraction,"
Jay S. Brown, Gregor Koblmüller, Feng Wu, Robert Averbeck, Henning Riechert and James S. Speck, J. Appl. Phys. **99**, 074902 (2006)

"Quadrupole mass spectrometry desorption analysis of Ga adsorbate on AlN (0001),"
Jay S. Brown, Gregor Koblmüller, Robert Averbeck, Henning Riechert, James S. Speck, J. Vac. Sci. Tech.J. Vac. Sci. Technol. A **24**, 1979 (2006).

"In situ investigation of growth modes during plasma-assisted molecular beam epitaxy of (0001) GaN,"
G. Koblmuller, S. Fernandez-Garrido, E. Calleja, J. S. Speck, *Appl. Phys. Lett.* **91**, 161904 (2007).

"High electron mobility GaN grown under N-rich conditions by plasma-assisted molecular beam epitaxy,"
G. Koblmueller, F. Wu, T. Mates, J. S. Speck, S. Fernandez-Garrido, E. Calleja, *Appl. Phys. Lett.* **91**, 221905 (2007).

"Improved properties of In-polar InN grown by plasma-assisted molecular beam epitaxy,"
C. S. Gallinat, G. Koblmüller, S. Bernardis, J. S. Brown, J. S. Speck, G. D. Chern, E. D. Readinger, H. Shen, and M. Wraback, Appl. Phys. Lett. **89**, 032109 (2006).

"Optimization of the surface and structural quality of N-face InN grown by molecular beam epitaxy,"
G. Koblmüller, C. S. Gallinat, S. Bernardis, J. S. Speck, G. D. Chern, E. D. Readinger, H. Shen, and M. Wraback, Appl. Phys. Lett. **89**, 071902 (2006).

"Characterisation of multiple carrier transport in indium nitride, grown by molecular beam epitaxy,"
T. B. Fehlberg, G. A. Umana-Membreno, B. D. Nener, G. Parish, C. S. Gallinat, G. Koblmuller, S. Rajan, S. Bernardis, and J. S. Speck, Jpn. J. Appl. Phys., Part 2 **45**, L1090 (2006).

"Excitation wavelength dependence of terahertz emission from InN and InAs,"
G. Chern, E. D. Readinger, H. Shen, and M. Wraback, C. S. Gallinat, G. Koblmüller, and J. S. Speck, Appl. Phys. Lett. **89**, 141115 (2006).

"Surface kinetics and thermal instability of N-face InN grown by plasma-assisted molecular beam epitaxy,"
G. Koblmuller, C. S. Gallinat, J. S. Speck, *J. Appl. Phys.* **101**, 083516 (2007)

"A growth diagram for plasma-assisted molecular beam epitaxy of In-face InN,"
C. S. Gallinat, G. Koblmueller, J. S. Brown, J. S. Speck, *J. Appl. Phys.* 102, 064907 (2007).

Appendices

T. B. Fehlberg, G. A. Umana-Membreno, B. D. Nener, G. Parish, C. S. Gallinat, G. Koblmuller, S. Rajan, S. Bernardis, and J. S. Speck, Jpn. J. Appl. Phys., Part 2 **45**, L1090 (2006).

Appendix X   "Excitation wavelength dependence of terahertz emission from InN and InAs,"
G. Chern, E. D. Readinger, H. Shen, and M. Wraback, C. S. Gallinat, G. Koblmüller, and J. S. Speck, Appl. Phys. Lett. **89**, 141115 (2006).

Appendix XI   "Surface kinetics and thermal instability of N-face InN grown by plasma-assisted molecular beam epitaxy,"
G. Koblmuller, C. S. Gallinat, J. S. Speck, *J. Appl. Phys.* **101**, 083516 (2007)

Appendix XII   "A growth diagram for plasma-assisted molecular beam epitaxy of In-face InN,"
C. S. Gallinat, G. Koblmueller, J. S. Brown, J. S. Speck, *J. Appl. Phys.* **102**, 064907 (2007).

In situ characterization of GaN quantum dot growth with reflection high-energy electron diffraction and line-of-sight mass spectrometry

Jay S. Brown and Gregor Koblmüller
Materials Department, University of California, Santa Barbara, California 93106-5050

Robert Averbeck and Henning Riechert
Infineon Technologies AG, Corporate Research Photonics, D-1730 Munich, Germany

James S. Speck[a)]
Materials Department, University of California, Santa Barbara, California 93106-5050

We have investigated the Ga-adlayer mediated growth of GaN quantum dots at 707 °C on AlN (0001) by simultaneous use of *in situ* reflection high-energy electron diffraction and line-of-sight quadrupole mass spectrometry during rf-plasma assisted molecular beam epitaxy (PA-MBE). We have found that the Ga-adsorbate coverage of 1.0 ML (monolayer) is critical in the mediation of a fundamental change in the GaN Stranski-Krastanov (SK) growth mode on AlN. When the Ga-adsorbate coverage was less than 1.0 ML, the SK transition occurred during GaN growth. For larger Ga-adsorbate coverages, the SK transition occurred after the desorption of the Ga coverage in excess of 1.0 ML. We performed variable GaN coverage growth experiments followed by desorption of the Ga adsorbate and subsequent GaN thermal decomposition to determine that the critical GaN coverage for the SK transition was less than 2.0 ML under Ga-droplet PA-MBE growth conditions. © 2006 American Institute of Physics. [DOI: 10.1063/1.2206375]

I. INTRODUCTION

Isolated GaN quantum dots (QDs) in AlN (0001) are attractive for fundamental investigation of bound electronic states and for potential room temperature quantum information device applications. Due to their three-dimensional confinement of carriers, large type-I band offsets[1] (>0.5 eV), and spontaneous and piezoelectric induced electric fields[2] (~5 MV/cm), GaN QD ensembles are potentially useful for optimizing the performance of high temperature conventional optoelectronics including emitters for light emitting diodes, laser diodes, and for intersubband infrared (IR) detectors.

Recent experimental and theoretical reports have provided substantial evidence for the utility of GaN QDs [in AlN (0001)] in conventional and quantum information devices. Electronic band structure calculations[3,4] of GaN QDs in AlN (0001) are consistent with experimentally measured recombination energies, tunable from 3.8 to 2.9 eV, in photoluminescence and cathodoluminescence experiments.[5,6] Ground state optical recombination from ensembles of GaN QDs has been observed up to 750 K, providing evidence for the viability of GaN QDs in high temperature device applications.[7] Analysis of room temperature optical absorption of GaN QD superlattices in AlN (0001) has demonstrated electric field dependent IR intersubband transitions in the conduction band of QD ensembles.[8] The recent observation of photon antibunching in isolated GaN QDs up to a temperature of ~100 K has demonstrated that GaN QDs may be described as single quantum systems, useful for quantum information related emission and detection.[9] Despite recent advances in fundamental investigations, the achievement of devices using GaN QD active regions has yet to be reported. As low defect density AlN substrates become widely available and QD growth technology matures, such devices should soon be possible.

In rf-plasma assisted molecular beam epitaxy (PA-MBE), *in situ* techniques have assisted in the investigation of growth condition dependent kinetics to manipulate GaN QD ensemble dimensions and areal densities. The "Ga autosurfactant modified" Stranski-Krastanov (SK) growth of GaN QDs has been demonstrated when GaN growth is performed under Ga-rich flux conditions.[10] The presence of the Ga adsorbate was reported to completely suppress the SK transition during growth under Ga-rich conditions.[11] The modified SK growth mode has now been observed for both the (0001) and (000$\bar{1}$) AlN substrate orientations.[12,13] Growth of GaN QDs under N-rich conditions, as compared to Ga-rich conditions, has been demonstrated to produce smaller, higher density QDs.[12,14] Reports from several groups have converged on the nominal critical GaN coverage for the SK transition to be ~2.0 ML (monolayer).[10-12,14-16] Further fundamental characterization of the Ga adsorbate mediated kinetics may be useful in the direction of continuous tuning of GaN QD ensemble dimensions and areal density towards optimized device implementation via PA-MBE.

Theoretical calculations and study of homoepitaxial growth of GaN (0001) by PA-MBE have converged on the importance of the Ga adsorbate in N-adatom surface mobility. The most energetically favorable configuration of the Ga adsorbate has been found to be a laterally contracted Ga bilayer on the GaN (0001) surface.[17] The Ga bilayer has been predicted by first principles calculations to provide a low-energy barrier path to N-adatom surface diffusion relative to

[a)]Electronic mail: speck@mrl.ucsb.edu

99, 124909-1

the stoichiometric GaN (0001) surface.[18] The exponential temperature dependence of critical incident Ga flux for Ga-droplet formation during GaN growth by PA-MBE was observed by *ex situ* optical microscopy.[19] Recent investigations of the details of GaN (0001) growth mode, using line-of-sight desorption quadrupole mass spectrometry (QMS), have indicated that the Ga adsorbate coverage is continuously variable depending on the Ga flux during growth or adsorption experiments.[20–22] The continuous evolution of GaN morphology[20] has been attributed to the Ga adsorbate coverage variation in accordance with the conclusions from theory. We have recently observed the formation of a laterally contracted Ga bilayer on AlN (0001), with similar apparent desorption activation energies to the Ga bilayer on GaN (0001).[23] This observation has identified the importance of the Ga bilayer coverage during the compressively strained GaN heteroepitaxy on AlN (0001) that typically results in the SK transition and the formation of QDs.

In this work, simultaneous *in situ* investigation of PA-MBE GaN SK growth on AlN (0001) via reflection high-energy electron diffraction (RHEED) and QMS experiments were performed. The surfaces were monitored by RHEED during growth to determine the onset of in-plane relaxation and monolayer-scale roughening associated with the SK transition. The Ga adsorbate coverage was assessed by the integration of the desorption Ga flux after growth. Two classes of experiments were performed to assess critical Ga adsorbate coverage in mediating the SK transition and the critical GaN coverage for the SK transition. We follow the nomenclature of Gogneau *et al.* in referring to the GaN SK transition that we have observed to occur after partial Ga adsorbate desorption as the Ga autosurfactant modified SK transition.[12] We discuss the GaN SK growth mode on AlN (0001) with regard to the incident Ga flux and the resultant Ga adsorbate coverage in the context of a previously developed GaN growth diagram for PA-MBE.[19]

II. EXPERIMENTS

The *in situ* investigation of GaN SK growth on AlN (0001) during PA-MBE was performed in a VH80 (VG Semicon) equipped with standard Ga and Al effusion cells and radio frequency plasma source (Epi/Veeco). Prior to GaN growth experiments, 150 nm AlN (0001) buffers were grown on 50.8 mm diameter $6H$-SiC (0001) wafers under Al-rich intermediate (3.25 nm/min Al flux) conditions at 790 °C, with N-limited AlN growth rate of 2.4 nm/min.[24] After AlN growth, the excess Al was consumed by exposure to N flux for ~5 min at 790 °C.[16] Prior to all GaN growths, the substrate temperature was decreased to 707 °C and stabilized for a minimum of 20 min. After each GaN growth under Ga-rich conditions, and the observation of the complete desorption of the Ga adsorbate to below the QMS detection limit (0.2 nm/min), the substrate temperature was subsequently increased in each case to 790 °C for the AlN growth conditions as described above. To reproduce similar AlN surfaces, a 25 nm AlN buffer was grown in between each GaN growth experiment. As described in detail for the variable GaN coverage experiments, the result of increasing

the substrate temperature prior to AlN recovery growths caused complete sublimative desorption (decomposition) of the exposed GaN layer.

Prior to the experiments described below, we performed a series of calibrations to ensure consistency with our previous reports of substrate temperature and fluxes.[19] The substrate temperature was controlled by a thermocouple and monitored directly by pyrometer. The self-consistent pyrometer temperatures reported in this work are based upon the calibration of pyrometer response at 743 °C, 20 nm/min Ga flux (critical Ga flux for droplet formation at 743 °C),[19] with a reproducibility of ±1 °C. The group-III fluxes reported in these experiments were measured by cross-sectional scanning electron microscopy (SEM) imaging of metal flux-limited 1–2 μm films grown on SiC (0001) with an absolute uncertainty less than 0.5 nm/min. The SEM growth rate measurements were correlated to ion gauge flux measurements, and fluxes were calibrated to cell temperature prior to all measurements. All Ga fluxes reported in this work are expressed in terms of GaN equivalent growth rate. We calibrated the linear response of the line-of-sight QMS detector by adsorption of calibrated Ga fluxes (1–30 nm/min) on a 50.8 mm diameter sapphire wafer at a temperature of 804 °C.[21]

Two classes of *in situ* GaN SK growth experiments on AlN (0001) were performed to investigate the role of excess Ga flux and to investigate the GaN coverage dependence at a fixed substrate temperature of 707 °C. In the first class of experiments, the incident Ga flux was varied with fixed N fluence (3 ML GaN nominal coverage equivalent). Two separate variable Ga flux experiments are presented, in which the Ga shutter was opened simultaneously with the N shutter and in which the Ga flux was exposed to the substrate for 10–60 s before the N flux. In the second class of experiments, the incident Ga flux was fixed, and the N fluence was varied to investigate the critical GaN thickness for the SK transition under Ga-droplet conditions.

During the experiments, the RHEED pattern along the $[11\bar{2}0]$ azimuth was recorded with a charge coupled device (CCD) camera (k-Space Associates) in 0.2–0.4 s intervals for subsequent analysis. The temporal evolution of the interplanar $(1\bar{1}00)$ lattice spacing and integrated Bragg spot $(10\bar{1}2)$ intensity[10] were subsequently analyzed to correlate the SK transition via the onset of relaxation and increased Bragg spot intensity with the QMS data. Ga desorption from the surface was monitored by QMS and subsequently analyzed to determine both the total Ga-adsorbate coverage after growth and the Ga-adsorbate coverage that desorbed after the SK transition. In the variable GaN coverage experiment, the total GaN coverage during thermal decomposition was determined by the integration of desorption Ga flux as the temperature was increased to 790 °C.

A. Stranski-Krastanov GaN growth: Variable Ga flux

In the first class of experiments, the incident Ga flux was varied to realize a continuous variation of Ga-adsorbate coverage during 3 ML GaN growth on AlN (0001) with a substrate temperature of 707±1 °C.[20,22] In the first experiment
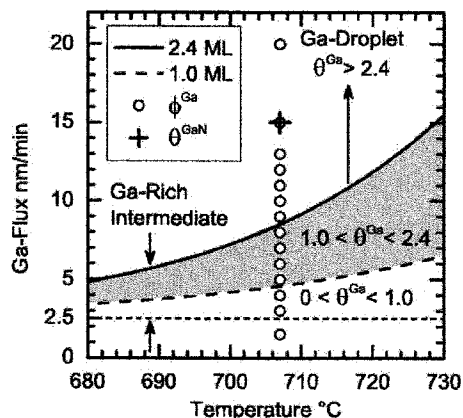
FIG. 1. The previously developed GaN (0001) growth diagram relates the temperature dependence of critical Ga fluxes for specific Ga-adsorbate coverages during GaN growth by PA-MBE. The Ga fluxes used in this work during GaN growth on AlN (0001) realized similar coverage transitions to GaN homoepitaxy.
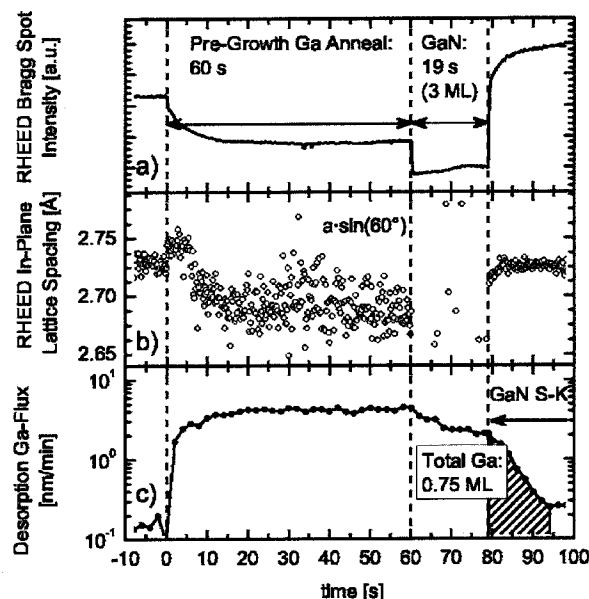

FIG. 2. *In situ* data during 60 s pregrowth Ga wetting, 19 s GaN growth, subsequent SK transition, and Ga-adsorbate desorption with a 707 °C substrate temperature. The Ga flux was 5 nm/min. The N fluence corresponded to 3.0 ML nominal GaN coverage. The conventional GaN SK transition occurred during GaN growth. The total Ga-adsorbate coverage was 0.75 ML. (a) RHEED Bragg spot intensity variation. (b) RHEED in-plane lattice spacing along the [$1\bar{1}00$] azimuth. (c) QMS desorption Ga flux.

of this type, the Ga and N shutters were opened simultaneously after preparation of the AlN surface. In the second variable Ga flux experiment, the AlN surface was exposed to a Ga flux for 10–60 s to realize a steady state Ga-adlayer coverage prior to opening the N shutter and GaN growth initiation. The Ga prewetting duration was 10 s for Ga-droplet fluxes to minimize Ga-droplet accumulation during adsorption. For Ga fluxes below the Ga-droplet GaN growth Ga flux at 707 °C (~8 nm/min, see Fig. 1), the pregrowth Ga adsorption duration was 60 s.

In both variable Ga flux experiments, with and without pregrowth Ga exposure, the GaN coverage was 3.0 ML, as determined by the N fluence, 19 s with a N-limited GaN growth rate of 2.5 nm/min. As shown in Fig. 1, the Ga flux for both experiments was varied from 1.5 to 20 nm/min in 1–5 nm/min Ga flux increments.

B. Ga autosurfactant modified SK: Variable GaN coverage

To further investigate the Ga autosurfactant modified SK growth mode characterized by the variable Ga flux experiments, we explored several nominal GaN coverages via N fluence under Ga-droplet growth conditions. In this experiment, the incident Ga flux was fixed at 15 nm/min, with 10 s pregrowth Ga adsorption before variable durations of GaN growth. The N shutter was opened for 9–31 s to obtain 1.5–5 ML GaN nominal coverage with a substrate temperature of 707±1 °C. After the GaN growth and subsequent desorption of the Ga-adsorbate, the substrate temperature was increased to 790 °C which resulted in the thermal decomposition of GaN as monitored by the desorbing Ga flux.

III. RESULTS

The variable Ga flux experiments, with and without pregrowth Ga wetting at 707 °C, revealed the 1.0 ML critical Ga-adsorbate coverage that defined a change from the usual SK to the Ga autosurfactant modified SK surface transition. In the investigation of Ga-droplet growth with variable GaN

coverage from 1.5 to 5 ML, we found that the critical GaN coverage for the SK transition was between 1.5 and 2.0 ML GaN at 707 °C.

A. Variable Ga flux SK GaN growth

We first describe two general cases of GaN SK growth and Ga autosurfactant modified SK growth, as mediated by the Ga-adsorbate coverage on the surface during growth. We next describe the results from both variable Ga flux series, with and without pregrowth Ga wetting, with specific regard to the Ga-adsorbate coverages that were determined in relation to the onset of the SK transition.

1. Pregrowth Ga wetting results

The temporal evolution of the desorption Ga flux measured by QMS, RHEED Bragg spot intensity, and RHEED in-plane relaxation data is presented for the incident Ga fluxes of 5 nm/min (Fig. 2) and 12 nm/min (Fig. 3) for pregrowth Ga wetting and subsequent GaN growth and Ga-adlayer desorption. The exposure of the surface to Ga flux is indicated by an immediate increase in desorption Ga flux, followed by the steady state Ga desorption flux consistent with the realization of a steady state Ga-adsorbate coverage prior to the opening of the N shutter (Figs. 2 and 3). In both Figs. 2 and 3, the onset of the SK transition, indicated by the RHEED data, is superimposed on the QMS desorption transient. As indicated by the hatched regions in Figs. 2 and 3, the total Ga-adsorbate coverage on the GaN surface during growth was determined by the integration of the QMS data corresponding to Ga desorption flux after the GaN growth. In all experiments the total Ga-adsorbate coverage was defined as the integration of desorption Ga flux from the time when
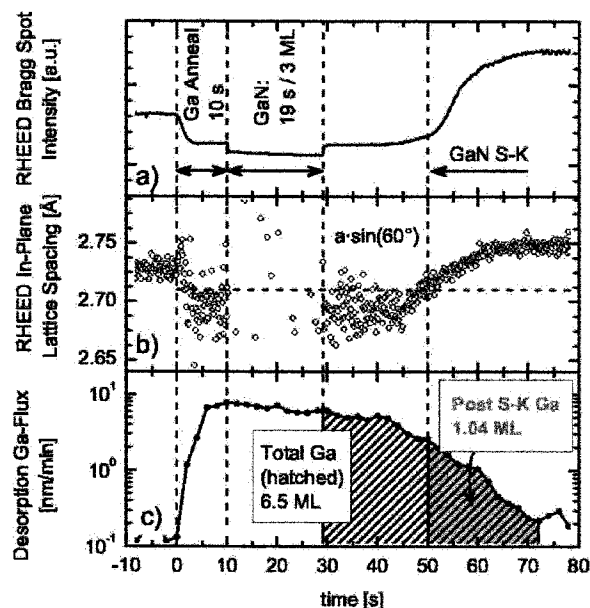
FIG. 3. *In situ* data during 10 s pregrowth Ga wetting, 19 s GaN growth, Ga-adsorbate desorption, and subsequent SK transition with a 707 °C substrate temperature. The Ga flux was 12 nm/min and the N fluence corresponded to 3.0 ML nominal GaN coverage. The total Ga-adsorbate coverage was 6.5 ML. The Ga autosurfactant GaN SK transition occurred after GaN growth and desorption of 5.5 ML Ga-adsorbate. The Ga-adsorbate coverage that desorbed after the SK transition in this case was 1.04 ML. (a) RHEED Bragg spot intensity variation. (b) RHEED in-plane lattice spacing along the [$1\bar{1}00$] azimuth. (c) QMS desorption Ga flux.
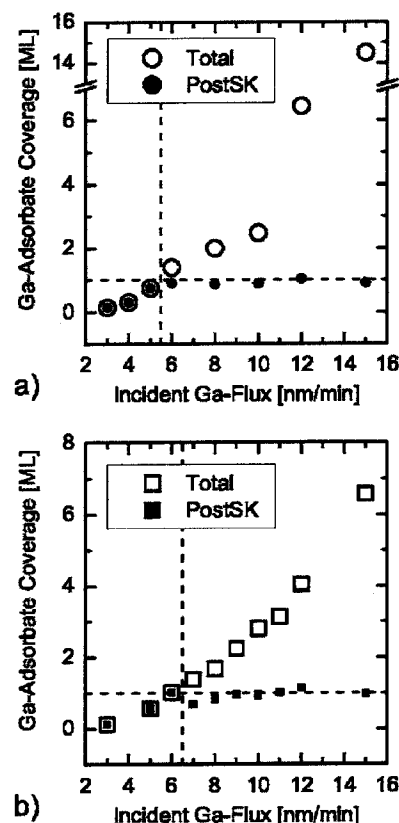

FIG. 4. Dependence of the total and post-SK Ga-adsorbate coverage on incident Ga flux realized after growth of 3 ML GaN on AlN (0001). (a) Ga wetting of 10–60 s prior to GaN growth. (b) GaN growth initiated by simultaneously opening the Ga and N shutters.

both the Ga and N shutters were closed to the time at which desorption flux reached the background detection limit of the QMS.

As shown in Fig. 2, the GaN SK transition occurred towards the end of GaN growth, and the total Ga-adsorbate coverage was 0.75 ML corresponding to the incident Ga flux of 5 nm/min. In general, we observed that for all of the Ga flux experiments in which the total Ga-adsorbate coverage after growth was less than 1 ML, the SK transition occurred during growth after 12–19 s, corresponding to the time at which the nominal GaN coverage was 2–3 ML. This growth mode is consistent with the SK transition that has been intensely studied in other III-V heteroepitaxy alloy systems such as InAs on GaAs in which the initial growth mode is layer by layer and the SK transition occurs during growth.[25,26]

When the Ga-adsorbate coverage exceeded 1.0 ML, the SK transition was consistent with the previously described Ga autosurfactant modified SK.[12] In Fig. 3, the Ga flux (12 nm/min) resulted in a total Ga-adsorbate coverage of 6.5 ML due to pregrowth adsorption as indicated by the hatched region of the Ga flux desorption transient. In this case, and in all cases in which the total Ga-adsorbate coverage exceeded 1.0 ML, the SK transition did not occur until after the GaN growth and subsequent desorption of the Ga-adsorbate in excess of ~1.0 ML (1.04 ML in Fig. 3). In experiments in which the SK transition occurred after growth and subsequent partial Ga-adsorbate coverage desorption, as is shown in Fig. 3, we integrated the QMS desorption flux to determine the post-SK transition Ga-adsorbate coverage. We defined the post-SK Ga-adsorbate coverage as the integration

of desorption Ga flux from the SK transition, indicated by the appearance of RHEED Bragg spots and the onset of in-plane relaxation, to the time at which the desorbing flux reached the background detection limit of the QMS (0.2 nm/min).

The results for the entire variable Ga flux series clearly demonstrate that the Ga-adsorbate coverage of 1.0 ML mediated a fundamental transition between SK and Ga autosurfactant modified SK subtypes. In Fig. 4(a), we show the summary of results for the entire series of Ga fluxes investigated under pregrowth Ga wetting conditions. In all cases where the Ga-adsorbate coverage was less than 1.0 ML, the SK transition occurred during GaN growth [Fig. 4(a)]. In cases where the Ga-adsorbate coverage was greater than 1.0 ML during growth, the SK transition occurred after partial desorption of the Ga-adsorbate. For the Ga autosurfactant modified SK transition, the average Ga-adsorbate coverage that desorbed after the SK transition was 1.0±0.1 ML.

2. Variable Ga flux GaN SK growth without pregrowth Ga wetting

Figure 4(b) shows a summary of results for the variable Ga flux dependent total and post-SK Ga-adsorbate coverage and resulting GaN SK transition. The fundamental difference between the initiations of GaN growth without pregrowth wetting with Ga was that for all Ga fluxes the Ga-adsorbate coverage was lower than the case with pregrowth Ga wetting. We speculate that this is consistent with the continuous

Ga-adsorbate coverage accumulation during growth under excess Ga flux until steady state coverage was reached.[20,22]

3. Variable Ga flux experiments in relation to the PA-MBE GaN growth diagram

Figure 1 shows the variable Ga fluxes used in the QD growth experiments on the PA-MBE GaN growth diagram.[19] Based upon previously reported QMS measurements, two Ga flux transitions are depicted on the GaN growth diagram (Fig. 1).[21,23] The first Ga flux dependent transition that is indicated is the critical Ga-adsorbate coverage of 1.0 ML, and the second (at higher Ga fluxes) is the transition that corresponds to the completion of the laterally contracted bilayer (~2.4 ML) and Ga-droplet formation on the surface. The Ga-adsorbate coverage transitions indicated on the GaN growth diagram (Fig. 1) correspond to the maximum steady state Ga-adsorbate that was realized during adsorption and are similar to those obtained after growth for 90 s during GaN homoepitaxy.[22] In the variable Ga flux GaN SK growth experiments, the Ga-adsorbate coverages were similar to the expected coverages predicted by the flux transitions on the growth diagram (Fig. 1). We note that in all cases pregrowth Ga wetting resulted in higher Ga-adsorbate coverages than GaN SK growths without prior wetting.

We propose that future correlation of SK island size or density distributions to specific Ga-adlayer coverages (0–2.4 ML) could be used to achieve controlled GaN QD growth with direct reference to the PA-MBE growth diagram (Fig. 1). For example, with the use of two separate Ga effusion cells, it would be possible to realize a specific Ga-adsorbate coverage of 0–2.4 ML with pregrowth Ga wetting to obtain specified Ga coverage. The second Ga cell could be set to stoichiometric flux conditions with the N flux to avoid further accumulation of Ga-adsorbate during subsequent GaN growth to realize a target GaN QD size or density as mediated by the Ga-adsorbate coverage.

B. Variable GaN coverage during Ga autosurfactant modified SK

Comparison of the onset of the SK transition after partial Ga-adsorbate desorption with the nominal GaN coverage revealed that the critical GaN coverage for the Ga autosurfactant modified SK transition was between 1.5 and 2.0 ML GaN. Subsequent to the SK transition, the integration of thermally induced decomposition Ga flux was consistent with the nominal GaN coverage, limited by N fluence, for all GaN coverage experiments.

1. Critical GaN coverage under Ga autosurfactant modified SK growth

The temporal evolution of the desorption Ga flux measured by QMS, RHEED Bragg spot intensity, and RHEED in-plane relaxation data is presented for the GaN coverages of 1.5 ML (Fig. 5) and 2.0 ML (Fig. 6) for pregrowth Ga wetting and subsequent GaN growth and Ga-adlayer desorption. In Fig. 5, after growth of 1.5 ML nominal GaN coverage, the SK transition was not observed, based upon the invariance of RHEED in-plane lattice spacing. In Fig. 6, the
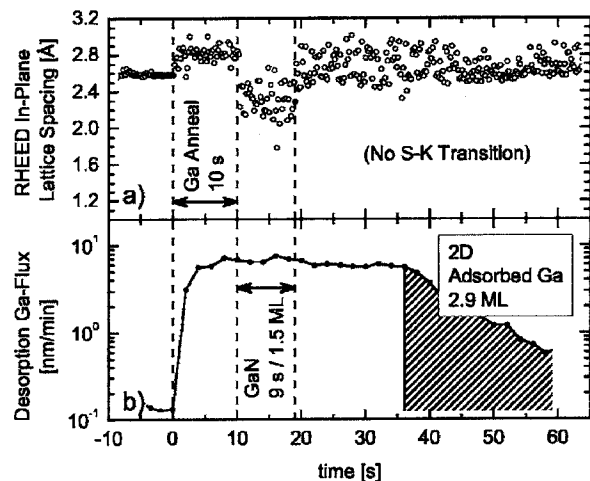

FIG. 5. *In situ* data during 10 s pregrowth Ga wetting, 9 s GaN growth under Ga-droplet conditions, and subsequent Ga-adsorbate desorption with a 707 °C substrate temperature. The Ga flux was 15 nm/min and the N fluence corresponded to 1.5 ML nominal GaN coverage. In this case, the nominal GaN coverage was below the critical thickness required for the SK transition. (a) RHEED in-plane lattice spacing along the [1$\bar{1}$00] azimuth. (b) QMS desorption Ga flux.

onset of the SK transition occurred as previously described above, concurrent with the onset of the desorption of the remaining 1.0±0.1 ML Ga adsorbate.

Previous experiments indicated that a critical GaN coverage of at least 2.0 ML was required for the GaN SK transition under Ga-droplet growth conditions on partially relaxed AlN (0001) surfaces.[10–12,14–16] We speculate that the moderately lower critical thickness, at most several tenths of a monolayer, observed in this work could be attributed to the degree of relaxation in the AlN grown on SiC as opposed to the partially relaxed AlN on GaN used in previous reports.

2. Nominal GaN coverage determination by subsequent thermal decomposition

Figure 7(a) shows the temporal evolution of the desorption Ga flux measured by QMS for the entire growth se-

FIG. 6. *In situ* data during 10 s pregrowth Ga wetting, 12 s GaN growth under Ga-droplet conditions, subsequent Ga-adsorbate desorption, and SK transition with a 707 °C substrate temperature. The Ga flux was 15 nm/min, and the N fluence corresponded to 2.0 ML nominal GaN coverage. In this case, the nominal GaN coverage was above the critical thickness required for the SK transition. The Ga-adsorbate coverage that desorbed after the SK transition was 0.98 ML. (a) RHEED Bragg spot intensity variation. (b) QMS desorption Ga flux.

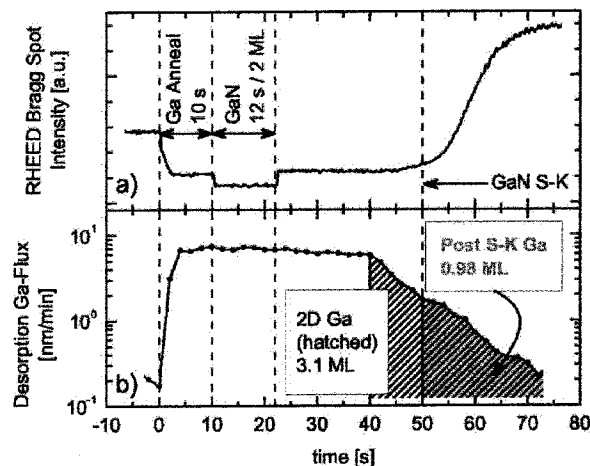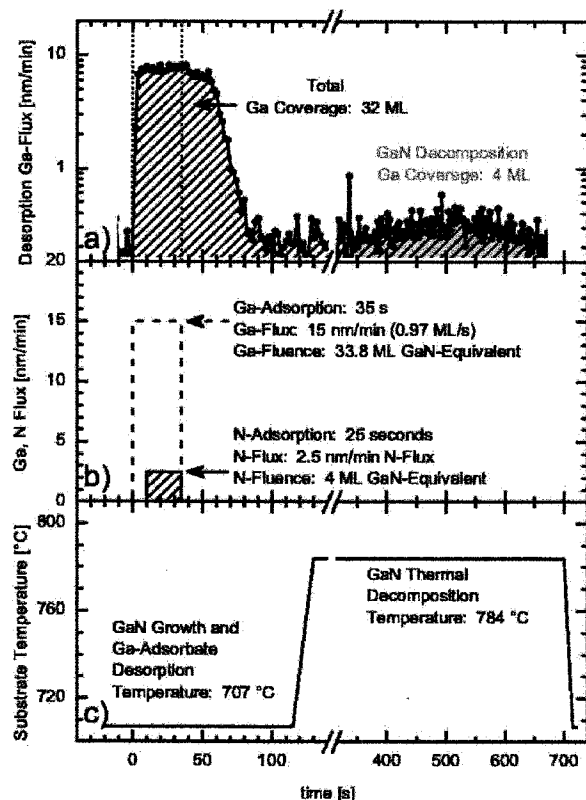FIG. 7. *In situ* Ga desorption data with flux and substrate temperature schematics during 10 s pregrowth Ga wetting, 25 s GaN growth under Ga-droplet conditions, subsequent Ga-adsorbate desorption, and SK transition with a 707 °C substrate temperature. The Ga flux was 15 nm/min, and the N fluence corresponded to 4.0 ML nominal GaN coverage. After complete desorption of the Ga-adsorbate, the substrate temperature was increased to 784 °C, and the increased Ga desorption flux was attributed to GaN thermal decomposition. (a) QMS desorption Ga flux. (b) Ga and N flux schematics and total Ga and N fluences. (c) Substrate temperature schematic.

FIG. 8. Dependence of the integrated desorption Ga flux during GaN thermal decomposition on N-limited GaN nominal coverage.

quence of 4 ML GaN on AlN (0001) followed by apparent subsequent thermal decomposition of the GaN SK surface. Figure 7(c) shows the corresponding temperature sequence for the growth experiment [Fig. 7(b)]. We surmise that after the Ga desorption and subsequent increase of substrate temperature up to 790 °C for surface recovery by AlN growth, the entire GaN SK layer thermally decomposed. In separate QMS measurements, we have measured similar GaN thermal decomposition rates for bulk GaN template wafers. In the case of bulk (0001) GaN, at the temperature of 780 °C, we measured a thermal decomposition rate of 9.6 nm/min. As indicated in Fig. 7(a) by the hatched region, we integrated the desorption Ga flux during GaN thermal decomposition for comparison to the nominal GaN deposition. In Fig. 8, we present the dependence of GaN nominal coverage, measured by QMS during GaN thermal decomposition, to the nominal GaN coverage (1.5–5 ML) as determined by N fluence.

The agreement between integrated GaN decomposition Ga flux and nominal GaN coverage provides an indication that the specified N fluence remained on the growth front. We conclude that the N-adatom incorporation rate (or sticking coefficient) on the time scale of the GaN growth experiments was ~1, and that all of the N flux was ultimate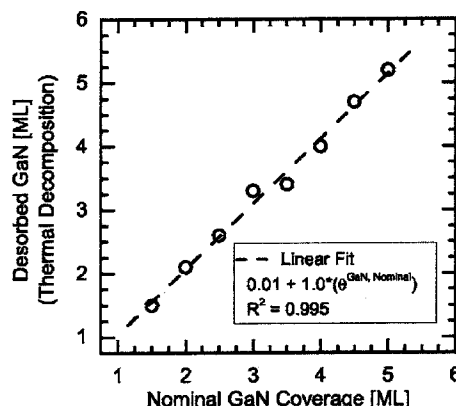ly incorporated as GaN prior to thermal decomposition. These results do not provide an indication of the N-adatom solubility in the Ga-adsorbate, which we speculate is finite due to theoretical and experimental indications that the N-adatom diffusion is dependent on the Ga-adsorbate coverage. However, these results may indicate that the N adatoms have a strong preference to diffuse out of the Ga adsorbate and nucleate as GaN when the Ga-adsorbate desorbs from the surface. In addition, the measurement of decomposition Ga flux corresponding to the nominal GaN coverage verifies the confidence that may be placed in the GaN critical thickness measurement, ~2 ML and in our previous correlation between GaN SK island density and nominal N-limited GaN coverage.[16]

IV. DISCUSSION AND CONCLUSIONS

We conclude that the Ga-adsorbate coverage that mediates a transition to Ga autosurfactant modified SK is 1.0 ML. We have confirmed that the critical GaN coverage for the SK transition under Ga autosurfactant modified (Ga-droplet) conditions on AlN (0001) is approximately 2.0 ML. Based upon these results, theoretical models for N-adatom diffusion in the Ga bilayer,[18] morphological investigations of Ga-adlayer mediated GaN growth,[20,22] and the experimental finding that indium functions as a surfactant during PA-MBE growth,[27] we provide the following suggestions for further experimental studies.

A. Further experiments: GaN SK

As discussed in the Introduction, theoretical consideration of the Ga-adsorbate on GaN has postulated that the Ga bilayer[17] provides a low-energy barrier path for N-adatom diffusion relative to diffusion on the bare GaN (0001) surface.[18] Experimental GaN homoepitaxial growth investigations have found that the Ga-adsorbate coverage varies continuously from 0 to 2.4 ML commensurate with increasing Ga flux during Ga adsorption and GaN growth by PA-MBE.[21,22] Additional GaN PA-MBE morphological investigation has found that the GaN morphology varies continuously with incident Ga flux, believed to be mediated by the continuous Ga-adlayer coverage variation.[20] *In situ*

examination by RHEED and QMS has indicated that the initial GaN homoepitaxial growth mode is mediated by the Ga-adsorbate coverage, and a transition from layer by layer to step-flow growth has been observed.[23] Investigation of Ga adsorption on AlN (0001) has determined that a Ga bilayer is formed on the AlN surface at temperatures of 634−704 °C.[23] In morphological and photoluminescence experiments to be presented separately, we have found that the GaN QDs formed by growth under standard and Ga autosurfactant modified SK conditions give rise to markedly different GaN SK island size distributions. We speculate that further detailed investigation of the GaN SK surface, corresponding to variable Ga flux and resultant Ga-adsorbate coverage, may find continuous mediation of island height and diameter due to the kinetic effect of the Ga bilayer, analogous to the continuous morphology evolution of GaN surfaces grown by PA-MBE.

B. Future directions: In surfactant and InGaN QD growth

Recently, other groups have documented the role of In as a surfactant during GaN and AlN (0001) growth.[27,28] Due to the much higher vapor pressure of In at typical GaN growth temperatures, PA-MBE growth of low roughness bulk GaN without the pit formation has been demonstrated. Theoretical calculations have indicated that In also forms an adlayer on GaN,[18] and a reduced energy barrier N-adatom diffusion channel has been predicted to exist for this adsorbate on GaN. We speculate that investigation of In adsorption on GaN and on AlN could give rise to steady state coverages corresponding to incident In flux. This approach could give rise to further mediation of GaN growth kinetics during QD or quantum well (QW) growth on AlN (0001).

ACKNOWLEDGMENTS

[1] A. Rizzi, R. Lantier, F. Monti, H. Luth, F. Della Sala, A. Di Carlo, and P. Lugli, J. Vac. Sci. Technol. B **17**, 1674 (1999).
[2] F. Bernardini, V. Fiorentini, and D. Vanderbilt, Phys. Rev. B **56**, 10024 (1997).
[3] A. D. Andreev and E. P. O'Reilly, Phys. Rev. B **62**, 15851 (2000).
[4] A. D. Andreev and E. P. O'Reilly, Appl. Phys. Lett. **79**, 521 (2001).
[5] F. Widmann, J. Simon, B. Daudin, G. Feuillet, J. L. Rouviere, N. T. Pelekanos, and G. Fishman, Phys. Rev. B **58**, R15989 (1998).
[6] F. Widmann, B. Daudin, G. Feuillet, Y. Samson, J. L. Rouviere, and N. Pelekanos, J. Appl. Phys. **83**, 7618 (1998).
[7] J. Brown, C. Elsass, C. Poblenz, P. M. Petroff, and I. S. Speck, Phys. Status Solidi B **228**, 199 (2001).
[8] K. Moumanis *et al.*, Appl. Phys. Lett. **82**, 868 (2003).
[9] C. Santori, S. Gotzinger, Y. Yamamoto, S. Kako, K. Hoshino, and Y. Arakawa, Appl. Phys. Lett. **87**, 051916 (2005).
[10] G. Mula, C. Adelmann, S. Moehl, J. Oullier, and B. Daudin, Phys. Rev. B **64**, 195406 (2001).
[11] C. Adelmann, N. Gogneau, E. Sarigiannidou, J. L. Rouviere, and B. Daudin, Appl. Phys. Lett. **81**, 3064 (2002).
[12] N. Gogneau, D. Jalabert, E. Monroy, T. Shibata, M. Tanaka, and B. Daudin, J. Appl. Phys. **94**, 2254 (2003).
[13] N. Gogneau, E. Sarigiannidou, E. Monroy, S. Monnoye, H. Mank, and B. Daudin, Appl. Phys. Lett. **85**, 1421 (2004).
[14] C. Adelmann, B. Daudin, R. A. Oliver, G. A. D. Briggs, and R. E. Rudd, Phys. Rev. B **70**, 125427 (2004).
[15] C. Adelmann, J. Brault, J. L. Rouviere, H. Mariette, G. Mula, and B. Daudin, J. Appl. Phys. **91**, 5498 (2002).
[16] J. Brown, F. Wu, P. M. Petroff, and J. S. Speck, Appl. Phys. Lett. **84**, 690 (2004).
[17] J. E. Northrup, J. Neugebauer, R. M. Feenstra, and A. R. Smith, Phys. Rev. B **61**, 9932 (2000).
[18] J. Neugebauer, T. K. Zywietz, M. Scheffler, J. E. Northrup, H. Chen, and R. M. Feenstra, Phys. Rev. Lett. **90**, 056101 (2003).
[19] B. Heying, R. Averbeck, L. F. Chen, E. Haus, H. Riechert, and J. S. Speck, J. Appl. Phys. **88**, 1855 (2000).
[20] G. Koblmüller, J. S. Brown, R. Averbeck, H. Riechert, P. Pongratz, and J. S. Speck, Jpn. J. Appl. Phys., Part 2 **44**, L906 (2005).
[21] G. Koblmüller, R. Averbeck, H. Riechert, and P. Pongratz, Phys. Rev. B **69**, 035325 (2004).
[22] G. Koblmüller, J. Brown, R. Averbeck, H. Riechert, P. Pongratz, and J. S. Speck, Appl. Phys. Lett. **86**, 041908 (2005).
[23] J. S. Brown, Ph.D. dissertation, University of California at Santa Barbara, 2005.
[24] G. Koblmueller, R. Averbeck, L. Geelhaar, H. Riechert, W. Hosler, and P. Pongratz, J. Appl. Phys. **93**, 9591 (2003).
[25] D. Leonard, M. Krishnamurthy, C. M. Reaves, S. P. Denbaars, and P. M. Petroff, Appl. Phys. Lett. **63**, 3203 (1993).
[26] D. Leonard, K. Pond, and P. M. Petroff, Phys. Rev. B **50**, 11687 (1994).
[27] C. Adelmann, R. Langer, E. Martinez-Guerrero, H. Mariette, G. Feuillet, and B. Daudin, J. Appl. Phys. **86**, 4322 (1999).
[28] C. Kruse, S. Einfeldt, T. Bottcher, and D. Hommel, Appl. Phys. Lett. **79**, 3425 (2001).

Optical Properties of GaN/AlN(0001) Quantum Dots Grown by Plasma-Assisted Molecular Beam Epitaxy

Jay S. Brown[1], Pierre M. Petroff[1,2], Feng Wu[1,3] and James S. Speck[1,3]

[1]Materials Department, University of California, Santa Barbara, CA 93106-5050, U.S.A.
[2]Electrical and Computer Engineering Department, University of California, Santa Barbara, CA 93106-5050, U.S.A.
[3]JST/ERATO UCSB Group, University of California, Santa Barbara, CA 93106-5050, U.S.A.

We have investigated the Ga-flux dependence of growth morphology and optical properties of GaN quantum dots (QDs) in AlN(0001). The QDs formed either by Stranski–Krastanov (S–K) or autosurfactant modified S–K growth depending on the incident Ga-flux during rf-plasma assisted molecular beam epitaxy. We correlated reflection high-energy electron diffraction specular intensity transients to the QD dimensions measured by atomic force microscopy. Single QD layers with growth mode dependant size, density, and wetting layer thickness were characterized by room temperature photoluminescence (PL) with a pulsed 193 nm excitation source. We used a self-consistent one-dimensional Schrödinger–Poisson calculation to identify the contribution of wetting layer quantum wells (1–4 monolayer GaN) and QDs in the PL spectra.
[DOI: 10.1143/JJAP.45.L669]

The three-dimensional electron confinement and the large type-I band offsets associated with self-assembled GaN quantum dots (QDs) in AlN(0001) make them potentially useful for improving optoelectronic device performance in light emitting diodes, lasers, and infrared detectors. Electronic band structure calculations[1,2] of GaN QDs in AlN(0001) have been consistent with the observed luminescence spectra which show characteristic emission intensity maxima between 2.9 and 3.8 eV.[3,4] The viability of high temperature performance has been demonstrated by luminescence from ensembles of GaN QDs up to 750 K.[5] Room temperature optical absorption of GaN QD superlattices in AlN(0001) has provided evidence for infrared (1.3 to 2.4 μm) intersubband electron transitions in QD ensembles.[6] Photon antibunching from single GaN QDs up to ~100 K has demonstrated that GaN QDs may be described as an "atom-like" system which could be useful for quantum information systems related emission and detection.[7]

In rf-plasma assisted molecular beam epitaxy (PA-MBE), *in situ* techniques have been instrumental for investigating growth kinetics and control of GaN QD dimensions and areal densities. Reflection high-energy electron diffraction (RHEED) has been used to investigate the role of a Ga-adsorbate on the GaN/AlN(0001) surface during the Stranski–Krastanov (S–K) transition under Ga-rich conditions.[8] Previous reports have shown that the accumulation of a Ga-adsorbate may suppress the GaN S–K transition, a phenomenon which has been termed the *Ga-autosurfactant modified S–K transition*. In contrast, a classic S–K transition is observed under N-rich growth conditions[9] of GaN on AlN resulting in smaller (1.6 ± 0.3 nm height) QDs in comparison to Ga-rich conditions[8] (2.7 ± 0.2 nm height). The critical GaN coverage for the S–K transition has been found to be approximately 2.0 monolayer (ML).[9–11] Control of the nominal GaN coverage from 2.2 to 3.0 ML under N-limited growth conditions has resulted in GaN QDs with densities from 3×10^8 to 9×10^{10} cm^{-2} as determined by atomic force microscopy (AFM) measurements.[11]

Theoretical calculations[12,13] and experimental studies of PA-MBE growth of GaN(0001) have been consistent in identifying the importance of the Ga-adsorbate in the mediation of adatom surface mobility. Recent PA-MBE GaN(0001) growth investigations, using line-of-sight desorption quadrupole mass spectrometry (QMS), have demonstrated that the Ga-adsorbate coverage[14,15] and GaN morphology[16] are continuously variable with respect to the Ga-flux during growth or adsorption experiments. Our recent observation of a laterally contracted Ga-bilayer on AlN(0001), similar to Ga on GaN(0001),[17] is consistent with previous descriptions of Ga-rich and N-rich GaN QD growth kinetics in the context of Ga-adsorbate mediation of N adatoms.

In this work, we varied the incident Ga-flux during PA-MBE GaN QD growth as a direct method to control the GaN growth kinetics on AlN(0001). The dependence of GaN growth mode on AlN(0001) on incident Ga-flux and Ga-adsorbate coverage 740 °C substrate temperature [Fig. 1(a)] was analyzed in the context of a previously developed GaN growth diagram for PA-MBE.[18] As shown schematically in Fig. 2, we demonstrate the growth of size-controlled GaN QDs on AlN(0001) under excess Ga growth conditions by PA-MBE via monitoring RHEED during the S–K transition. We have found that the S–K transition is not suppressed up to a Ga-adsorbate coverage of approximately 1 ML. We investigated the optical properties of size and density controlled GaN QDs ensembles with room temperature photoluminescence (PL).

GaN growth experiments were performed on partially relaxed 100 nm AlN buffers grown on ~2 μm thick metal-organic chemical vapor deposition (MOCVD)-GaN on sapphire templates in a Varian GEN II MBE system equipped with standard Ga effusion cells and a VEECO Unibulb rf-plasma N source. The GaN template wafers were cleaved into ~2 × 2 cm pieces, degreased with solvents, and indium bonded to 76 mm diameter Si(111) wafers. AlN buffers were grown under excess Al-flux conditions, and the excess Al-adsorbate was consumed by exposure to N-flux prior to GaN growth experiments. Several representative GaN S–K layers were cooled after the observation of the S–K transition for subsequent AFM characterization to compare island size and density distributions to *in situ* RHEED observations. Single layers of GaN QDs were overgrown
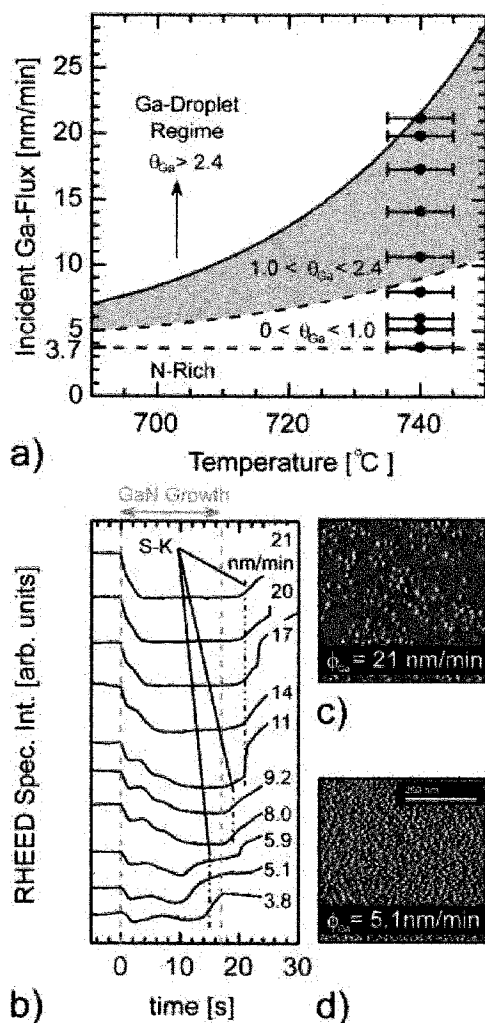
a)

b)

c)

d)

Fig. 1. The dependence of GaN QD growth on excess Ga-flux was investigated via *in situ* RHEED data and *ex situ* AFM morphology. (a) A GaN growth diagram for PA-MBE describes the dependence of Ga adsorbate coverage on (excess) incident Ga-flux. The temperature dependence of critical Ga-flux for gallium droplets formation was previously reported in the context of GaN growth (e.g., see ref. 18). Closed circles indicate Ga-fluxes used during QD growth experiments. (b) RHEED specular intensity transients along the [11$\bar{2}$0] azimuth during growth of 4 ML GaN (17 s, indicated by dashed lines) with variable Ga-flux (as shown, nm/min GaN growth rate potential). The Stranski–Krastanov (S–K) transition is denoted by dashed and dotted lines, as observed via RHEED transmission electron diffraction pattern appearance (not shown). (c) Amplitude AFM image of GaN S–K islands grown with Ga-droplet flux (21 nm/min) and step-flow wetting layer growth. (d) Amplitude AFM image of GaN S–K islands grown with low Ga-flux (5.1 nm/min) and layer-by-layer wetting layer growth.
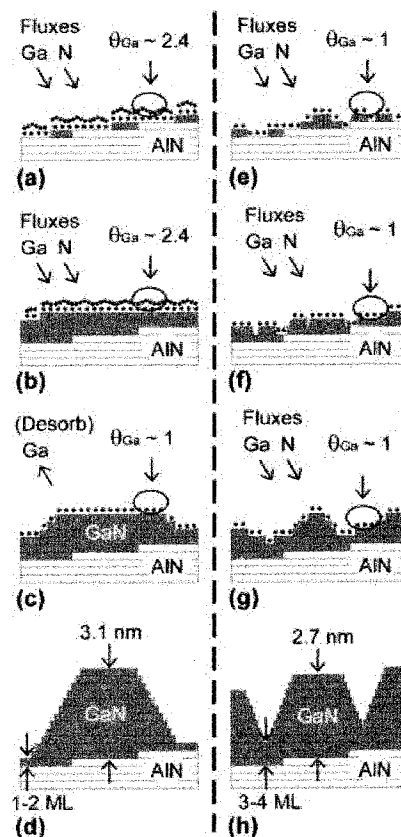

Fig. 2. Schematic representation of GaN wetting layer and subsequent Stranski–Krastanov (S–K) transition on AlN(0001) for Ga autosurfactant modified (a–d) and unmodified S–K conditions (e–h). (a) and (b) Under excess Ga flux conditions such that 1.0–2.4 ML Ga adsorbate is present on the growth surface, the GaN wetting layer grows in the step-flow mode. (c) After GaN wetting layer growth of 2–3 ML, and subsequent partial desorption of the Ga adsorbate, the onset of the S–K transition is observed via RHEED. (d) GaN quantum dots grown under autosurfactant modified S–K conditions with total thickness (including the wetting layer) of 3.1 nm, and a wetting layer of 1–2 ML. (e) and (f) Under excess Ga flux conditions such that less than 1.0 ML Ga adsorbate is present on the growth surface, the GaN wetting layer grows in the layer-by-layer mode. (g) After GaN wetting layer growth of 3–4 ML, the onset of the S–K transition is observed via RHEED. (h) GaN quantum dots grown under S–K conditions with total thickness (including the wetting layer) of 2.7 nm, and a wetting layer of 3–4 ML.

with ~100 nm AlN layers for PL experiments. Fluxes are expressed in (0001)GaN growth rate units, as measured by cross section transmission electron microscopy of Ga-limited and N-limited GaN films. The growth details of variable density GaN QDs samples under Ga-rich conditions were described in a previous report.[11]

The PA-MBE growth of size-controlled GaN QDs on AlN(0001) was monitored by RHEED specular intensity variation along the [11$\bar{2}$0] azimuth, as shown in Fig. 1(b). The N-flux used in this work was 3.6 nm/min, corresponding to 250 W rf power and 0.3 sccm N_2 flow. The growth of GaN on AlN(0001) with variable Ga-flux (3.8–21 nm/min) was performed to investigate the initial GaN "wetting layer"

growth mode prior to the S–K transition with a fixed substrate temperature of 740 °C. As shown in Fig. 1(b), Ga and N shutters were simultaneously opened (at $t = 0$ s) and closed ($t = 17$ s) after the growth of a nominal N-limited GaN coverage of 4 ML. The onset of the S–K transition for each incident Ga-flux was noted by the appearance of Bragg spots in the RHEED pattern, as indicated in Fig. 1(b).

Room temperature PL experiments were performed using a 193 nm pulsed laser (Lambda-Physik) to optically excite carriers in the AlN barriers of the GaN QDs ensembles. The 193 nm laser was operated at 6.5 mJ pulse energy (8 ns FWHM pulse duration) with 100 Hz repetition, focused by refractive optics to achieve maximum (cw) excitation power of 6.4 kW/cm^2. The PL experiments were performed at room temperature, and the luminescence was detected by a grating spectrometer (J-Y Horiba) with spectral resolution <1 nm. We used a least-squares Gaussian peak fitting algorithm to determine mean emission energies for the spectra.

During the growth of 4 ML GaN on AlN(0001), we observed an evolution of RHEED specular intensity variation during the growth of the GaN wetting layer (prior to the S–K transition) with the variation of incident Ga-flux. As shown in Fig. 1(b), with a Ga-flux of 3.8–5.9 nm/min, RHEED oscillations consistent with the layer-by-layer N-limited GaN wetting layer growth rate[9] were observed upon growth initiation. After the growth of a ~3 ML GaN wetting layer, Bragg spots appeared which indicated the onset of the S–K transition. For Ga-fluxes in excess of 14 nm/min, the rapid quenching of RHEED intensity oscillations was observed consistent with step-flow wetting layer growth prior to the S–K transition [Fig. 1(b)]. Consistent with previous reports of the Ga-autosurfactant effect, we observed that with sufficient Ga-fluxes (above 14 nm/min at 740 °C) the S–K transition did not occur until partial desorption of the Ga-adsorbate, i.e., 2–4 sec after the Ga/N shutter closure [Fig. 1(b)]. We believe that the Ga-adsorbate coverage directly mediated the GaN wetting layer growth mode on AlN prior to the S–K transition.

By comparing the steady-state Ga-adsorbate coverage predicted by the QMS-measured critical flux for the completion of 1.0 ML Ga-adsorbate on GaN at 740 °C[17] [Fig. 1(a)], we established that the transition to step-flow wetting layer GaN growth on AlN occurred for Ga-adsorbate coverages above 1.0 ML. As summarized by a growth sequence schematic in Fig. 2, we conclude that the S–K transition was not suppressed when the Ga-adsorbate coverage was less than 1.0 ML and the wetting layer growth mode was consistent with layer-by-layer via RHEED oscillations. When the Ga-adsorbate coverage was greater than about 1 ML, no RHEED oscillations were observed, consistent with step-flow mode growth prior to the Ga-autosurfactant modified S–K transition, as shown in Fig. 2. We conclude that above ~1 ML Ga-adsorbate coverage a reduced energy barrier path for N-adatom surface diffusion was present, allowing the transition from low adatom mobility (layer-by-layer) to high adatom mobility (step-flow) wetting layer growth.[12,13]

As shown in Figs. 1 and 2, the S–K morphology of representative layers grown under identical Ga- and N-flux conditions to those described in the RHEED experiment showed a dramatic difference in GaN island height and diameter as measured by AFM. For the GaN QDs grown under Ga-autosurfactant modified S–K (Ga-droplet) conditions [Fig. 1(c)] with 3 ML nominal GaN coverage, the mean island height was 2.6 ± 0.6 nm, and the mean island diameter was 13.5 ± 3.5 nm. The GaN QDs grown under layer-by-layer conditions [Fig. 1(d)] resulted in S–K island height of 1.8 ± 0.5 nm, and mean island diameter 9.5 ± 3.5 nm. We attribute this difference to the kinetic effect of the Ga-adlayer coverage mediated N-diffusion during GaN growth. The dependence of island size on incident Ga flux is consistent with previous reports.[19–21]

In Fig. 3(a) we present the PL spectra for two representative GaN QDs samples grown under Ga-autosurfactant modified [Fig. 1(c)] and by layer-by-layer [Fig. 1(d)] S–K conditions. In the autosurfactant modified GaN QDs sample, we observed PL emission at 3.4 (GaN substrate), 3.5, 4.2, 4.7, and 5.1 eV. The nominal GaN coverage for this QDs layer was 3.0 ML with two-dimensional GaN wetting layer
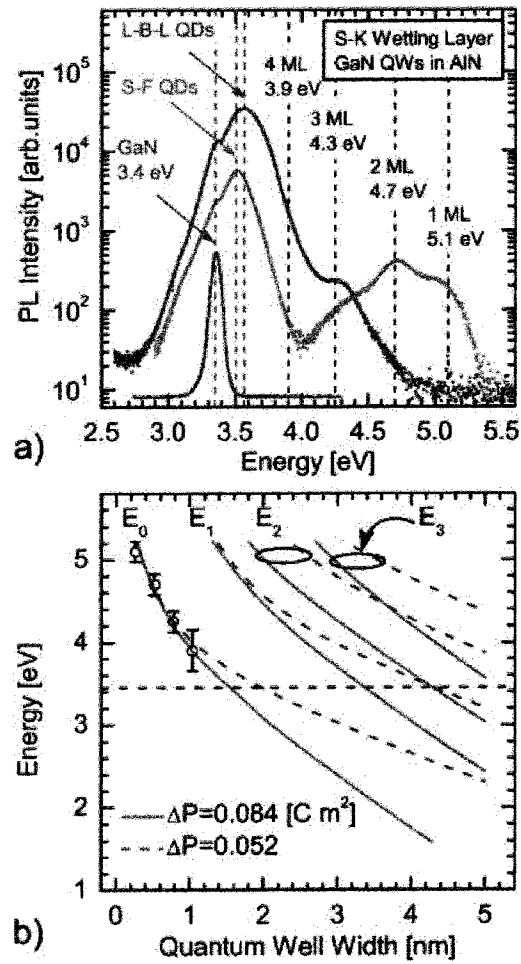

Fig. 3. Room temperature photoluminescence measurements of GaN QDs ensembles in AlN(0001) and calculation of the recombination photon energy for a GaN quantum well wetting layer formed prior to the Stranski–Krastanov transition. (a) Photoluminescence of step-flow (S-F), layer-by-layer (L-B-L) GaN QDs heterostructures and GaN substrate with 193 nm pulsed laser excitation source. (b) One-dimensional effective mass self-consistent Schrödinger–Poisson calculation of bound state interband recombination energy in GaN quantum wells in AlN with polarization induced sheet charge corresponding to fully relaxed and fully strained GaN. The ground state (E_0) and first three excited (E_1, E_2, E_3) recombination energies are shown.

thickness ($w = 2$ ML $= 0.518$ nm) formed prior to the S–K transition. By comparison to reported calculations for GaN QDs in an AlN matrix parameterized in terms of the total QD height ($h = 2.6$ nm) and wetting layer (w) thickness, we attribute the 3.5 eV emission to the QD ground state ($h + w = 3.1$ nm).[1] As shown in Fig. 3(a), the GaN QDs grown under layer-by-layer growth mode S–K conditions exhibited PL emission at 3.4, 3.6, and 4.2 eV. These results are consistent with a 3.6 eV QD ground state with total QD thickness ($h + w$) 2.7 nm.[1] These PL energies are consistent with the reduced QD height ($h = 1.8$ nm), and with GaN quantum well (QW) wetting layer ($w = 0.78$–1.04 nm) due to the increased GaN apparent critical thickness (3–4 ML) observed during in situ experiments [Fig. 1(b)]. We used an effective mass ($m_{GaN}^{electron} = 0.2m_0$; $m_{AlN}^{electron} = 0.3m_0$; $m_{GaN}^{heavy-hole} = 0.8m_0$; $m_{AlN}^{heavy-hole} = 2.0m_0$) self-consistent Schrödinger–Poisson calculation[19] to calculate the ground and first three excited bound electronic states in GaN wetting layer QWs in AlN of varying QW thickness. We approxi-
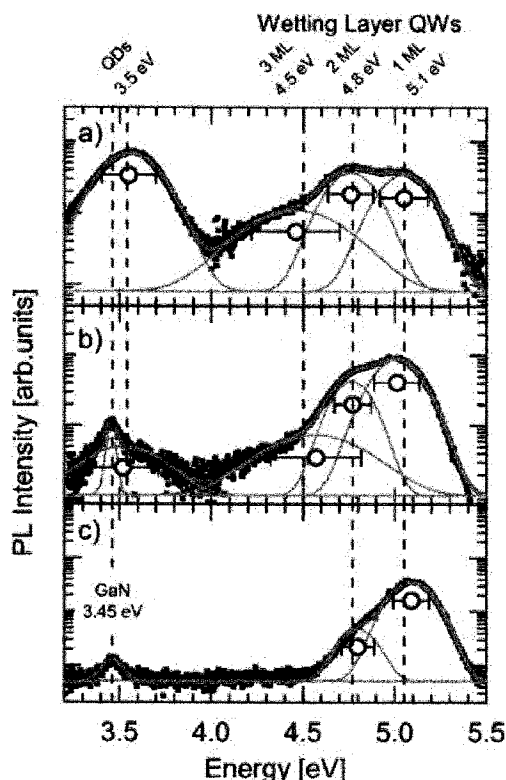
Fig. 4. Photoluminescence of separate single layers of GaN QDs in AlN with variable QD density grown under step-flow (Ga-droplet flux) conditions. The excitation source was a 193 nm pulsed laser. (a) 3.0 ML GaN nominal coverage, 9.2×10^{10} cm^{-2} GaN QDs density. (b) 2.6 ML GaN nominal coverage, 2.8×10^{10} cm^{-2} GaN QDs density. (c) 2.2 ML GaN nominal coverage, 1.7×10^9 cm^{-2} GaN QDs density.

mated two values of the polarization induced electron sheet charge[20] $\Delta P = 0.052-0.084$ C·m^{-2} with 1 Å delta-doped regions at the GaN/AlN interfaces of $(3.25-6.1) \times 10^{21}$ cm^{-3}, corresponding to fully relaxed and fully strained GaN QWs in relaxed AlN. As shown in Fig. 3(b), the energy difference between the ground state electron and the heavy-hole eigenvalues indicated ground state optical transitions corresponding to 1, 2, 3, and 4 ML GaN QWs in AlN at 5.1, 4.7, 4.2, and 3.9 eV, respectively. We therefore attribute the higher energy peaks in the step-flow GaN QDs PL [Fig. 3(a)] to the GaN wetting layer QWs formed prior to the S–K transition of 1–3 ML GaN. We assign the energy peak above the QD transition in the layer-by-layer GaN QDs samples to 3 ML GaN wetting layer QWs.

In Figs. 4(a)–4(c), the PL results for separate samples of variable GaN QD density[11] are shown for nominal GaN coverages of 3.0, 2.6, and 2.2 ML resulting in GaN QD densities of 9.2×10^{10}, 2.8×10^{10}, and 1.7×10^9 cm^{-2}. Separate samples showed a decrease in QD PL intensity commensurate with the QD density. With decreasing nominal GaN coverage, the maximum GaN QW wetting layer peak distribution shifted from 3 ML GaN to 1 ML GaN, consistent with the decreasing nominal GaN coverage. This trend agrees with our assignment of the higher energy PL transitions to GaN QW wetting layers formed prior to the S–K transition, and not to excited states in the GaN QDs.

The optical emission from GaN QDs and QW wetting layers in PL experiments have been demonstrated to span the energy range of 3.5 to 5.1 eV. Our assignment of wetting layer QW PL transitions in the PL spectra is similar to previous reports for GaN QDs grown in AlN by MOCVD.[21] Our observation of the dependence of GaN QDs size and QW thickness on wetting layer growth mode Ga-adsorbate coverage is unique to the PA-MBE growth technique. The direct correlation we have observed between GaN S–K island height, wetting layer thickness, and calculated ground state QD recombination energy[1] indicates that the effect of AlN overgrowth on the GaN S–K surfaces is negligible in PA-MBE. The Ga-adlayer mediation of growth kinetics observed in situ via RHEED has allowed the control of GaN QD size and resulted in a simultaneous change of the wetting layer critical thickness. We conclude that the increase of wetting layer thickness with decreasing island height has given rise to an overall negligible shift in QD emission energy, consistent with reported calculations for GaN QDs.

Acknowledgements

1) A. D. Andreev and E. P. O'Reilly: Phys. Rev. B **62** (2000) 15851.
2) A. D. Andreev and E. P. O'Reilly: Appl. Phys. Lett. **79** (2001) 521.
3) F. Widmann, J. Simon, B. Daudin, G. Feuillet, J. L. Rouviere, N. T. Pelekanos and G. Fishman: Phys. Rev. B **58** (1998) R15989.
4) F. Widmann, B. Daudin, G. Feuillet, Y. Samson, J. L. Rouviere and N. Pelekanos: J. Appl. Phys. **83** (1998) 7618.
5) J. Brown, C. Elsass, C. Poblenz, P. M. Petroff and J. S. Speck: Phys. Status Solidi B **228** (2001) 199.
6) K. Moumanis, A. Helman, F. Fossard, M. Tchernycheva, A. Lusson, F. H. Julien, B. Damilano, N. Grandjean and J. Massies: Appl. Phys. Lett. **82** (2003) 868.
7) C. Santori, S. Gotzinger, Y. Yamamoto, S. Kako, K. Hoshino and Y. Arakawa: Appl. Phys. Lett. **87** (2005) 051916.
8) C. Adelmann, N. Gogneau, E. Sarigiannidou, J. L. Rouviere and B. Daudin: Appl. Phys. Lett. **81** (2002) 3064.
9) C. Adelmann, B. Daudin, R. A. Oliver, G. A. D. Briggs and R. E. Rudd: Phys. Rev. B **70** (2004) 125427.
10) C. Adelmann, J. Brault, J. L. Rouviere, H. Mariette, G. Mula and B. Daudin: J. Appl. Phys. **91** (2002) 5498.
11) J. Brown, F. Wu, P. M. Petroff and J. S. Speck: Appl. Phys. Lett. **84** (2004) 690.
12) J. E. Northrup, J. Neugebauer, R. M. Feenstra and A. R. Smith: Phys. Rev. B **61** (2000) 9932.
13) J. Neugebauer, T. K. Zywietz, M. Scheffler, J. E. Northrup, H. Chen and R. M. Feenstra: Phys. Rev. Lett. **90** (2003) 056101.
14) G. Koblmuller, R. Averbeck, H. Riechert and P. Pongratz: Phys. Rev. B **69** (2004) 035325.
15) G. Koblmuller, J. Brown, R. Averbeck, H. Riechert, P. Pongratz and J. S. Speck: Appl. Phys. Lett. **86** (2005) 041908.
16) G. Koblmueller, J. S. Brown, R. Averbeck, H. Riechert, P. Pongratz and J. S. Speck: Jpn. J. Appl. Phys. **44** (2005) L906.
17) J. S. Brown, G. Koblmuller, F. Wu, R. Averbeck, H. Riechert and J. S. Speck: J. Appl. Phys. **99** (2006) 074902.
18) B. Heying, R. Averbeck, L. F. Chen, E. Haus, H. Riechert and J. S. Speck: J. Appl. Phys. **88** (2000) 1855.
19) I. H. Tan, G. L. Snider, L. D. Chang and E. L. Hu: J. Appl. Phys. **68** (1990) 4071.
20) F. Bernardini, V. Fiorentini and D. Vanderbilt: Phys. Rev. B **56** (1997) 10024.
21) K. Hoshino and Y. Arakawa: J. Cryst. Growth **272** (2004) 161.

Ga adsorbate on (0001) GaN: *In situ* characterization with quadrupole mass spectrometry and reflection high-energy electron diffraction

Jay S. Brown and Gregor Koblmüller
Materials Department, University of California, Santa Barbara, California 93106-5050

Feng Wu
*JST/ERATO UCSB Group and Materials Department, University of California,
Santa Barbara, California 93106-5050*

Robert Averbeck and Henning Riechert
Infineon Technologies AG, Corporate Research Photonics, D-1730 Munich, Germany

James S. Speck[a]
*JST/ERATO UCSB Group and Materials Department, University of California,
Santa Barbara, California 93106-5050*

We have investigated the adsorption and subsequent desorption of Ga on (0001) GaN using simultaneous line-of-sight quadrupole mass spectrometry (QMS) and reflection high-energy electron diffraction (RHEED). The *in situ* QMS and RHEED desorption transient measurements demonstrate the Ga flux dependent accumulation of the theoretically predicted laterally contracted Ga bilayer [J. E. Northrup *et al.*, Phys. Rev. B **61**, 9932 (2000)] under conditions similar to those used during GaN growth by rf-plasma molecular beam epitaxy. We correlated biooscillatory RHEED desorption transients [C. Adelmann *et al.*, J. Appl. Phys. **91**, 9638 (2002)] to QMS-measured Ga-adsorbate coverage and found both to be consistent with layer-by-layer desorption of the Ga-adsorbate bilayer. The QMS-measured steady-state Ga-adlayer coverage exhibited a continuous increase from 0 to 2.4 ML (monolayer) with respect to impinging Ga flux at substrate temperatures of 640–700 °C. We observed an exponential dependence of the Ga flux corresponding to 1.0 ML Ga-adsorbate coverage on substrate temperature and we measured an apparent activation energy of 2.43±0.11 eV and an attempt prefactor of 6.77×10^{12} nm/min (4.36×10^{11} Hz) for this transition. © 2006 American Institute of Physics. [DOI: 10.1063/1.2181415]

I. INTRODUCTION

Recent improvements in GaN-based electronic[1] and optoelectronic devices[2] grown by rf-plasma assisted molecular beam epitaxy (PA-MBE) have demonstrated several important advantages as compared to chemical vapor deposition III-nitride growth technology. The key features of III-nitride growth by PA-MBE include complete composition control of the AlGaN (Ref. 3) and InGaN (Ref. 4) ternary alloys, abrupt *p*-type Mg doping profiles without postgrowth activation,[5] and heterostructure growth control on the monolayer scale[6] to take advantage of the spontaneous and piezoelectric polarization-induced electric fields[7] in device engineering. Further optimized GaN growth, resulting in smooth surfaces, low structural defect densities, and the elimination of morphological features, including pitting or metal droplets in PA-MBE, is desirable for improved device yield across full wafers.

Homoepitaxial GaN growth by PA-MBE has been characterized *ex situ* by atomic force microscopy, electron microscopy, x-ray diffraction, photoluminescence, and optical microscopy to establish a flux and substrate temperature diagram with three distinct regimes.[8,9] As the Ga flux is increased above stoichiometric conditions, the surface rough-

ness is observed to decrease until the Ga flux is sufficient for Ga droplet accumulation. Rough and faceted GaN growth, indicative of low adatom diffusion lengths, is observed when the N flux exceeds the Ga flux. Under Ga-droplet formation flux conditions, step-flow GaN morphology without pits is observed, indicative of high mobility adatoms. Under conditions where the Ga flux is intermediate to the Ga-droplet and N-rich regimes, GaN morphology ranges from rough to step flow with faceted pits. The pit formation is associated with threading dislocations and is the MBE analog of V defects commonly observed under low surface mobility conditions of metal-organic chemical vapor deposition of GaN.[10,11] Under typical PA-MBE GaN growth conditions, with substrate temperatures of 700–750 °C, optimized electrical and optical quality GaN has been obtained with excess Ga fluxes just below the Ga-droplet formation flux.[12] The critical excess Ga flux required for Ga-droplet formation during GaN growth was found to increase exponentially with substrate temperature with an activation energy of ∼2.83 eV, which is the same as the activation energy associated with the Ga partial pressure over liquid Ga.[8]

More recent morphological investigation of the GaN growth dependence on Ga flux has found that by varying the Ga flux from N-rich to Ga-droplet conditions the surface pit density decreases monotonously up to the Ga-droplet formation flux commensurate with increasing Ga-adsorbate

[a]Electronic mail: speck@mrl.ucsb.edu

coverage.[13] The PA-MBE GaN morphology is consistent with the continuously increasing adatom mobility with increasing Ga flux from stoichiometry up to the Ga-droplet formation flux.[9]

Neugebauer *et al.*[14] and Zywietz *et al.*[15] provided theoretical and experimental evidence that N-adatom mobility on the GaN growth surface may be directly mediated by the presence or the absence of Ga adsorbate on GaN. The two N-adatom limited diffusion cases that have been found are complete Ga-bilayer coverage [~2.4 ML (monolayer)] and the bare GaN (0001) surface. For complete bilayer coverage, the energy barrier for N diffusion was predicted to be as low as 0.5 eV, representing a significant decrease from the 1.4 eV energy barrier for N diffusion on the bare GaN (0001) surface. This theoretical prediction is consistent with the empirical GaN morphology of PA-MBE grown under N-rich and Ga-droplet conditions.[8,9]

Static first principles total energy calculations by Northrup *et al.* have predicted the stability of several phases of Ga adsorbate on the Ga-polar (0001) GaN surface.[16] In the Ga-rich limit, the energetically favorable Ga-adsorbate structure was found to be a laterally contracted bilayer. The first Ga-adsorbate monolayer was found to be pseudomorphic (PM) to the (0001) GaN lattice with an areal density of 1.14×10^{15} cm^{-2}, in terms of (0001) GaN density. The second Ga-adsorbate monolayer was found to prefer a lateral contraction (LC) toward the bulk Ga nearest neighbor distance, with a GaN-equivalent coverage of ~1.4 ML. Additional Ga monolayers were found to be less energetically favorable than the bilayer, a result that is consistent with the experimental conclusion that sufficient Ga fluxes result in liquid Ga-droplet formation beyond the bilayer completion.[17]

Analysis of GaN (0001) surfaces after PA-MBE growth under excess Ga conditions via scanning tunneling electron microscopy (STM), low energy electron diffraction (LEED), and Auger electron spectroscopy (AES) has been consistent with the laterally contracted bilayer model predicted by theory.[18] Observation of 1×1 STM corrugation patterns consistent with the underlying GaN wurtzite (WZ) bond length, 3.19 Å, may be assigned to the PM Ga adlayer which retains the hexagonal structure of the GaN (0001) surface. The diffraction satellite rings in the vicinity of the (0,1) LEED intensity maxima were assigned to an incommensurate adlayer that was laterally contracted toward the bulk Ga–Ga bond length of 2.7 Å. Finally, the AES measurements indicated the presence of 2–3 ML Ga adsorbate on the pseudo-1×1 GaN (0001) surface. An analysis of several measurements of the Ga/GaN (0001) pseudo-1×1 surface was consistent with an incommensurate fluid Ga adlayer above 350 °C.

The correlation between GaN surface PA-MBE growth morphology and excess adsorbed Ga on the GaN surface has motivated further detailed investigation of the structure and dynamics of adsorbed Ga phases on GaN in the absence of N flux. In Fig. 1(a), we show a Ga/GaN adsorption diagram, which is equivalent to the GaN growth diagram in the limit of zero N flux. Following previous work,[19] we note the important distinction between the GaN growth diagram[8] that is strictly valid only in the presence of N flux, and the Ga/GaN adsorption diagram in the absence of N flux. However, based
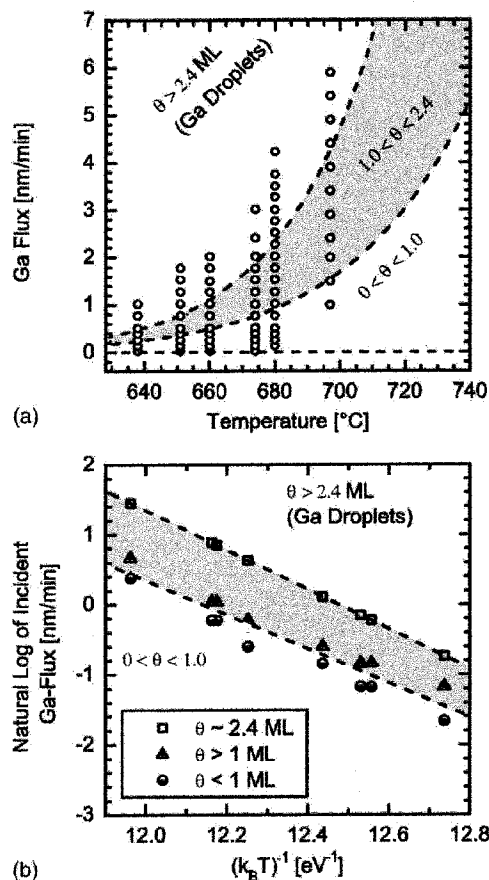

FIG. 1. (a) The "Ga/GaN (0001) adsorption diagram" correlates the exponential Ga-flux dependence of Ga-adsorbate coverage and Ga droplet formation on substrate temperature. The activation energy for 1 ML Ga-adsorbate was determined from *in situ* temperature dependent measurements, as shown in (b). The Ga fluxes and substrate temperatures used for 90 s adsorption in this work are indicated as open circles. (b) Arrhenius plot for the determination of single exponential activation energies and atomic attempt frequencies for critical fluxes to realize 1.0 and 2.4 ML gallium adsorbate coverage. For the critical flux to form 1.0 ML Ga on GaN after 90 s Ga adsorption, we measured an activation energy of 2.43 ± 0.11 eV and a prefactor of 6.77×10^{12} nm/min. The activation energy and atomic attempt prefactor for the critical flux for 2.4 ML gallium coverage and droplet formation were previously reported in the context of GaN growth (e.g., see Ref. 8).

upon the invariance of the activation energies for the temperature dependence of the droplet formation flux on excess Ga flux in GaN growth and for bulk Ga vapor pressure,[8] it is reasonable to perform Ga-adsorption experiments and compare the results to the GaN growth diagram. Investigation of the temperature and flux dependences of Ga-adsorbate coverage on (0001) GaN is pursued in this work to improve control and understanding of the growth of GaN under Ga-rich conditions.

Adelmann *et al.* explored the correspondence of Ga-adsorbate coverage to the impinging Ga flux at substrate temperatures of 700–740 °C, using reflection high-energy electron diffraction (RHEED).[19,20] Adsorption and subsequent desorption of the Ga-adsorbate on (0001) GaN were investigated by monitoring the intensity of the RHEED specular spot (00) along the [11$\bar{2}$0] azimuth. The Ga-adsorbate coverage was observed to depend on the impinging Ga flux, based on the dependence of the desorption time

on adsorption time. It was shown that near the critical Ga flux to form droplets, the specular intensity exhibited two complete oscillations during adsorption and during desorption, consistent with the layer-by-layer growth and desorption of an adsorbate bilayer. A signature of Ga-droplet formation was observed by monitoring the RHEED desorption transient duration after Ga shutter closure. When Ga droplets had formed on the GaN surface during Ga adsorption, the onset of the RHEED intensity oscillations was preceded by a delay that increased monotonously with increasing Ga flux or adsorption time. When the impinging flux was below the critical flux for Ga-droplet formation, desorption time saturation was observed, consistent with steady-state Ga-adsorbate coverage. At fixed temperatures, the dependence of desorption time on the impinging Ga flux exhibited a flux-invariant region for a range of Ga fluxes just below and up to the critical flux to form Ga droplets. The flux-invariant duration regime measured by RHEED specular intensity was attributed to the completion of the laterally contracted bilayer over a range of Ga fluxes.

Another more quantitative technique that has been implemented in the investigation of the Ga adsorbate on GaN is a line-of-sight quadrupole mass spectrometry (QMS).[17] The QMS technique measures the temporal desorption of Ga from the wafer surface, providing a direct measure of mean Ga adatom lifetime and adlayer coverage. Previous QMS measurements have shown that the two-dimensional Ga-adsorbate coverage on (0001) GaN saturates at ~2.4 ML at temperatures of interest for MBE, and that additional Ga coverage may be accommodated in macroscopic Ga droplets, in agreement with the theoretically predicted Ga bilayer structure. Desorption activation energies derived from temperature dependent adatom lifetime measurements for both the PM (4.9 eV) and LC (3.7 eV) monolayers of the Ga adsorbate were used in a macroscopic rate equation analysis to model the QMS-measured desorption Ga-flux transients. The QMS-measured Ga-adsorbate coverage was found to increase continuously with increasing impinging Ga flux both in the absence of N flux and during GaN growth, in contrast to the RHEED experiments which were interpreted to reveal a regime of constant Ga coverage independent of adsorption flux.

In this work, we present the results of simultaneous RHEED and QMS *in situ* experiments of Ga-adsorbate desorption from (0001) GaN to investigate the correspondence of the information provided by both *in situ* MBE techniques. Both techniques have practical advantages in routine use to monitor the N and Ga fluxes and substrate temperature. Large sample size, similar to full wafers (50.8 mm diameter) used in this work, is required for the QMS signal detection in our MBE system, whereas small samples as small as ~2 mm diameter provide sufficient contrast for use in RHEED experiments. Our experiments have been motivated both to realize a fundamental understanding of the kinetics of the Ga adsorbate on (0001) GaN, and with the more practical goal of developing reliable growth control techniques for samples of various sizes.

II. EXPERIMENTS

The Ga adsorption experiments were performed on (0001) GaN with simultaneous QMS and RHEED in a Varian GEN II MBE system equipped with standard Ga effusion cells and a VEECO Unibulb rf-plasma N source. All experiments were performed on 2 inch (Lumilog) wafers of 2 μm metal-organic chemical vapor deposition (MOCVD)-grown (0001) GaN on sapphire. Electron beam evaporation was used to deposit 0.5 μm titanium films on the backside of the sapphire substrates to facilitate radiative heating. The substrates were degreased with solvents and outgassed in vacuum prior to introduction into the growth chamber. Prior to adsorption experiments, ~200 nm thick GaN buffers were grown under Ga droplet conditions to realize smooth GaN surfaces and avoid surface contamination.[21] After GaN buffer growth, the desorption of Ga-adsorbate bilayer and droplets was monitored by QMS. Fluxes are expressed in (0001) GaN growth rate units, as measured by cross section transmission electron microscopy of Ga-limited and N-limited GaN films. For convenience of conversion to a.u., we note that in WZ GaN along [0001], 2.59 Å is the height of 1 ML.

A quadrupole mass spectrometer (Stanford Research Systems AMU-200) installed in a source port of the GEN II was used for QMS measurements. An aperture was placed between the substrate and the ionization grid to reduce the line-of-sight acceptance angle of the detector to exclude Ga atoms that do not originate on the wafer surface. The linear proportionality constant of the response of the QMS detector was measured by exposure of a sapphire wafer at ~850 °C to impinging Ga fluxes (1–30 nm/min) well below the critical flux for Ga-droplet accumulation (~430 nm/min). Under these conditions, steady-state conservation of Ga flux allows a direct correlation from the QMS-measured ^{69}Ga partial pressure to total desorption Ga flux in GaN-equivalent growth rate units.

The QMS-measured temporal desorption Ga flux was integrated to determine the Ga-adsorbate steady-state coverage. The substrate temperature was measured *in situ* by pyrometer, but the temperatures we report were determined by comparing maximum steady-state Ga desorption rates to the Ga/GaN adsorption diagram (Fig. 1). This method provided a precise self-consistent correlation of substrate temperature to (critical) Ga droplet Ga flux, based upon previous *ex situ* measurements that were in agreement with the bulk Ga partial pressure.[8] At steady state, the critical flux to form droplets at fixed temperature is the same as the maximum Ga desorption rate from the wafer surface. When the impinging Ga flux, or excess Ga flux in the case of GaN growth, was in excess of the maximum Ga desorption rate, Ga-droplet accumulation occurred. Consequently, when the impinging Ga flux was incrementally increased up to and beyond the critical flux for droplet formation at fixed substrate temperature, we observed an increase in the maximum Ga desorption rate up to the critical (Ga-droplet formation) flux, followed by a saturation of the maximum rate of Ga desorption independent of further increases in Ga flux. By averaging the maximum Ga steady-state desorption rate from several adsorption

experiments, it was possible to determine the self-consistent substrate temperature with standard variation ± 1 °C via flux calibration and the response calibration of the QMS detector.

We monitored the integrated intensity of the RHEED specular spot (00) along the $[11\bar{2}0]$ azimuth to characterize the structural organization of the Ga adsorbate. We used a 7 keV beam energy, a 2.7 mA filament current, and an $\sim 1°-2°$ incident angle. The time resolution of the charge-coupled device (CCD) detection system (k-Space Associates) was less than 0.5 s. We defined the RHEED desorption duration as the elapsed time after closing the Ga shutter to the time at which the derivative of the specular intensity reached zero. For comparison to RHEED desorption time, the QMS desorption duration was defined as the time elapsed after closing the Ga shutter for the desorbing Ga flux to decrease below 0.2 nm/min, the minimum detectable desorption flux.

A. Ga adsorption: Variable adsorption time

We investigated Ga adsorption with variable adsorption time from 10 to 600 s, with impinging Ga fluxes of 0.8 and 3 nm/min and substrate temperature of 678 ± 1 °C. The adsorbed Ga coverage was determined from the QMS measurements. The Ga-desorption duration was measured from the RHEED specular intensity oscillations. Variable adsorption time experiments were designed to confirm the presence of steady-state Ga-adsorbate coverage on (0001) GaN, previously observed by monitoring the dependence of RHEED desorption time on adsorption time.[19]

B. Ga adsorption: Variable impinging Ga flux

In the second series of adsorption experiments, the impinging flux was varied incrementally (0.25–1.0 nm/min steps) to sample the Ga/GaN adsorption diagram [Fig. 1(a)] at selected substrate temperatures. For all fluxes and temperatures, the adsorption duration was held constant at 90 s for consistency with previous reports.[19] Variable Ga-flux experiments were performed at six substrate temperatures, from 638 to 697 °C as depicted by open circles in Fig. 1, to characterize the effect of temperature on the transition fluxes. We used substrate temperatures below 700 °C to minimize the contribution of GaN thermal decomposition to the Ga flux desorbing from the wafer.[22] The total adsorbed Ga coverage resulting from each impinging flux was determined by direct integration of the desorption Ga flux measured by QMS. The desorption duration was defined, as described above, for the fixed Ga-flux experiments for both QMS and RHEED data. Variable impinging flux experiments were performed to realize different initial Ga-adlayer coverages for comparison of adlayer morphology (characterized by RHEED) and coverage (measured by QMS) over a range of substrate temperatures.

III. RESULTS

A. Dynamic stability of Ga-adlayer coverage with impinging Ga flux

The QMS-measured Ga-adsorbate coverage and RHEED desorption duration are shown as a function of adsorption
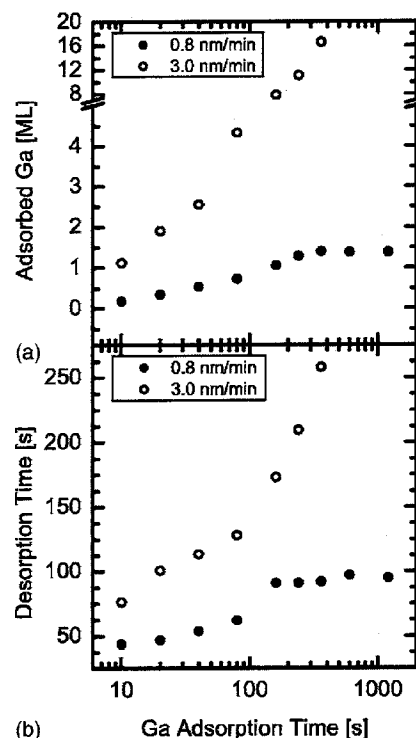

FIG. 2. Ga adsorption with variable adsorption time for impinging fluxes above (3.0 nm/min) and below (0.8 nm/min) the droplet formation flux at a substrate temperature of 678 °C. (a) QMS-measured total adsorbate coverage as a function of adsorption time. (b) RHEED measured desorption time evolution as a function of adsorption time.

time for two impinging Ga fluxes in Fig. 2. From the Ga/GaN adsorption diagram (Fig. 1), at the substrate temperature of 678 °C, the critical Ga flux for Ga droplet formation is 2.2 nm/min. For a subcritical impinging Ga flux of 0.8 nm/min, the Ga-adsorbate coverage [Fig. 2(a)] saturated at 1.4 ± 0.01 ML beyond 360 s of adsorption. This result provides an independent confirmation that stable steady-state Ga coverages exist, corresponding to Ga fluxes that are less than the critical Ga-droplet flux.[19] The total desorption time [Fig. 2(b)] determined from the RHEED specular intensity oscillations also showed an invariant adsorption time regime for 0.8 nm/min impinging flux, but the onset of the saturation occurred at 160 s of adsorption. We note that the RHEED spot size is ~ 1 mm $\times$ 100 μm, while the QMS measures the desorbing flux from the full 50.8 mm diam wafer. Due to the nonuniformity of the impinging flux, we speculate that the onset of steady-state coverage occurred inhomogeneously across the entire wafer.

With a supercritical impinging Ga flux of 3.0 nm/min, as shown in Fig. 2, neither the coverage or desorption time saturated, rather the adsorbed Ga coverage and desorption time increased monotonically with adsorption time. These Ga coverage and desorption time behavior are attributed to the completion of the Ga bilayer followed by accumulation of Ga in droplets, which is identical to the analysis of previous RHEED experiments[19] and QMS experiments.[17]

The results of this experiment are consistent with previous reports[17,19] and establish the foundation for variable Ga-flux experiments over a range of temperatures. We have observed this dichotomy of coverage stability for subcritical
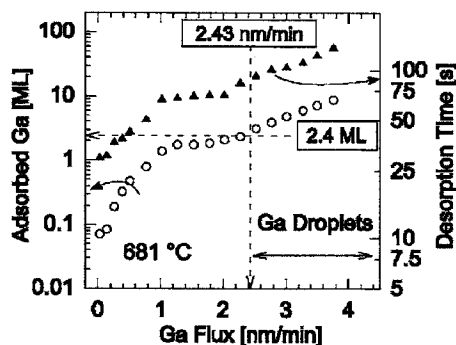
FIG. 3. Evolution of adsorbate Ga coverage and desorption time as a function of impinging Ga flux after 90 s adsorption at a substrate temperature of 681 °C. The droplet transition flux from the Ga/GaN(0001) growth diagram of 2.43 nm/min and the adsorbate coverage of 2.4 ML are indicated in relation to the measured adsorbed coverage.

and supercritical Ga fluxes at all temperatures presented in this work, in accordance with the Ga/GaN adsorption diagram [Fig. 1(a)].

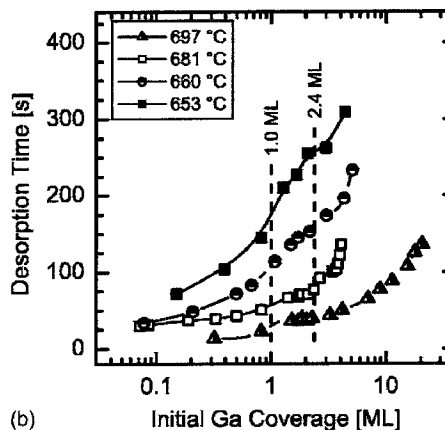## B. Ga-adsorbate coverage and desorption time evolution with impinging Ga flux

Figure 3 shows the dependence of the QMS-measured Ga-adsorbate coverage and QMS-measured desorption time on the impinging Ga flux at a substrate temperature of 681 °C. As shown in Fig. 3, the Ga-adsorbate coverage increased continuously with impinging Ga flux. From the Ga/GaN adsorption diagram [Fig. 1(a)], at 681 °C substrate temperature the critical Ga flux for Ga droplets formation is 2.43 nm/min. When the impinging Ga flux was subcritical (below 2.43 nm/min), the Ga-adsorbate coverage was between 0 and 2.4 ML. For supercritical Ga fluxes, the Ga coverage increased monotonically from 2.4 to 10 ML.

The duration of the desorption process increased over the same range of impinging Ga flux and resultant Ga-adsorbate coverages, with two subtle exceptions in the form of an abrupt increase and a flux-invariant plateau (Fig. 3). The Ga-adsorbate desorption time increased monotonically to 51 s as the adsorbed coverage reached 0.8 ML. Then, for a modest increase in coverage to 1.02 ML, the desorption time abruptly increased to 67 s. As the initial adsorbed coverage was subsequently increased further from 1.02 to 2.02 ML, the desorption time was nearly insensitive to the impinging flux, with a gradual increase to 71 s. Therefore, the PM monolayer accounted for approximately 94% of the total desorption time for the full 2.4 ML bilayer. We speculate that despite the larger coverage (1.4 ML) of the LC monolayer, the higher mean adatom desorption rate and the rapid transfer of adatoms from the LC to PM monolayer due to the energy minimization give rise to the negligibly small increase in total desorption time from the coverage range of 1.0–2.4 ML.

For all substrate temperatures, we observed qualitatively similar evolution of Ga-adsorbate coverage and desorption time with impinging Ga flux, as shown in Fig. 4. The transition flux for bilayer completion and droplet formation increased exponentially with substrate temperature [Fig. 4(a)], as expected from the Ga/GaN adsorption diagram. As the
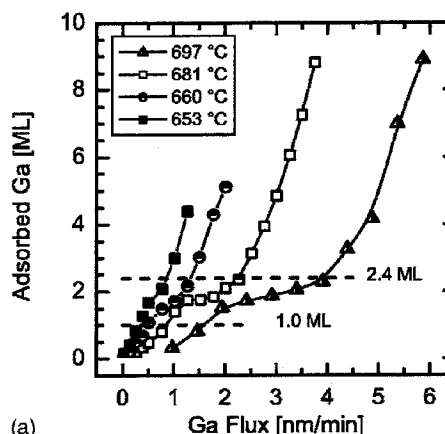
FIG. 4. (a) Dependence of the QMS-measured adsorbate Ga coverage on the impinging Ga flux for the substrate temperatures in the range of 653–697 °C. (b) Dependence of the Ga-adsorbate desorption time on the initial Ga-adsorbate coverage over the same range of substrate temperatures.

substrate temperature was increased, the desorption time decreased with respect to the initial coverage, and the flux-invariant desorption time plateau became more pronounced [Fig. 4(b)]. For example, the flux-invariant desorption time increased only a few seconds over the entire range of coverage at 697 °C, appearing to be nearly invariant with respect to the impinging flux. By comparison of desorption time to the QMS-measured initial coverage, our experiments demonstrate that the flux-invariant desorption time plateaus correspond to a region of gradually increasing Ga-adsorbate coverage. We propose that the abrupt increase in desorption time is a direct result of coverage sensitivity to adsorption flux in the vicinity of the completion of 1.0 ML total coverage. The subsequent slow increase of desorption time with increasing coverage is attributed to the difference in desorption rates between the 2 ML of the bilayer structure.[17] Desorption time as a function of Ga-adsorbate coverage is dominated by the first (PM) monolayer, due to the higher mean adatom lifetime of Ga atoms which are strongly bound to the underlying GaN.[17]

C. Ga-adsorbate morphology and coverage

We assessed the correlation between the RHEED transient oscillations and the Ga-adsorbate coverage measured by QMS for the variable impinging Ga-flux experiments (Fig. 5). Zeros in the first derivative of the RHEED intensity,
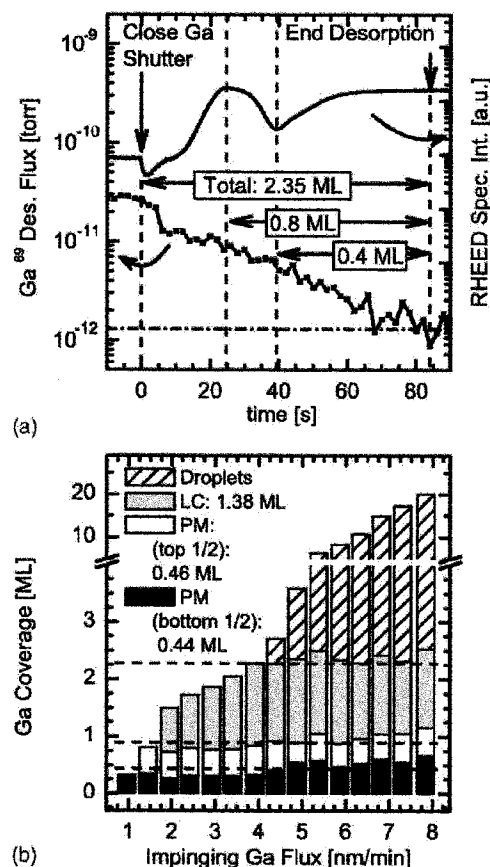
FIG. 5. (a) An example of RHEED delineated QMS integration experiment with 2.35 ML total adsorbed coverage after 90 s Ga adsorption with 2.2 nm/min impinging flux and a substrate temperature of 681 °C. (b) Correlation between laterally contracted (LC) and pseudomorphic (PM) monolayer intervals indicated by RHEED specular intensity extrema along [11$\bar{2}$0] azimuths and desorbed Ga-adsorbate coverage, obtained via integration of Ga-flux desorption transient intervals. The histogram plot indicates the breakdown of Ga-adsorbate coverage between the monolayer intervals as the incident Ga flux was increased from 1 to 8 nm/min with 697 °C substrate temperature.

corresponding to local extrema in the RHEED oscillation intensity, were used to delineate specific integration limits of the QMS signal. Under the assumption that the Ga bilayer adatoms adsorb and desorb via a sequential layer-by-layer process, the maxima in the RHEED intensity correspond to planar surfaces of completed monolayers. However, interpretation of the origin of the RHEED contrast may also depend on the GaN surface roughness evolution, substrate vicinality, azimuthal beam orientation, multiple (dynamic) scattering effects, disorder of individual monolayers, and the electron beam conditions.[23]

An example of simultaneous RHEED intensity oscillations and QMS desorption Ga-flux data is shown in Fig. 5(a), for an initial Ga coverage of 2.35 ML at a substrate temperature of 681 °C. The RHEED-delineated Ga-adsorbate coverage dependence measured by QMS on impinging Ga flux at a substrate temperature of 697 °C is shown in Fig. 5(b). The consistency between RHEED intensity oscillations and the QMS-measured coverage evolution shows that both types of measurements are in agreement with the predicted laterally

contracted Ga bilayer. These results confirm that the RHEED contrast is dominated by Ga-adlayer structure desorption by a sequential layer-by-layer process.

D. Activation energy for completion of 1.0 ML

As shown in Fig. 1(a), for 90 s adsorption, the Ga flux corresponding to 1.0 ML total Ga-adsorbate coverage increased exponentially with temperature, and was lower than the critical flux for 2.4 ML completion and subsequent Ga-droplet formation. Following the approach used to determine the activation energy for Ga droplets formation in GaN growth by PA-MBE,[8] we determined a thermal activation energy of 2.43±0.11 eV and an attempt frequency prefactor of 6.77×10^{12} nm/min $(4.36 \times 10^{11}$ Hz) for the completion of 1.0 ML total adsorbate coverage. For each of the substrate temperatures of the variable Ga-flux adsorption experiments, we found the nearest fluxes above and below 1.0 ML coverage and interpolated to estimate the critical transition flux. An Arrhenius plot, shown in Fig. 1(b), demonstrates the single exponential behavior of both the 1.0 and 2.4 ML transition fluxes and the corresponding linear fits to extract the activation energies and attempt frequency prefactors. The temperature and flux dependent 1.0 ML formation flux was then superimposed on the Ga/GaN adsorption diagram. According to our measurements of Ga-adsorbate coverage corresponding uniquely to subcritical adsorption flux, a transition flux for any arbitrary coverage below 2.4 ML may be defined. We draw attention to the 1.0 ML coverage transition flux as a result of separate GaN growth experiments. The preliminary growth mode results have indicated that 1.0 ML coverage may mediate a transition in GaN growth mode. These results will be presented separately after further *in situ* QMS and RHEED experiments during GaN growth by PA-MBE.

IV. DISCUSSION AND CONCLUSIONS

The experimental results show the complementary nature of the information provided by the RHEED oscillations and the Ga-adlayer coverage measured by QMS. We have confirmed that steady-state Ga-adlayer coverages may be established below the critical impinging Ga flux necessary to form Ga droplets. The steady-state coverage dependence on adsorption time was directly observed by QMS and was consistent with the dependence of desorption time measured by QMS or RHEED. In principle, the correlation of desorption time with QMS-measured adlayer coverage, demonstrated at the substrate temperature of 678 °C in this work, could be used to estimate the Ga-adsorbate coverage at any substrate temperature. Below the critical Ga flux for Ga-droplet formation, the steady-state Ga-adlayer coverages increased continuously with impinging Ga flux. As demonstrated for the Ga-adsorbate coverage of 1.0 ML, the critical Ga flux corresponding to a specific Ga-adsorbate coverage up to 2.4 ML increased exponentially with substrate temperature. We have shown that each half period of RHEED specular reflection oscillation is associated with the corresponding (bottom) PM and (top) LC monolayers. This result confirms that the

RHEED specular intensity transients observed during adsorption and subsequent desorption are primarily due to the Ga-adsorbate bilayer.

We have argued that the discontinuous dependence of transient desorption time on increasing Ga flux is consistent with the continuously increasing Ga-adsorbate coverage due to the different desorption rates that have been measured for each monolayer.[17] Previous analyses of desorption time from RHEED specular reflection intensity transient oscillations have led to the conclusion that a 2.4 ML (complete bilayer) coverage may be established over a range of impinging Ga fluxes,[20] indicating a first order surface phase transition[24] between the Ga-adsorbate PM (1.0 ML) and LC (2.4 ML total Ga coverage) Ga-adsorbate phases. However, the QMS-measured Ga-adsorbate coverage has been found to increase monotonically with respect to impinging Ga flux from 0 to 2.4 ML, indicative of a continuous transition from 1.0 to 2.4 ML Ga-adsorbate coverage.[13,17,25] We propose that the large difference in adlayer desorption rates may be responsible for an error in coverage assessment exclusively based upon analysis of RHEED transients.

A. Relevance for GaN growth

These results are relevant in a detailed description of the evolution of Ga-adsorbate coverage and resultant GaN growth mode in the intermediate regime, where the excess Ga fluxes are intermediate to stoichiometric and Ga-droplet conditions, of the PA-MBE GaN growth diagram, in accordance with previous studies.[8,12,13,20] The existence of a continuous increase[24] in Ga-adsorbate surface coverage with increasing Ga flux does not exclude the possibility of a PA-MBE GaN "growth window" under excess Ga growth conditions, in which fluctuations from nominal temperature and flux values do not adversely affect growth morphology. However, we propose that several of the important details of the diffusion pathways for the Ga/GaN (0001) growth surface and excess constituent vapor pressures, as manifested in growth experiments[13] and theoretical investigation,[14] are different than in the case of previously characterized materials[26] grown by MBE.

In MBE, the expression *growth window* is typically used to refer to a regime in which the growth mode and surface structure are insensitive to variations in flux and substrate temperature. Although molecular beam epitaxy cannot be explained in simple terms, thermodynamics provides a useful frame of reference for predicting stable surface phases.[27] In the most common applications, epitaxial growth of GaAs (001) occurs at substrate temperatures and excess As flux such that the As-rich 2×4 reconstruction is observed.[28] The 2×4 reconstruction occurs over a range of As coverage from 0.31 to 0.53 ML equivalent coverage, and a continuous increase in As coverage occurs with increasing As flux up to ~ 0.5 ML when the $c(4 \times 4)$ reconstruction is observed.[29,30] In typical GaAs MBE growth at substrate temperatures of 500–650 °C, typical As fluxes are several orders of magnitude smaller than the As flux required to form As precipitates.[27] In addition, impinging As_2 molecules have a sticking coefficient of ~ 1 on exposed Ga adatoms on GaAs,

but the sticking coefficient is negligible for As_2 molecules impinging on the complete (2×4) reconstruction, providing a mechanism for self-limited As coverage at normal substrate temperatures during GaAs growth.[31]

The continuous morphology evolution of GaN commensurate with Ga flux variation and Ga-adsorbate coverage may be related to some of the important differences in surface kinetic mechanisms in comparison of GaAs (001) and GaN (0001) surfaces. Under As-rich 2×4 GaAs (001) growth, Ga adatom surface diffusion has an apparent measured[32] and theoretical[33] activation energy of 1.3–1.5 eV. The As_2 molecules have been observed to diffuse with lower activation energy[31] of 0.25 eV, but the As_2 dissociation activation energy required for incorporation[34] is around 1.4 eV. In the case of GaN, as demonstrated by the two limiting cases of zero Ga-adsorbate coverage and full bilayer plus droplets, two different surface diffusion pathways have been proposed.[14,15] The lowest known activation energy barrier for N diffusion exists inside the bilayer, between the PM and LC monolayers. We speculate that the rapid Ga-adsorbate domain diffusion that has been observed by STM measurements[18] may lead to an averaging effect of diffusion mediation corresponding to Ga-adsorbate coverage of less than 2.4 ML. Domains of the LC phase that rapidly diffuse on top of the PM adlayer on the GaN growth surface could give rise to locally modulated surface diffusivity during growth. Under the assumption that LC domains may diffuse much more rapidly than N adatoms, this effect could give rise to a composite N-adatom surface diffusion that corresponds to LC occupation when the total surface coverage is between 1.0 and 2.4 ML. This proposed mechanism is consistent with the Ga-adsorbate coverage results presented here that show that coverage may increase systematically with impinging Ga flux, thereby increasing the local N diffusion length on the growth surface. It is also possible that further theoretical investigation of the Ga adlayer may find that intermediate barrier diffusion pathways exist, for example, on or through the PM monolayer.

Our previous experiments and current investigation of the Ga adsorbate are consistent with the absence of an intermediate GaN growth regime where the surface morphology may be invariant with respect to small variations in flux. However, with accurate flux calibration and QMS and RHEED *in situ* monitoring techniques, we note several routes for improved uniformity of growth of GaN by PA-MBE. With precision flux control, Ga-droplet density and surface pit density may be simultaneously minimized.[13] As mentioned in the discussion of experimental techniques, we propose that the most direct method for monitoring flux ratios and growth temperature is the QMS measurement of steady-state desorption Ga-flux during growth. Another route that has been demonstrated is the intentional modulation of the Ga flux, making use of two Ga effusion cells with Ga flux above and below the droplet formation flux, to achieve a net flux that is just below the droplet formation flux to obtain smooth GaN surfaces without droplets.[35] Finally, we suggest that it may be possible to grow under conditions of complete bilayer coverage and unstable droplet size. Classical nucleation and growth theory predict a balance between surface

energy and volume energy that results in a minimum (critical) nucleus volume, whereas droplets of supercritical volume may decrease their free energy with further volume increase.[36] Theoretical consideration of critical Ga-droplet volume and kinetic stability with respect to Ga vapor and substrate temperature could form the basis for GaN growth approaches that maximize adatom diffusion and minimize Ga-droplet formation.

[1] S. Rajan, P. Waltereit, C. Poblenz, S. J. Heikman, D. S. Green, J. S. Speck, and U. K. Mishra, IEEE Electron Device Lett. **25**, 247 (2004).

[2] C. Skierbiszewski *et al.*, Appl. Phys. Lett. **86**, 011114 (2005).

[3] C. R. Elsass, Jpn. J. Appl. Phys., Part 2 **39**, L1023 (2000).

[4] Y. Nanishi, Y. Saito, and T. Yamaguchi, Jpn. J. Appl. Phys., Part 1 **42**, 2549 (2003).

[5] I. P. Smorchkova, Appl. Phys. Lett. **76**, 718 (2000).

[6] I. P. Smorchkova *et al.*, J. Appl. Phys. **90**, 5196 (2001).

[7] F. Bernardini, V. Fiorentini, and D. Vanderbilt, Phys. Rev. B **56**, R10024 (1997).

[8] B. Heying, R. Averbeck, L. F. Chen, E. Haus, H. Riechert, and J. S. Speck, J. Appl. Phys. **88**, 1855 (2000).

[9] E. J. Tarsa, B. Heying, X. H. Wu, P. Fini, S. P. DenBaars, and J. S. Speck, J. Appl. Phys. **82**, 5472 (1997).

[10] B. Heying, E. J. Tarsa, C. R. Elsass, P. Fini, S. P. DenBaars, and J. S. Speck, J. Appl. Phys. **85**, 6470 (1999).

[11] X. H. Wu *et al.*, Appl. Phys. Lett. **72**, 692 (1998).

[12] B. Heying, I. Smorchkova, C. Poblenz, C. Elsass, P. Fini, S. Den Baars, U. Mishra, and J. S. Speck, Appl. Phys. Lett. **77**, 2885 (2000).

[13] G. Koblmueller, J. S. Brown, R. Averbeck, H. Riechert, P. Pongratz, and J. S. Speck, Jpn. J. Appl. Phys., Part 2 **44**, L906 (2005).

[14] J. Neugebauer, T. K. Zywietz, M. Scheffler, J. E. Northrup, H. Chen, and R. M. Feenstra, Phys. Rev. Lett. **90**, 056101 (2003).

[15] T. Zywietz, J. Neugebauer, and M. Scheffler, Appl. Phys. Lett. **73**, 487 (1998).

[16] J. E. Northrup, J. Neugebauer, R. M. Feenstra, and A. R. Smith, Phys. Rev. B **61**, 9932 (2000).

[17] G. Koblmuller, R. Averbeck, H. Riechert, and P. Pongratz, Phys. Rev. B **69**, 035325 (2004).

[18] A. R. Smith, R. M. Feenstra, D. W. Greve, M. S. Shin, M. Skowronski, J. Neugebauer, and J. E. Northrup, J. Vac. Sci. Technol. B **16**, 2242 (1998).

[19] C. Adelmann, J. Brault, G. Mula, B. Daudin, L. Lymperakis, and J. Neugebauer, Phys. Rev. B **67**, 165419 (2003).

[20] C. Adelmann, J. Brault, D. Jalabert, P. Gentile, H. Mariette, G. Mula, and B. Daudin, J. Appl. Phys. **91**, 9638 (2002).

[21] C. Poblenz, T. Mates, M. Craven, S. P. DenBaars, and J. S. Speck, Appl. Phys. Lett. **81**, 2767 (2002).

[22] Temperature dependent QMS measurements of Ga partial pressure above GaN were carried out to estimate the rate of GaN decomposition into vacuum. At 716 °C, the GaN decomposition rate was 0.5 nm/min. Below 705 °C, the rate of GaN decomposition was below the detection limit of the QMS instrument (0.2 nm/min).

[23] W. Braun, *Applied RHEED: Reflection High-Energy Electron Diffraction During Crystal Growth* (Springer, Berlin, 1999), p. 219.

[24] M. E. Fisher, Rep. Prog. Phys. **30**, 615 (1967).

[25] G. Koblmuller, J. Brown, R. Averbeck, H. Riechert, P. Pongratz, and J. S. Speck, Appl. Phys. Lett. **86**, 041908 (2005).

[26] B. A. Joyce and D. D. Vvedensky, Mater. Sci. Eng., R. **46**, 127 (2004).

[27] J. Y. Tsao, *Materials Fundamentals of Molecular Beam Epitaxy* (Academic, San Diego, CA, 1992), p. 285.

[28] A. Y. Cho, J. Appl. Phys. **42**, 2074 (1971).

[29] C. Deparis and J. Massies, J. Cryst. Growth **108**, 157 (1991).

[30] J. R. Arthur, Surf. Sci. **43**, 449 (1974).

[31] C. T. Foxon and B. A. Joyce, Surf. Sci. **50**, 434 (1975).

[32] J. H. Neave, P. J. Dobson, B. A. Joyce, and J. Zhang, Appl. Phys. Lett. **47**, 100 (1985).

[33] A. Kley, P. Ruggerone, and M. Scheffler, Phys. Rev. Lett. **79**, 5278 (1997).

[34] C. G. Morgan, P. Kratzer, and M. Scheffler, Phys. Rev. Lett. **82**, 4886 (1999).

[35] C. Poblenz, P. Waltereit, and J. S. Speck, J. Vac. Sci. Technol. B **23**, 1379 (2005).

[36] J. W. Christian, *The Theory of Transformations in Metals and Alloys: An Advanced Textbook in Physical Metallurgy*, 2nd ed. (Oxford, New York, 1981).

Quadrupole mass spectrometry desorption analysis of Ga adsorbate on AlN (0001)

Jay S. Brown and Gregor Koblmüller
Materials Department, University of California, Santa Barbara, California 93106-5050

Robert Averbeck and Henning Riechert
Infineon Technologies AG, Corporate Research Photonics, D-1730 Munich, Germany

James S. Speck[a)]
Materials Department, University of California, Santa Barbara, California 93106-5050

The authors have investigated the adsorption and subsequent desorption of Ga on AlN (0001) with line-of-sight quadrupole mass spectrometry (QMS). The authors present desorption data consistent with a continuous Ga-flux dependent accumulation of a laterally contracted Ga bilayer on AlN (0001) from 0 to 2.7 ± 0.3 ML GaN equivalent coverage, and further Ga accumulation in macroscopic Ga droplets. The temperature dependence of Ga-adsorbate QMS desorption transients was investigated and the authors determined that the desorption activation energies for individual monolayers of the Ga adsorbate on AlN (0001) were similar to Ga desorption from GaN (0001). For the (first) pseudomorphic Ga-adsorbate monolayer on AlN, the authors measured a maximum Ga coverage of 1.0 ± 0.1 ML and desorption activation energy of 6.2 ± 0.3 eV. For the (second) laterally contracted Ga monolayer (1.7 ± 0.3 ML) the desorption activation energy was 3.8 ± 0.1 eV. © *2006 American Vacuum Society.* [DOI: 10.1116/1.2338554]

I. INTRODUCTION

High Al-content III-nitride semiconductor heterostructures have been the subject of intense study due to a variety of applications such as ultraviolet III-nitride light emitting diodes,[1–3] as well as GaN-based high electron mobility transistors.[4,5] Improved fundamental understanding of the growth of AlN by rf plasma assisted molecular beam epitaxy (PA-MBE) is necessary for further improvement of interfaces in heterostructures.[6,7] Under conditions similar to AlN growth by MBE, the stability of a laterally contracted Al bilayer has been predicted by first principles calculations and directly observed by scanning tunneling microscopy.[8,9] In both Ga/GaN (Ref. 10) and Al/AlN,[8] the first monolayer of adsorbate metal has been proposed to be pseudomorphic to the underlying wurtzite structure and the second metal adsorbate monolayer has been found to be laterally contracted (LC) with GaN (AlN) equivalent coverage of 1–2 ML. In the case of Ga/GaN, the LC monolayer has been found to be an incommensurate fluid with respect to the underlying substrate at temperatures above 200 °C, while the Al adsorbate retains hexagonal symmetry and shows surface reconstructions at growth temperatures (up to 850 °C).[9] Under conditions similar to GaN homoepitaxy by PA-MBE, calculations of N diffusion on the bare GaN (0001) surface and within the Ga-adsorbate bilayer have indicated that the Ga-adsorbate bilayer provides a lower energy barrier to surface diffusion.[11] Recent experiments, using line-of-sight quadrupole mass spectrometry (QMS), have demonstrated a continuously increasing Ga-adsorbate coverage[12,13] and improved surface morphology[14,15] for GaN growth with increasing Ga flux.

During AlN-based GaN heterostructure growth by PA-MBE, GaN quantum wells (QWs) or quantum dots (QDs), the presence of a Ga adsorbate on the AlN surface during GaN growth initiation has been recognized as crucial in the mediation of growth mode and adatom surface mobility.[16] The presence of a dynamically stable Ga adlayer on AlN during GaN growth was reported to result in step-flow morphology and to prevent the partial elastic relaxation during Stranski-Krastanov (SK) transition, which provided a viable route to QW growth.[17] In the growth of GaN QDs on AlN (0001) by PA-MBE, further reports have clarified the importance of excess Ga flux in determining GaN growth mode on AlN. Under N-rich growth conditions, the initial GaN growth mode on AlN was found to be layer by layer, and the SK transition occurred after 2–3 ML GaN deposition, consistent with previous reports of the SK growth mode in other material systems.[18] However, under Ga-rich flux conditions, desorption of the Ga adsorbate preceded the SK transition, which has been referred to as "Ga-autosurfactant modified" SK GaN growth.[17,19] A comparison of the size and density for both types of GaN QDs, grown under SK (Ref. 8) and modified SK (Refs. 17 and 19) conditions, is consistent with reduced adatom mobility under zero Ga-adsorbate coverages as compared to finite coverages (2–3 ML) predicted by the theory.[11] Under modified SK (Refs. 17 and 19) conditions, GaN QDs are relatively larger and of lower areal density[12] than GaN QDs grown under conventional SK (Ref. 18) conditions.

In light of recent experiments[12–15] and the importance of the Ga adsorbate in the mediation of GaN growth on AlN,[16–19] we have investigated the structure and kinetics of the Ga adlayer on AlN (0001) by performing Ga adsorption

a)Electronic mail: speck@mrl.ucsb.edu

with AlN (0001) substrate temperatures similar to those used during PA-MBE growth of GaN/AlN heterostructures. In the following sections, we present experimental evidence for the presence of a LC Ga adlayer on AlN (0001).

II. EXPERIMENT

In this work, growth of AlN (0001) on SiC and subsequent Ga adsorption experiments were carried out in a VH80 (VG Semicon) reactor equipped with standard Ga and Al effusion cells and radio frequency plasma source (EPI). The substrate temperature was controlled by thermocouple located inside the substrate heater. The wafer surface temperature was monitored directly by a normal incidence emissivity corrected (0.63) pyrometer with maximum sensitivity at 940 nm. Routine growth of GaN by PA-MBE under excess metal conditions results in a gradual accumulation of metal on the pyrometer window and leads to observable pyrometer temperature changes, depending on growth temperatures and excess fluxes, because of absorption losses. Prior to the adsorption experiments described below, we calibrated the pyrometer temperature response by comparison of the substrate temperature at Ga-droplet formation for known Ga flux.[12,20] All pyrometer temperatures reported in this work are based upon the calibration of pyrometer response at 743 °C, 20 nm/min Ga flux.[12]

The group-III fluxes were measured by cross sectional scanning electron microscopy (SEM) imaging of metal flux-limited 1–2 μm films grown on SiC. The SEM growth rate measurements were used to calibrate the beam flux monitor (ion gauge) measurements, and we calibrated the fluxes to effusion cell temperature prior to all measurements.

We calibrated the linear response of the line-of-sight QMS detector by adsorption of Ga fluxes (1–30 nm/min) on a 50.8 mm diameter sapphire wafer at a temperature of 804 °C. As previously described,[12,13] Ga adatoms have a negligible surface residence time under these adsorption conditions and we observed steady-state desorption Ga fluxes that were directly dependent on incident Ga flux.[12,13]

As previously described, ~225 nm AlN (0001) was grown by PA-MBE on 50.8 mm diameter 6H-SiC (0001) wafers under Al-rich intermediate (3.25 nm/min Al flux) conditions at 784 °C, with N-limited AlN growth rate of 2.5 nm/min.[21] After AlN growth, the excess Al was consumed by exposure to N flux for 15 min at 784 °C. During exposure to the N flux, the AlN surface was monitored by the reflection high energy electron diffraction (RHEED) specular intensity, and evolution of the two-dimensional diffraction pattern.[22] In general, the AlN RHEED pattern intensity increased and became more diffuse during N-flux exposure, indicative of the incorporation of excess Aluminum.

Two classes of Ga adsorption experiments on AlN (0001) were performed by changing the incident Ga flux with fixed substrate temperature and by changing the substrate temperature with fixed Ga incident flux. These studies were designed to follow the analysis of Ga on GaN (0001) and GaN (000$\bar{1}$) by Koblmüller *et al.*[13]

A. Variable Ga-flux adsorption on AlN (0001)

The incident Ga flux was varied from 1 to 20 nm/min, with 30 s Ga adsorption with each Ga flux at a substrate temperature of 672±2 °C. After each adsorption wetting pulse, the Ga shutter was closed to allow adsorbed Ga to desorb from the AlN (0001) surface under vacuum. The Ga effusion cell temperature was stabilized for at least 8 min prior to each wetting experiment.

B. Temperature dependence of Ga desorption from AlN (0001)

Adsorption on AlN (0001) with a Ga flux sufficient for Ga droplet formation[20] with substrate temperatures in the range of 634–704 °C, with incremental temperature changes of 5±1 °C was performed. In each case, a total Ga fluence of 8 ML was deposited with a Ga flux of 3.9 nm/min (0.25 ML/s). The substrate temperature was stabilized for 4 min after complete desorption of the Ga adsorbate from the AlN (0001) surface under vacuum prior to each adsorption experiment. This experiment was used to assess the temperature variation of the mean adatom lifetimes according to the bilayer desorption model presented for Ga on GaN (0001).[13]

III. RESULTS

A. Variable Ga-flux adsorption on AlN (0001)

We first discuss the salient features of an individual Ga adsorption wetting pulse on AlN (0001) at 672 °C. Distinct time intervals of the temporal Ga-desorption flux were integrated to determine the Ga-adsorbate coverage on AlN (0001), in accordance with the LC Ga bilayer desorption characteristic that has been observed on GaN (0001).[13] We compared the saturation of desorption Ga flux with respect to incident Ga flux to the case of Ga-droplet desorption on GaN (0001), and we attribute the steady-state desorption flux after Ga adsorption on AlN (0001) to Ga-droplet desorption.

Typical QMS data are shown in Fig. 1 a for 30 s Ga adsorption with 6 nm/min incident flux on AlN (0001). The initiation of Ga adsorption is evidenced by an abrupt increase in desorption Ga flux from the detection limit to an adsorption steady state. After the Ga shutter was closed, the steady-state Ga desorption flux provided a direct indication that Ga droplets were formed on the surface during adsorption.[12,13] The steady-state desorpiton of Ga under vacuum is consistent with adsorption from the two-dimensional adsorbate surface, which is maintained near full coverage by diffusion from a Ga-droplet reservoir, as shown schematically in Fig. 2(a). For comparison, a 1 nm/min Ga-flux adsorption pulse is depicted in Fig. 1(b), in which Ga droplets did not form and immediate desorption flux decay was observed after Ga-shutter closure, as shown in the schematic for PM monolayer desorption in Fig. 2(d).

Assessment of Ga-adsorbate coverage corresponding to incident Ga flux was realized by integration of QMS data as indicated by the shaded and hatched regions in Fig. 1. Similar to the case of the Ga-adsorbate accumulation on GaN (0001),[12,13] the total Ga-adsorbate coverage on AlN (0001),
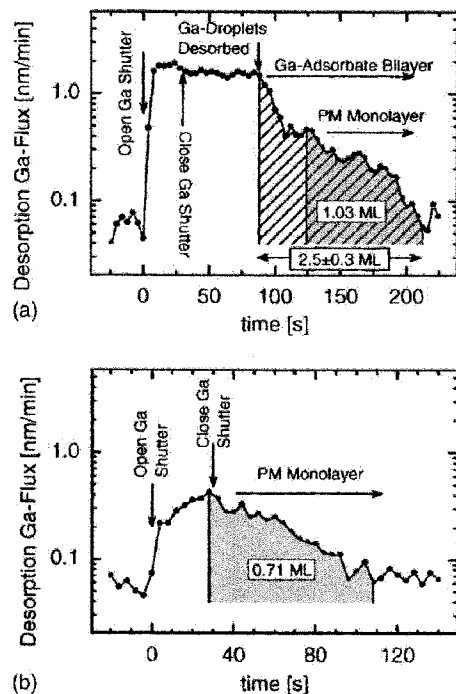
FIG. 1. Typical line-of-sight quadrupole mass spectrometry desorption flux measurements of ^{69}Ga during and after 30 s Ga adsorption on AlN (0001) with substrate temperature of 672 ± 2 °C. The hatched and shaded regions indicate integration of desorption Ga flux for the determination of the LC and PM monolayer coverages, respectively. (a) Adsorption with 6 nm/min Ga flux. Subsequent steady-state Ga-droplet desorption and a 2.46 ML Ga bilayer. (b) Adsorption with 1 nm/min Ga flux. Subsequent desorption of an incomplete PM monolayer, 0.71 ML Ga-adsorbate coverage.
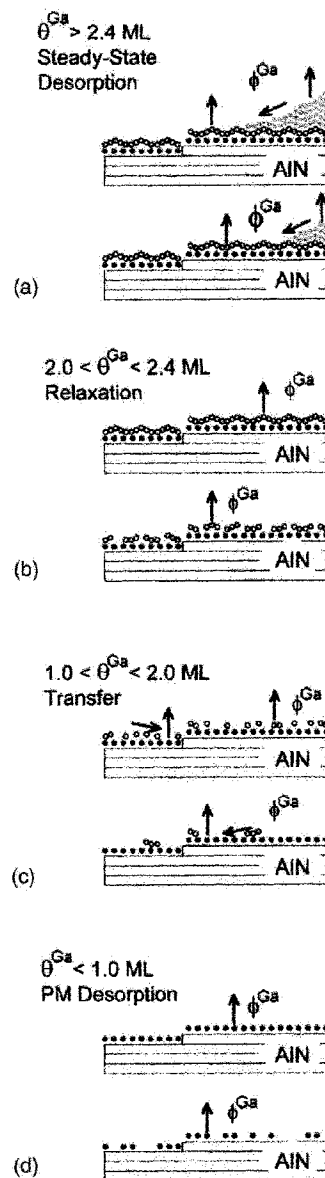

FIG. 2. Desorption schematic sequence of adsorbed Ga droplets and Ga bilayer on AlN (0001) [see Ref. 13 for further details regarding Ga on GaN (0001) surfaces]. Black circles represent Ga atoms in the PM monolayer, open circles represent Ga atoms in the LC monolayer, and solid gray circles represent Ga atoms in liquid droplets. (a) Steady-state desorption is observed while Ga droplets remain on the surface and the total adsorbate coverage is greater than ~2.4 ML. Desorption flux is dominated by the LC Ga-adsorbate monolayer, and the Ga droplets maintain the LC monolayer at full coverage via surface diffusion. (b) In the *relaxation* stage, the total Ga-adsorbate coverage is between ~2.4 and 2.0, the desorption flux evidences exponential decay from the steady-state level while desorption is dominated by the LC monolayer. (c) During the *transfer* stage, the total Ga-adsorbate coverage is between 2.0 and 1.0, the desorption flux is momentarily at a steady-state level while the PM monolayer is maintained at 1.0 ML by surface diffusion from the LC monolayer. (d) When the total coverage is 1.0 ML, the desorption flux from the PM monolayer decays exponentially to the background detection limit.

determined by integration of desorption Ga flux after the Ga shutter was closed, was observed to continuously increase with increasing incident Ga flux (Fig. 3). For all desorption Ga-flux transients with Ga fluxes greater than 2.5 nm/min resulting in Ga-adlayer completion and Ga-droplet formation at 672 °C, we integrated the desorption flux from the onset of desorption transient decay (nearest data point) which resulted in an Ga-adsorbate coverage of 2.7 ± 0.3 ML. As shown in Fig. 3, it is apparent that the measured decay coverage increased minimally beyond the critical Ga flux for Ga-droplet formation. We note that near the critical Ga flux (2.5 nm/min) the integrated decay coverage was found to be in the range of 1.99–2.46 ML, an average of 2.2 ± 0.2 ML, which is close to the predicted Ga bilayer on GaN coverage of 2.33 ML.[10] Sources of error in our measurements include the time resolution of QMS data (4 s), the ambiguity of determining the point of desorption flux decay in several instances, and nonuniformity across the wafer surface due to temperature and flux distribution. These sources of error are consistent with the large standard deviation (0.3 ML) obtained for the dataset of all decay coverages. It is also plausible that (unintentional) AlN roughness could have contributed to a higher than expected total bilayer coverage. However, previous experiments with Ga adsorption from GaN has indicated that GaN roughness was not a significant source of error in adsorbate coverage measurements.[13]

For each incident Ga-flux adsorption experiment, specific intervals of the distinct three-stage transient decay of desorption Ga flux were integrated as indicated in Fig. 1 to determine the Ga-adsorbate coverage corresponding to the three-
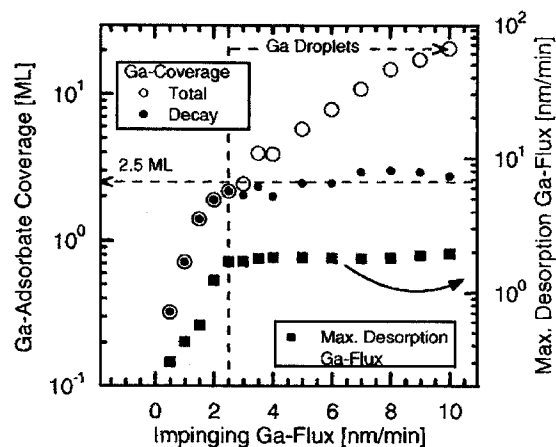
FIG. 3. Dependence of the total decay (two dimensional) Ga coverage, and maximum Ga desorption flux on the incident Ga flux from AlN (0001) (672 °C substrate temperature).

FIG. 4. Representative line-of-sight quadrupole mass spectrometry desorption flux measurements of ^{69}Ga during and after 8 ML Ga adsorption on AlN (0001). The solid and dashed lines indicate integration intervals of the total desorption transient used for determination of mean adatom lifetime (inset) for the LC and PM desorption Ga adsorbate phases, respectively. (a) Adsorption with 687 °C substrate temperature. (b) Adsorption with 659 °C substrate temperature.

stage model for bilayer desorption.[13] In the analysis of Ga on GaN, up to a measured Ga adsorbate coverage of 1.0 ML, a single exponential (linear on semilog scale) desorption flux decay was observed,[23] which was attributed to the desorption of a pseudomorphic monolayer (PM) on GaN (0001) as shown in Fig. 2(d).[13] Similarly, for Ga on AlN (0001), we integrated the desorption Ga flux for time intervals corresponding to the final single exponential flux decay for all of the variable Ga-flux adsorption experiments and determined the Ga-adsorbate coverage to be 1.0±0.1 ML, similar to the PM monolayer in the Ga bilayer on GaN (0001).[13]

As shown in Fig. 3, the maximum steady-state Ga desorption flux increased with increasing incident Ga flux, up to the incident Ga flux at which the Ga droplets formed, approximately 2.5 nm/min. This saturation point corresponded to the Ga flux at which the Ga-adsorbate coverage reached 2.2±0.2 ML. As shown in Fig. 3, the Ga-adsorbate coverage of the transient desorption flux decay, indicated by the hatched region in Fig. 1, did not increase significantly with respect to experimental error for all incident Ga fluxes above 2.5 nm/min. These results are consistent with the Ga adsorption and accumulation of a bilayer (2.2±0.2 ML) and Ga droplets on GaN (0001).[13]

At the 672±2 °C substrate temperature in the variable Ga-flux study on AlN (0001), the observed Ga-droplet desorption flux saturation value, 1.55±0.07 nm/min, was consistent with a substrate temperature of 668–669 °C predicted by the Ga/GaN adsorption diagram, based upon the assumption that the saturation desorption flux corresponds to the maximum surface desorption flux.[12,20] This agreement provides an independent validation of our previously described pyrometer calibration at 743 °C, 20 nm/min Ga flux. We conclude that for total Ga coverage beyond the saturation of the two-dimensional 2.2±0.2 ML Ga-adsorbate phase, the bulk liquid Ga-droplet phase was formed on the surface as shown by the schematic in Fig. 2(a). The variable Ga-flux experimental results are consistent with the preliminary conclusion that the excess Ga on the AlN (0001) surface that is accumulated beyond the 2.2±0.2 ML bilayer is sub-
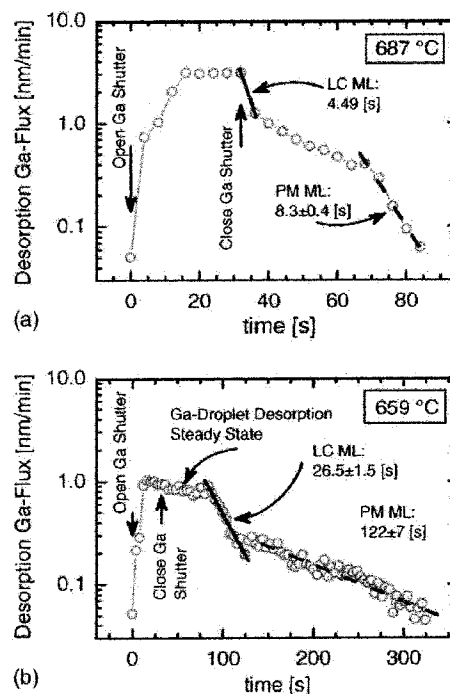
ject to its bulk liquid-Ga attraction, just as in the case of adsorbed Ga on GaN (0001).[12,13,20] The temperature dependent desorption kinetics, presented in the next section, help to further elucidate the similarities and differences between the desorption activation energies of the PM, LC, and Ga-droplet adsorbate phases on GaN and AlN (0001).

B. Temperature dependence of Ga desorption from AlN (0001)

Temperature dependent experiments were performed to determine an apparent desorption activation energy for each of the monolayers of the Ga bilayer on AlN (0001). As shown in Fig. 4 for two substrate temperatures, 687 and 659 °C, desorption transient intervals corresponding to the Ga adsorbate coverage attributed to the LC monolayer and the PM monolayer were linear on a logarithmic flux scale versus desorption time t. This observation is consistent with the Ga-adsorbate bilayer desorption process proposed for the laterally contracted Ga bilayer on GaN (0001),[13] as shown schematically in Fig. 2. In the proposed desorption model the Ga-droplet phase and the LC and PM monolayers are depleted sequentially via desorption and surface diffusion, and corresponding intervals of the desorption transients may be used to extract an apparent desorption activation energy for each phase of the adsorbate. The decay of LC and PM desorption rates of Ga on AlN (0001), similar to the case of Ga on GaN (0001), was consistent with exponential desorption
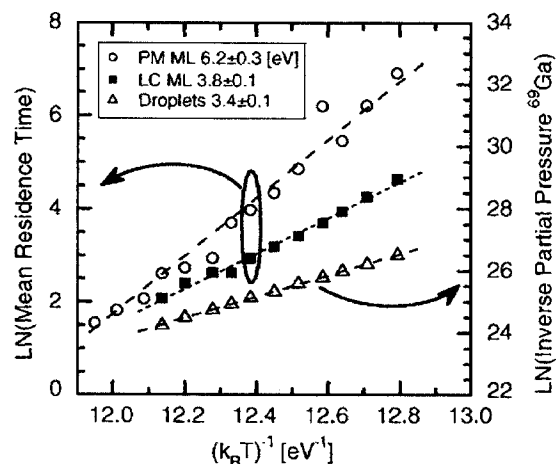
FIG. 5. Ga-adsorbate phase Arrhenius plots of mean adatom residence time and inverse partial pressure (proportional to inverse maximum Ga-desorption flux) used to determine the apparent desorption activation energies from temperature dependent line-of-sight quadrupole mass spectrometry measurements of Ga on AlN (0001).

rate processes, where the Ga surface population and total desorption flux is proportional to $\exp(-t/\tau_A)$. As indicated in Fig. 4, the mean adatom lifetimes τ_A were determine for both the LC and PM monolayers for each adsorption temperature. As previously described,[13] linear fits to Arrhenius plots of mean adatom lifetime versus thermal energy (Fig. 5) were used to determine apparent desorption activation energies E_A and desorption attempt prefactors v_0 for the PM and LC Ga-adsorbate adlayers on AlN (0001), based upon the application of the Frenkel equation[24] for the temperature dependence of adatom lifetime, $\tau_A=(v_0)^{-1}\exp(E_A/k_BT)$. The mean adatom lifetime for steady-state desorption processes, such as the steady-state desorption attributed to the Ga-droplet phase, was taken to be inversely proportional to the desorption Ga flux.[13] The Ga-droplet steady-state desorption is indicated in Fig. 4(b) and is also apparent in Fig. 1(a). In Fig. 5, the temperature dependence of the Ga-droplet inverse steady-state desorption Ga flux is shown, along with the measured Ga-droplet desorption activation energy on AlN (0001) of 3.4 ± 0.1 eV.

As shown in Fig. 5, we have measured increasing desorption activation energies for Ga-droplet phase of 3.4 ± 0.1 eV, LC monolayer of 3.8 ± 0.1 eV, and PM monolayer of 6.2 ± 0.3 eV, which compares favorably with the Ga adsorption on GaN (0001) results reported by Koblmüller *et al.*[13] The Ga-droplet desorption activation energy on GaN, determined from separate QMS measurements on different GaN surfaces, was found to be 3.1 ± 0.2.[13] The activation energy for the desorption of bulk liquid Ga has been reported to be 2.9 eV.[25] We note that in the case of relatively small Ga droplets on GaN or AlN surfaces, kinetic effects are likely to modify the activation energy from that observed from bulk Ga desorption. The LC monolayer desorption activation energy for Ga on GaN (0001) was found to be ~3.7 eV.[13] We note that while the LC and Ga-droplet activation energies for Ga on AlN (0001) are nearly the same as those for Ga on

GaN (0001) within experimental error, the PM monolayer desorption activation energy was found in this work to be significantly larger for the Ga adsorbate on AlN (0001).[13] In the next section, we discuss the similarities and differences between desorption kinetics for the Ga bilayer on both AlN and GaN (0001) surfaces.

IV. DISCUSSION

For the Ga-adsorbate PM monolayer on AlN (0001) we measured a maximum Ga coverage of 1.0 ± 0.1 ML and apparent desorption activation energy of 6.2 eV, that is greater than the 4.9 eV which was measured in the case of Ga on GaN (0001).[13] In contrast, the similar desorption activation energies for the LC Ga adlayer on both GaN and AlN (0001) are consistent with the conclusion that the Ga atoms within the LC monolayer are bound primarily to the Ga atoms in the PM monolayer.[10] This is in accord with the lateral contraction of the adlayer toward the bulk Ga lattice constant[10] and the corresponding observation of the higher atomic density, $(1.4)\pm0.3$ ML, in the LC adlayer on both surfaces. A similar argument may be made for the temperature dependent increase of Ga flux sufficient for Ga-droplet formation; in both GaN and AlN (0001) the Ga-droplet desorption activation energy is in the range of 3.1–3.4 eV. The activation energy for desorption in vacuum for bulk liquid Ga has been well established to be close to 2.9 eV over a wide range of temperatures.[25] In the present analysis of Ga on AlN (0001) we have applied a simplistic model for thermally activated desorption (single exponential behavior) to quantify the relative desorption behavior for the Ga-droplet phase and the LC and PM monolayers. This model may not be sufficient to describe the more detailed atomistic behavior, which is likely to be influenced by kinetic processes such as diffusion and multiple activation barriers to desorption.

V. SUMMARY AND CONCLUSIONS

We have demonstrated the presence of a laterally contracted (LC) Ga bilayer on AlN (0001) for substrate temperatures in the range of 634–704 °C. We have found that the phase-dependent desorption activation energies for the Ga adsorbate on AlN (0001) are similar to the Ga-adsorbate bilayer on GaN (0001), but that the first (PM) Ga-adsorbate monolayer is more tightly bound to the AlN surface than to the GaN surface. The conditions under which we have characterized the Ga bilayer on AlN (0001) are similar to GaN growth by PA-MBE, and we expect that enhanced surface diffusion of N adatoms[11] may be present during GaN growth on AlN.

We propose that the existence of a LC Ga bilayer on AlN (0001) has direct relevance for GaN heterostructure growth kinetics on AlN (0001) during PA-MBE, based upon previous results from experiment[13-15] and theory[11] for GaN growth. We have demonstrated that the Ga-adsorbate coverage may be controlled continuously from 0 to 2.7 ML, and we anticipate that this result could be used for the direct mediation of GaN growth kinetics during the Stranski-Krastanov transition of GaN on AlN (0001). Calculations of

the interfacial energy between several monolayers of GaN on AlN and a Ga bilayer could provide further insight into the Ga-adlayer mediated SK transition in GaN.

ACKNOWLEDGMENT

[1]A. J. Fischer *et al.*, Appl. Phys. Lett. **84**, 3394 (2004).

[2]K. Iida *et al.*, J. Cryst. Growth **272**, 270 (2004).

[3]C. G. Moe *et al.*, Jpn. J. Appl. Phys., Part 2 **44**, L502 (2005).

[4]L. Shen *et al.*, J. Electron. Mater. **33**, 422 (2004).

[5]S. Rajan, P. Waltereit, C. Poblenz, S. J. Heikman, D. S. Green, J. S. Speck, and U. K. Mishra, IEEE Electron Device Lett. **25**, 247 (2004).

[6]D. Jena, A. C. Gossard, and U. K. Mishra, Appl. Phys. Lett. **76**, 1707 (2000).

[7]D. Jena, I. Smorchkova, A. C. Gossard, and U. K. Mishra, Phys. Status Solidi B **228**, 617 (2001).

[8]C. D. Lee, Y. Dong, R. M. Feenstra, J. E. Northrup, and J. Neugebauer, Phys. Rev. B **68**, 205317 (2003).

[9]R. M. Feenstra, Y. Dong, C. D. Lee, and J. E. Northrup, J. Vac. Sci. Technol. B **23**, 1174 (2005).

[10]J. E. Northrup, J. Neugebauer, R. M. Feenstra, and A. R. Smith, Phys. Rev. B **61**, 9932 (2000).

[11]J. Neugebauer, T. K. Zywietz, M. Scheffler, J. E. Northrup, H. Chen, and R. M. Feenstra, Phys. Rev. Lett. **90**, 056101 (2003).

[12]J. S. Brown, G. Koblmuller, F. Wu, R. Averbeck, H. Riechert, and J. S. Speck, J. Appl. Phys. **99**, 074902 (2006).

[13]G. Koblmuller, R. Averbeck, H. Riechert, and P. Pongratz, Phys. Rev. B **69**, 035325 (2004).

[14]G. Koblmueller, J. S. Brown, R. Averbeck, H. Riechert, P. Pongratz, and J. S. Speck, Jpn. J. Appl. Phys., Part 2 **44**, L906 (2005).

[15]G. Koblmuller, J. Brown, R. Averbeck, H. Riechert, P. Pongratz, and J. S. Speck, Appl. Phys. Lett. **86**, 041908 (2005).

[16]G. Mula, C. Adelmann, S. Moehl, J. Oullier, and B. Daudin, Phys. Rev. B **64**, 195406 (2001).

[17]C. Adelmann, N. Gogneau, E. Sarigiannidou, J. L. Rouviere, and B. Daudin, Appl. Phys. Lett. **81**, 3064 (2002).

[18]C. Adelmann, B. Daudin, R. A. Oliver, G. A. D. Briggs, and R. E. Rudd, Phys. Rev. B **70**, 125427 (2004).

[19]N. Gogneau, D. Jalabert, E. Monroy, T. Shibata, M. Tanaka, and B. Daudin, J. Appl. Phys. **94**, 2254 (2003).

[20]B. Heying, R. Averbeck, L. F. Chen, E. Haus, H. Riechert, and J. S. Speck, J. Appl. Phys. **88**, 1855 (2000).

[21]G. Koblmueller, R. Averbeck, L. Geelhaar, H. Riechert, W. Hosler, and P. Pongratz, J. Appl. Phys. **93**, 9591 (2003).

[22]J. Brown, F. Wu, P. M. Petroff, and J. S. Speck, Appl. Phys. Lett. **84**, 690 (2004).

[23]S. Guha, N. A. Bojarczuk, and D. W. Kisker, Appl. Phys. Lett. **69**, 2879 (1996).

[24]K. L. Chopra, *Thin Film Phenomena* (McGraw-Hill, New York, 1969).

[25]I. Barin, *Thermochemical Data of Pure Substances* (VCH, Weinheim, 1993).

In situ investigation of growth modes during plasma-assisted molecular beam epitaxy of (0001) GaN

G. Koblmüller[a)]
Materials Department, University of California, Santa Barbara, California 93106-5050, USA

S. Fernández-Garrido and E. Calleja
ISOM and Dpto. de Ingeniería Electrónica, Universidad Politécnica, 28040 Madrid, Spain

J. S. Speck
Materials Department, University of California, Santa Barbara, California 93106-5050, USA

Real-time analysis of the growth modes during homoepitaxial (0001) GaN growth by plasma-assisted molecular beam epitaxy was performed using reflection high energy electron diffraction. A growth mode map was established as a function of Ga/N flux ratio and growth temperature, exhibiting distinct transitions between three-dimensional (3D), layer-by-layer, and step-flow growth modes. The layer-by-layer to step-flow growth transition under Ga-rich growth was surfactant mediated and related to a Ga adlayer coverage of one monolayer. Under N-rich conditions the transition from 3D to layer-by-layer growth was predominantly thermally activated, facilitating two-dimensional growth at temperatures of thermal decomposition. © *2007 American Institute of Physics*. [DOI: 10.1063/1.2789691]

In recent years, the growth of high precision GaN-based structures for opto- and high-power microelectronic applications[1–3] was increasingly accomplished by the powerful growth technique of molecular beam epitaxy (MBE). Essentially, the development of growth surface diagrams[4,5] for the plasma-assisted (PA)MBE growth of (0001) GaN has become highly instrumental for identifying optimum growth regimes to produce device-quality GaN films. Within such growth regimes, the surface properties (roughness, morphology) were similar and given by two important growth parameters, i.e., Ga/N flux ratio and growth temperature.

Low Ga/N flux ratios (Ga/N < 1, N-rich growth regime) yielded overall heavily pitted and rough GaN surfaces.[5,6] Relatively smooth surfaces were acquired under Ga-rich conditions (Ga/N > 1), accentuated by a continuous reduction in surface pit density and growth planarization with increasing Ga flux.[6,7] Electron mobilities reached peak values under Ga-rich conditions near the limit for Ga droplet formation,[6] while impurity incorporation was reduced drastically.[8]

This enhancement in GaN material properties was interpreted by the existence of a stable Ga surface adlayer[5,9,10] and its strong impact on adatom diffusion[11,12] under Ga-rich conditions. Along its self-surfactant nature, the Ga adlayer was found to form steady-state coverages on the (0001) GaN surface, with values ranging from fractions of 1 ML to a 2.5-ML-thick bilayer depending on the excess Ga flux present during growth.[13]

Despite this progress, the exploration of the surface kinetics within the current GaN growth diagrams has been limited to temperatures below thermal decomposition (i.e., <750 °C). By encompassing the usually avoided temperature region far beyond 750 °C, we establish in this study the correlation between growth parameters and growth modes towards higher temperatures and provide a detailed growth mode map for the PAMBE growth of (0001) GaN.

The experiments were carried out in a Gen-II MBE system equipped with standard effusion cells for Ga and a Vecco Unibulb radio frequency plasma source for active nitrogen. As substrate we used a 2 in. (0001)GaN template grown by metal-organic chemical vapor deposition (MOCVD) on-axis (with surface vicinality defined <0.5°) on *c*-plane sapphire. The substrate temperature was measured by an optical pyrometer. Cross-sectional scanning electron microscopy of thick Ga- and N-limited GaN films grown at low temperatures (680 °C) was used to calibrate Ga and N fluxes in GaN growth rate units (nm/min).[4] 1 nm/min is equivalent to 0.064 ML/s, where 1 ML of GaN corresponds to $c/2 = 0.259$ nm or 1.14×10^{15} GaN/cm^2 areal density.

The growth mode and surface roughness were analyzed by monitoring the reflection high energy electron diffraction (RHEED) Bragg spot intensity along the $[11\bar{2}0]$ azimuth during homoepitaxial GaN nucleation experiments.[14,15] Simultaneous recording of the postgrowth Ga desorption by quantitative line-of-sight quadrupole mass spectrometry (QMS) allowed us to determine the Ga adlayer coverage. To calibrate the desorbing Ga flux in GaN-equivalent growth rate units, the response function of the QMS was measured by exposure of a sapphire wafer at 800 °C to known impinging Ga fluxes (1–20 nm/min) well below the limit for Ga droplet formation.[10,13] Note that all experiments were performed on a single GaN template and were reproducible during successive growths and surface recovery cycles.

Figure 1 shows the QMS-measured desorbing Ga flux (blue datapoints) and the RHEED intensity profile (black curves) during the 50 s long homoepitaxial GaN nucleation for different Ga fluxes at fixed N flux (4.8 nm/min) and temperature (700 °C). Growth was varied from the N-rich to the Ga-rich growth regime, yielding different QMS desorption profiles and Ga adlayer coverages. According to previous work,[13] the maximum Ga desorption during GaN nucleation was defined as the excess Ga flux desorbing from the surface. Under N-rich conditions, apparently no Ga desorption was measured, as the impinging Ga flux was entirely

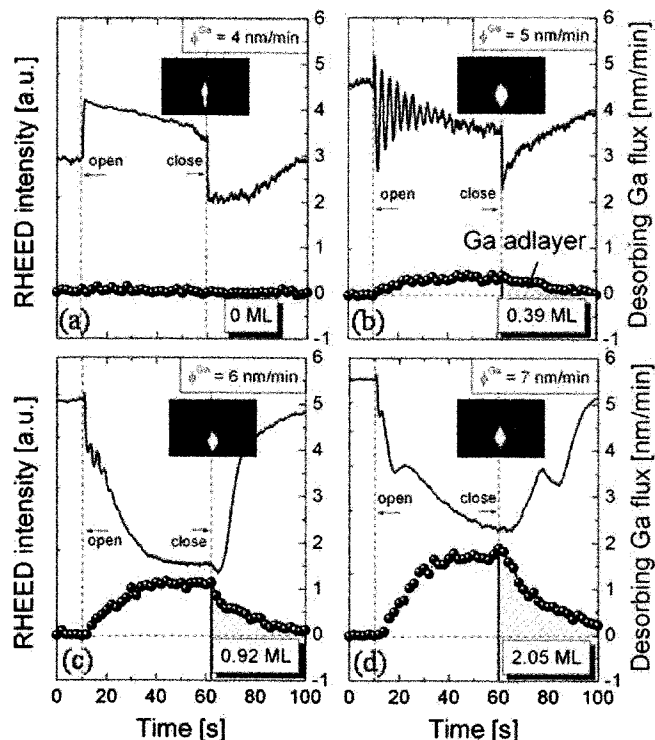[a)]Electronic mail: gregor@engineering.ucsb.edu

FIG. 1. (Color online) QMS-measured desorbing Ga flux and Ga adlayer coverages (blue curves and hatched areas) and RHEED intensity transients (black curves) during 50 s long homoepitaxial (0001) GaN nucleation on MOCVD-grown GaN templates at constant $T=700$ °C, $N=4.8$ nm/min, but variable Ga fluxes of (a) $\Phi^{Ga}=4$ nm/min, (b) $\Phi^{Ga}=5$ nm/min, (c) $\Phi^{Ga}=6$ nm/min, and (d) $\Phi^{Ga}=7$ nm/min. RHEED patterns of representative morphologies taken at the end of each experiment are shown as insets.
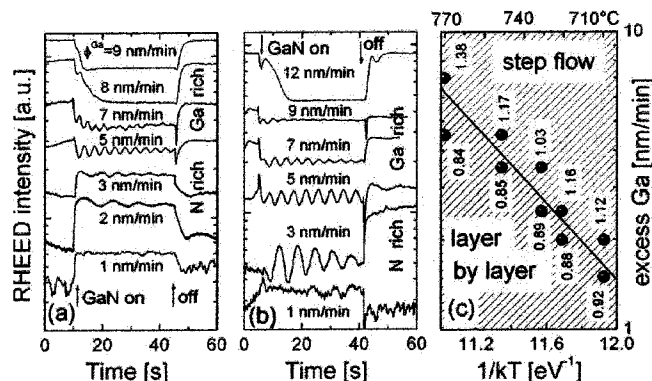

FIG. 2. (Color online) Ga flux dependent RHEED intensity transients during short GaN growth pulses on MOCVD-GaN templates at constant N flux (4.8 nm/min) and temperatures of (a) 750 °C and (b) 780 °C, showing 3D growth (black curves), layer-by-layer growth (blue curves), and step-flow growth (red curves). (c) Arrhenius plot of the boundary fluxes for the layer-by-layer to step-flow growth transition under Ga-rich growth. Note that each datapoint refers to the QMS-measured Ga adlayer coverage in units of ML.

consumed by nitrogen [Fig. 1(a)]. For Ga-rich growth [Figs. 1(b)–1(d)], the desorbing Ga flux increased and matched with the nominally expected excess Ga ($\Phi^{Ga}-\Phi^{N}$). This agreement holds only for moderate excess Ga fluxes, well below the critical Ga flux for droplet formation at the given temperature (i.e., $\Phi^{Ga}-\Phi^{N}\sim5$ nm/min at 700 °C).[4]

With increasing Ga flux, the Ga adlayer coverage, as determined by integration of the area below the desorbing Ga flux after each growth pulse (i.e., hatched areas),[13] increased steadily from 0 ML (N-rich growth) to more than a 2 ML thick Ga bilayer (Ga-rich). Error bars for these coverages are on the order of ±0.2 ML, resulting from the ~2 s time resolution of the QMS. We stress that these values present steady-state Ga coverages, independent of the growth time as far as steady-state growth and desorption was achieved.

In correlation with the Ga adlayer coverage, three different RHEED intensity transients were found and associated with three specific growth modes. Under the absence of the Ga adlayer (N-rich growth), the RHEED intensity showed no oscillatory behavior and decreased slightly during growth [Fig. 1(a)]. Concurrently, the RHEED pattern transformed from a streaky pattern (indicative of a smooth GaN template) to a pattern with slight intensity modulations towards the end of nucleation (typical for the onset of a roughening surface, see inset). These observations characterize the prevailing three-dimensional (3D) growth mode.[5,15]

For higher Ga adlayer coverages (0.39 and 0.92 ML, respectively), multiple intensity oscillations were observed [Figs. 1(b) and 1(c)], with their periodicity consistent with the N-limited GaN growth rate. These characteristics along with persistently streaky RHEED patterns are commonly at-

tributed to a two-dimensional (2D) layer-by-layer growth mode, describing the formation of single GaN monolayers.[14]

Note that the RHEED intensity oscillations were quickly damped for Ga adlayer coverages higher than 1 ML, resulting in only one or two lower-frequency oscillations (~3–6 s long) [Fig. 1(d)]. Such bioscillatory behavior at the onset and end of Ga-rich GaN growth was recently attributed to the layer-by-layer-like buildup and desorption of a Ga adlayer (bilayer) interfering with growth such that growth rate oscillations were obscured.[16,17] This transitory behavior was representative for the transition from 2D to one-dimensional (1D) step-flow growth mode.[14]

The RHEED intensity transients were further investigated for higher growth temperatures (750 and 780 °C), exhibiting distinct temperature dependencies of the transition Ga fluxes related with the two growth mode boundaries (Fig. 2). In specific, the 3D-to-layer-by-layer growth transition occurred at a boundary Ga flux of $\Phi^{Ga}\sim3$ nm/min at 750 °C and $\Phi^{Ga}\sim2$ nm/min at 780 °C, both well in the N-rich regime. For the layer-by-layer to step-flow growth transition this boundary Ga flux was much higher and in the Ga-rich regime, i.e., $\Phi^{Ga}\sim7.5$ nm/min at 750 °C and $\Phi^{Ga}\sim11$ nm/min at 780 °C.

Analysis of RHEED transients over a wider temperature range (680–780 °C) yielded more systematic data. With increasing temperature the 3D to layer-by-layer growth transition increased further into the N-rich growth regime (i.e., towards higher excess N fluxes). This demonstrates that at higher temperatures N-rich growth may lead to smooth layer-by-layer growth despite the absence of the Ga adlayer (i.e. no indication of pseudo-oscillatory RHEED transients at the end of each growth pulse). Indeed, we confirmed sustainable layer-by-layer growth with streaky RHEED patterns up to thicknesses larger than 0.5 μm, especially when growth conditions were selected further away from the transition boundary to 3D growth, i.e., moderately N-rich ($0.4<Ga/N<1$) and higher temperatures ($T>750$ °C).

Similarly, the boundary Ga fluxes defining the layer-by-layer to step-flow growth transition increased also with temperature with a clear Arrhenius dependency [Fig. 2(c)]. Following the procedure of Fig. 1, we determined for each boundary Ga flux (below and above the growth transition) at each temperature the absorbed Ga adlayer coverage by QMS,
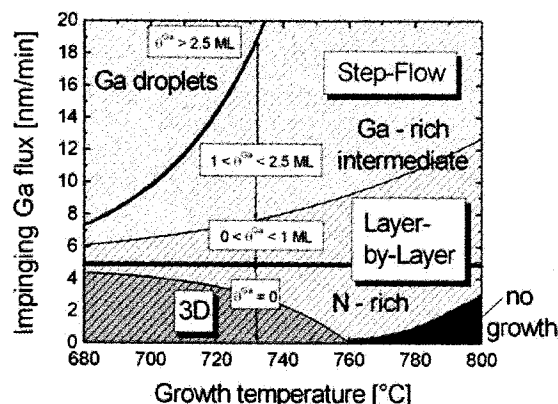
FIG. 3. (Color online) Summarized map of the growth modes as a function of Ga flux and growth temperature for constant N flux (4.8 nm/min) on on-axis (<0.5° surface vicinality) (0001) GaN, highlighting the interrelation with the three standard GaN growth regimes (Refs. 4 and 5: N-rich, Ga-rich intermediate and Ga-rich droplets) and Ga adlayer coverages.

as indicated for each data point. We concluded that a steady-state adlayer coverage of approximately 1 ML must be associated with this growth mode transition. Fits were made to the data separating the boundary Ga fluxes for each temperature, which resulted in an apparent activation energy of 1.45 ± 0.2 eV. This suggests that the processes involved with this transition are related to substantial increases in surface diffusion at Ga coverages >1 ML.

Both growth mode boundaries and their relation to the Ga adlayer coverage are summarized in the growth mode map of Fig. 3. With respect to the three characteristic growth regimes (N-rich, Ga-rich intermediate and Ga-rich droplets) defining the standard PAMBE growth diagram of GaN,[4,5] the present map highlights in particular the dependence of growth mode on impinging Ga flux and temperature, including regions of GaN thermal decomposition (>750 °C). We note that this map holds only for the given N flux (i.e., 4.8 nm/min) and the slight (<0.5°) surface vicinality of the given (0001) GaN template. Variations in these two parameters are expected to shift the transition boundaries of the growth modes, as they are crucially dependent on deposition rate (i.e., supplied N flux), surface diffusion rate and the nucleation of atomic steps on the surface. Such a map provides therefore not only a guide for the growth of high-quality GaN films but also substantial information about surface diffusion and island formation mechanisms.

The current manifestation of 3D growth under N-rich conditions[4,5] seems to break down for high temperature growth, where thermal decomposition comes into play (>750 °C). Under these conditions, the RHEED intensity oscillations indicated that the thermally activated diffusion seemed fast enough to produce higher adatom mobilities and layer-by-layer growth, as was recently observed even at moderate temperatures below the onset for decomposition.[5] However, in Ref. 5 layer-by-layer growth was unsustainable over time resulting in 3D growth, eventually due to insufficient surface diffusion or limitations of the rather narrow layer-by-layer growth region at these lower temperatures.

Utilizing temperatures of thermal decomposition, we assume that surface diffusion may be further enhanced by the reevaporating Ga atoms, which adsorb with possibly finite surface lifetimes as Ga adatoms and which migrate readily

over the generally N-rich GaN surface. This would yield reduced effective N surface coverages, which in turn may cause a strong decrease in Ga diffusion barrier according to theoretical calculations.[11] Such reduced nitrogen coverage and enhanced surface diffusivity during the competitive growth and decomposition processes have been recently also reported for the PAMBE growth of InN,[18] emphasizing the feasibility of high-quality group-III nitride growth by PAMBE under N-rich conditions. However, this scenario holds only for conditions, where the rate of GaN formation is larger than the rate of thermal decomposition. For insufficient Ga fluxes (i.e., <1 nm/min at 780 °C) GaN formation may be completely suppressed and thermal etching of the GaN surface may result in roughened surfaces.

The second important boundary defining the layer-by-layer to step-flow growth transition underlies a much stronger influence of surfactant mediated diffusion, given by the critical Ga adlayer of 1 ML. This is in accordance with similar observations of layer-by-layer to step-flow growth mode transitions identified between different Ga-rich growth regimes.[5] All these results agree favorably with the well known autosurfactant effect and the significant reduction in the Ga and N adatom diffusion barriers for Ga adlayer coverages >1 ML [$E^A = 0.4$ eV (Ga) and 0.9 eV (N)], as compared to dry GaN surfaces [$E^A = 1.8$ eV (Ga) and 1.4 eV (N)] or GaN surfaces with a submonolayer coverage of Ga.[11,12]

[1]R. P. Vaudo, I. D. Goepfert, T. D. Moustakas, D. M. Beyea, T. D. Frey, and K. Meehan, J. Appl. Phys. **79**, 2779 (1996).
[2]H. Riechert, R. Averbeck, A. Graber, M. Schienle, U. Strauß, and H. Thews, Mater. Res. Soc. Symp. Proc. **449**, 149 (1997).
[3]S. Rajan, P. Waltereit, C. Poblenz, S. J. Heikman, D. S. Green, J. S. Speck, and U. K. Mishra, IEEE Electron Device Lett. **25**, 247 (2004).
[4]B. Heying, R. Averbeck, L. F. Chen, E. Haus, H. Riechert, and J. S. Speck, J. Appl. Phys. **88**, 1855 (2000).
[5]C. Adelmann, J. Brault, D. Jalabert, P. Gentile, H. Mariette, G. Mula, and B. Daudin, J. Appl. Phys. **91**, 9638 (2002).
[6]B. Heying, I. Smorchkova, C. Poblenz, C. Elsass, P. Fini, S. P. DenBaars, U. K. Mishra, and J. S. Speck, Appl. Phys. Lett. **77**, 2885 (2000).
[7]G. Koblmüller, J. Brown, R. Averbeck, H. Riechert, P. Pongratz, and J. S. Speck, Jpn. J. Appl. Phys., Part 2 **44**, L906 (2005).
[8]C. R. Elsass, T. Mates, B. Heying, C. Poblenz, P. Fini, P. M. Petroff, S. P. DenBaars, and J. S. Speck, Appl. Phys. Lett. **77**, 3167 (2000).
[9]A. R. Smith, R. M. Feenstra, D. W. Greve, M.-S. Shin, M. Skowronski, J. Neugebauer, and J. E. Northrup, J. Vac. Sci. Technol. B **16**, 2242 (1998).
[10]G. Koblmüller, R. Averbeck, H. Riechert, and P. Pongratz, Phys. Rev. B **69**, 035325 (2004).
[11]T. Zywietz, J. Neugebauer, and M. Scheffler, Appl. Phys. Lett. **73**, 487 (1998).
[12]J. Neugebauer, T. Zywietz, M. Scheffler, J. E. Northrup, H. Chen, and R. M. Feenstra, Phys. Rev. Lett. **90**, 056101 (2003).
[13]G. Koblmüller, J. Brown, R. Averbeck, H. Riechert, P. Pongratz, and J. S. Speck, Appl. Phys. Lett. **86**, 041908 (2005).
[14]N. Grandjean and J. Massies, Appl. Phys. Lett. **71**, 1816 (1997).
[15]B. Daudin and F. Widmann, J. Cryst. Growth **182**, 1 (1997).
[16]J. S. Brown, G. Koblmüller, F. Wu, R. Averbeck, H. Riechert, and J. S. Speck, J. Appl. Phys. **99**, 074902 (2006).
[17]C. Adelmann, J. Brault, G. Mula, B. Daudin, L. Lymperakis, and J. Neugebauer, Phys. Rev. B **67**, 165419 (2003).
[18]G. Koblmüller, C. S. Gallinat, and J. S. Speck, J. Appl. Phys. **101**, 083516 (2007).

High electron mobility GaN grown under N-rich conditions by plasma-assisted molecular beam epitaxy

G. Koblmüller,[a) F. Wu, T. Mates, and J. S. Speck
Materials Department, University of California, Santa Barbara, California 93106-5050, USA

S. Fernández-Garrido and E. Calleja
ISOM and Departamento de Ingeniería Electrónica, Universidad Politécnica, 28040 Madrid, Spain

An alternative approach is presented for the plasma-assisted molecular beam epitaxy of high-quality GaN. Under N-rich growth conditions, an unexpected layer-by-layer growth mode was found for a wide range of growth temperatures in the GaN thermal decomposition regime (>750 °C). Consequently, superior surface morphologies with roughness of less than 1 nm (rms) have been achieved. For lightly Si-doped GaN films, room-temperature electron mobilities exceeding 1100 cm^2/V s were measured, surpassing the commonly insulating nature of GaN grown under N-rich conditions at low temperature. © *2007 American Institute of Physics.*
[DOI: 10.1063/1.2817597]

Many recent advances in the device performance of GaN-based materials have been realized by the powerful technique of plasma-assisted molecular beam epitaxy (PAMBE). Unlike the MBE growth of conventional III/V semiconductors (GaAs, InP, etc.), optimum surface, structural, and electrical properties of PAMBE GaN are currently produced under group-III-rich, i.e., Ga-rich, conditions.[1,2] Under these conditions, it has been well established that a metallic Ga wetting layer (adlayer) exists on the surface[3,4] with many beneficial effects, such as increased surface adatom diffusion,[5,6] a two-dimensional (2D) growth mode,[7] and consequently smoother surface morphologies.[2,8,9] In contrast, N-rich conditions typically yield poor crystal quality characterized by heavily pitted surfaces, a tilted columnar structure with a high density of stacking faults.[10]

The use of Ga-adlayer stabilized growth conditions helped to further improve the electron mobilities by reducing the density of unintentional impurities and point defects.[11] To date, the best morphological and electrical transport properties [with room-temperature electron mobilities ~ 1100 cm^2/V s (Ref. 12) and ~ 800 cm^2/V s (Ref. 13)] were achieved for (0001) GaN films grown under a 2.5 ML thick Ga adlayer (bilayer) at temperatures in the range of 700–720 °C. This criterion denotes a critical boundary condition, where large Ga droplets accumulate and degrade the GaN device performance if the excess Ga flux exceeds this Ga bilayer limit.[2,4,8,9,12] Therefore, precise growth control of the Ga-rich growth conditions marginally below the Ga droplet boundary[14] has become a standard method to achieve high-quality GaN films. However, this poses great challenges due to nonuniformities in temperature control, (especially for large-area wafer growth), but also due to limitations in the available Ga flux necessary to sustain a complete Ga wetting layer at high growth temperatures (e.g., $T>740$ °C).

In this study, we circumvented these issues and present an entirely different approach for achieving high-quality (0001) GaN films by PAMBE by utilizing N-rich growth conditions at high temperatures of thermal decomposition [>750 °C (Refs. 15 and 16)]. The high growth temperatures were demonstrated to yield sufficiently high adatom mobili-

ties without a Ga adlayer, leading to 2D layer-by-layer growth, smooth films, and room-temperature electron mobilities in excess of 1100 cm^2/V s for light doping. This opened a promising growth window for high-quality GaN growth by PAMBE, bringing the growth kinetics closer to the other main epitaxial techniques, i.e., ammonia MBE or metal organic chemical vapor deposition.

As substrates, we used two types of (0001) GaN templates grown by metal-organic chemical vapor deposition (MOCVD) on c-plane sapphire: (i) highly resistive ($\sim 10^8$ Ω, Fe doped) ~ 4 μm thick standard GaN templates with threading dislocation (TD) densities specified to $\sim 5 \times 10^8$ cm^{-2} (Ref. 17), and (ii) unintentionally doped (UID) ~ 10 μm thick two-step epitaxial lateral overgrowth (ELO) GaN templates with an average TD density of $\sim 4 \times 10^7$ cm^{-2}.[18] The rather low dislocation densities of these templates are expected to limit the extent of dislocation induced electron scattering, allowing the realization of higher mobilities as compared to standard heteroepitaxial MBE GaN films with dislocation densities $>5 \times 10^9$ cm^{-2}.[19,20]

All GaN films were grown in a Gen-II MBE system using standard effusion cells for Ga, Mg, and Si and a Veeco AppliedEPI Unibulb radio frequency plasma source for supplying active nitrogen. A pyrometer was used to measure the substrate temperature *in situ*, which was calibrated by the melting point of Al (660 °C). The molecular fluxes are expressed in (0001) GaN growth rate units (nm/min), as measured by cross-sectional scanning electron microscopy of Ga-limited and N-limited GaN films at temperatures of negligible thermal decomposition.[2] In wurtzite GaN, $c/2 = 0.259$ nm or 1.14×10^{15} GaN/cm^2 areal density refer to 1 monolayer.

To electrically isolate the MOCVD-GaN template and to obviate the typical degenerate n-type region at the MBE-GaN/template interface, we deposited initially an isolation structure consisting of 200-nm-thick UID GaN, followed by a 50-nm-thick p-type GaN layer [doped with Mg at a concentration of $\sim 8 \times 10^{18}$ cm^{-3}, as determined by secondary ion mass spectrometry (SIMS)]. To maintain high crystalline

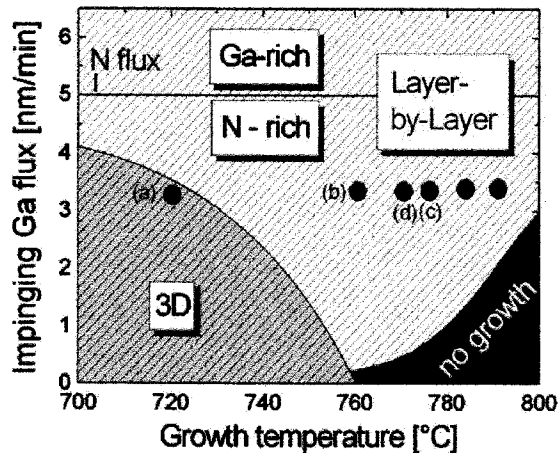a)Electronic mail: gregor@engineering.ucsb.edu.

FIG. 1. (Color online) (0001) GaN growth diagram describing the dependence of Ga flux and growth temperature on the growth regime (N rich vs Ga rich) and growth mode (3D vs 2D layer-by-layer growth). Note that under low Ga fluxes and very high temperatures, no growth is facilitated due to enhanced thermal decomposition. The closed symbols define the conditions used for the GaN films grown in this study.

FIG. 2. 3×3 and 1×1 μm^2 (insets) AFM images of 0.8-μm-thick MBE-GaN layers grown under identical N-rich conditions (Ga/N=0.7) at (a) T =720 °C, (b) 760 °C, and (c) T=775 °C on standard MOCVD-GaN templates, and at (d) T=770 °C on two-step ELO GaN template.

quality and avoid the formation of inversion domains (IDs),[21] both these layers were grown under Ga-rich droplet conditions at temperatures of 700 °C (UID-GaN) and 625 °C (*p*-GaN), respectively.[2] The conservation of the Ga face, i.e., (0001) polarity and successful inhibition of IDs, were confirmed *in situ* by the appearance of a characteristic 2×2 reconstruction during reflection high energy electron diffraction (RHEED) imaging at subsequent cooldown to 570 °C.[22] Using light doping by Si with concentrations in the low 10^{16} cm^{-3} region, the overlying GaN films (0.8 μm thickness, unless otherwise noted) were grown under constant N-rich conditions (Ga/N ratio=0.7 and N flux of 5 nm/min) at temperatures in the range of 720–790 °C, as shown in the growth diagram of Fig. 1.

This growth diagram exhibits a segment of a recently refined growth mode map for (0001) GaN homoepitaxy, which was developed by RHEED intensity profiling and quadrupole mass spectrometry (QMS) and has been described in detail elsewhere.[23] Central to this diagram is a growth mode transition in the N-rich growth regime from three-dimensional (3D) to 2D layer-by-layer growth at elevated temperatures, which coincides with the onset of thermal decomposition (as illustrated by the no growth region). In particular, for the selected Ga/N flux ratio and temperatures higher than 760 °C, multiple RHEED intensity oscillations were observed previously at the onset of GaN growth, indicative of a layer-by-layer growth mode.[23] At these increased temperatures, the thermally activated surface diffusion was significantly increased even by lacking the surfactant Ga adlayer. Thus, the growth surface is essentially N rich, as confirmed by the absence of pseudo-oscillatory RHEED transients and QMS-measured Ga desorption during growth interrupts,[23] which would indicate the existence of a finite Ga adlayer common under Ga-rich growth.[4,8,9]

The surface morphologies of GaN films (as indicated by the closed symbols in Fig. 1) were determined by atomic force microscopy (AFM), showing a series of representative images in Fig. 2. The surface of the film grown at T =720 °C [Fig. 2(a)] exhibited a columnar structure, typically observed for N-rich growth at low temperatures.[10] The rms (root-mean-square) roughness was as large as ~7.3 nm over
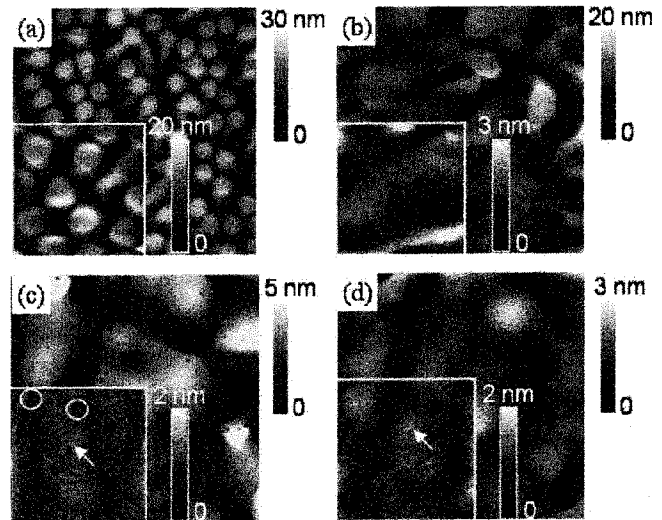
a 3×3 μm^2 area, evidencing further the predominance of 3D growth at these conditions.

In contrast, the surfaces of GaN films grown at higher growth temperatures (T=760, 770, and 775 °C) [Figs. 2(b)–2(d)] confirmed the 2D layer-by-layer growth mode. Surfaces shown in Figs. 2(b) and 2(c) are from of films grown on the highly resistive standard GaN templates (TD densities ~5×10^8 cm^{-2}). They indicate that with increasing temperature, gradually smoother surfaces were achieved, given also by the reduction in rms roughness from 3.7 nm (T=760 °C) to 1.5 nm (T=775 °C) over a 3×3 μm^2 area. Films grown at higher temperatures (up to 790 °C) revealed no change in surface quality and roughness, as compared to the surface shown in Fig. 2(c). The surface shown in Fig. 2(d) is from a film grown on the two-step ELO GaN template (maximum TD density ~4 $\times 10^7$ cm^{-2}), exhibiting even lower rms roughness of ~0.5 nm over the same scale.

All these improved surfaces produced at higher growth temperature share several common characteristics of typical layer-by-layer growth sequences, i.e., fairly distinguishable arrangements of stepped terraces and surface termination by 2D islands (marked by white arrows). Also, areas were observed on the surface, where the 2D islands have not fully coalesced to form completely continuous monolayers (marked by white circles). These layer-by-layer features are quite different from the features typically found for PAMBE growth of GaN under step-flow growth conditions. In the latter, steps and terraces are free of surface depressions and form characteristic arrays of hexagonally shaped spiral hillocks around mixed-type dislocations, where each hillock consists of two interlocking spiral ramps.[24]

Comparison between GaN films grown on standard GaN template and two-step ELO GaN template reveals a significant difference in the density of surface pits, which are commonly observed in MBE-grown GaN and have been associated with the surface termination of dislocations.[2,8,9,24] Quantitative assessment for two respective films resulted in surface pit densities of 5.8×10^8 cm^{-2} [Fig. 2(c)] and 2.2 $\times 10^7$ cm^{-2} [Fig. 2(d)], respectively. These values match

TABLE I. Average (and highest) room-temperature Hall mobilities and carrier concentrations in slightly Si-doped GaN films grown N-rich (Ga/N =0.7) at different temperatures on standard MOCVD-GaN templates (first five rows) and on one two-step ELO GaN template (last row).

T (°C)	d (μm)	Average (highest) mobility (cm^2/V s)	Carrier concentration (cm^{-3})
720	0.8	Insulating	Insulating
760	0.8	710 (750)	9.2×10^{15}
775	0.8	871 (934)	2.3×10^{16}
782	1	909 (936)	2.1×10^{16}
790	0.8	747 (784)	1.6×10^{16}
770	0.8	1125 (1150)	1.1×10^{16}

closely with the TD density given by the underlying GaN template, evidencing that under the selected growth conditions, no new dislocations were formed and the majority of TDs propagate to the surface. This conservation of microstructure was further confirmed by transmission electron microscopy, where the MBE-GaN film was found indistinguishable from the underlying MOCVD GaN template.

We further examined the unintentional impurity (i.e., oxygen) incorporation during the N-rich/high-T growth relative to standard Ga-rich growth conditions by SIMS. Identically, low oxygen levels were found in layers grown under these two different growth conditions. This demonstrates that even in the absence of the Ga adlayer, which generally promotes the oxygen desorption through the formation of a volatile gallium oxide under Ga-rich conditions,[25] low oxygen incorporation can be achieved under N-rich growth conditions at significantly increased growth temperature.

Considering the low oxygen levels, high surface and structural quality of GaN films grown under N-rich/high-T conditions, we expected great improvements in the electrical properties of these films. Hall measurements were performed at room temperature on the GaN films grown under the conditions denoted in Fig. 1, using 150×150 μm^2 van der Pauw (vdP) patterns defined through the top GaN film and the isolation structure. Table I summarizes the average and highest electron mobilities and carrier concentrations measured from six vdP patterns of each sample. The deviation in mobility and carrier concentration from the average values is less than ±6% and ±12%, respectively.

As obvious from Table I, the mobilities changed significantly with growth temperature and growth mode. While N-rich growth conditions at low temperatures (i.e., 720 °C, 3D growth regime) yielded highly resistive GaN films, which could not be measured, all GaN films grown at higher temperatures in the 2D layer-by-layer growth regime were conductive and revealed relatively high mobilities in excess of 700 cm^2/V s. The highest mobility measured for a GaN film grown on standard GaN template was 936 cm^2/V s and increased to 1150 cm^2/V s for a GaN film grown on a two-step ELO GaN template due to the lower TD density. Note that these values compare well with the highest ever reported RT mobilities in MBE-grown GaN.[12,13] Although, mobilities appear to increase with growth temperature under constant

Ga/N ratio, this trend may not hold completely true due to the slight deviations in carrier concentrations among this series. In addition, these preliminary results arise from yet unoptimized growth conditions and further exploration of the effect of Ga/N flux ratio, supplied N flux and doping concentration will be needed to elucidate clear correlations between growth conditions and mobilities and to further improve the electronic transport properties.

[1]H. Riechert, R. Averbeck, A. Graber, M. Schienle, U. Strauß, and H. Thews, *MRS Symposia Proceedings No. 449* (Materials Research Society, Pittsburgh, 1997), p. 149.

[2]B. Heying, R. Averbeck, L. F. Chen, E. Haus, H. Riechert, and J. S. Speck, J. Appl. Phys. **88**, 1855 (2000).

[3]J. E. Northrup, J. Neugebauer, R. M. Feenstra, and A. R. Smith, Phys. Rev. B **61**, 9932 (2000).

[4]G. Koblmüller, J. Brown, R. Averbeck, H. Riechert, P. Pongratz, and J. S. Speck, Appl. Phys. Lett. **86**, 041908 (2005).

[5]T. Zywietz, J. Neugebauer, and M. Scheffler, Appl. Phys. Lett. **73**, 487 (1998).

[6]J. Neugebauer, T. Zywietz, M. Scheffler, J. E. Northrup, H. Chen, and R. M. Feenstra, Phys. Rev. Lett. **90**, 056101 (2003).

[7]J. M. Myoung, O. Gluschenkov, K. Kim, and S. Kim, J. Vac. Sci. Technol. A **17**, 3019 (1999).

[8]C. Adelmann, J. Brault, D. Jalabert, P. Gentile, H. Mariette, G. Mula, and B. Daudin, J. Appl. Phys. **91**, 9638 (2002).

[9]G. Koblmüller, J. S. Brown, R. Averbeck, H. Riechert, P. Pongratz, and J. S. Speck, Jpn. J. Appl. Phys., Part 2 **44**, L906 (2005).

[10]E. J. Tarsa, B. Heying, X. H. Wu, P. Fini, S. P. Den Baars, and J. S. Speck, J. Appl. Phys. **82**, 5472 (1997).

[11]A. Hierro, A. R. Arehart, B. Heying, M. Hansen, U. K. Mishra, S. P. DenBaars, J. S. Speck, and S. A. Ringel, Appl. Phys. Lett. **80**, 805 (2002).

[12]B. Heying, I. Smorchkova, C. Poblenz, C. Elsass, P. Fini, S. DenBaars, U. Mishra, and J. S. Speck, Appl. Phys. Lett. **77**, 2885 (2000).

[13]E. Iliopoulos, M. Zervos, A. Adikimenakis, K. Tsagaraki, and A. Georgakilas, Superlattices Microstruct. **40**, 313 (2006).

[14]C. Poblenz, P. Waltereit, and J. S. Speck, J. Vac. Sci. Technol. B **23**, 1379 (2005).

[15]N. Grandjean, J. Massies, F. Semond, S. Yu. Karpov, and R. A. Talalaev, Appl. Phys. Lett. **74**, 1854 (1999).

[16]A. J. Ptak, M. R. Millecchia, T. H. Myers, K. S. Ziemer, and C. D. Stinespring, Appl. Phys. Lett. **74**, 3836 (1999).

[17]Z. Bougrioua, M. Azize, A. Jimenez, A.-F. Braña, P. Lorenzini, B. Beaumont, E. Muñoz, and P. Gibart, Phys. Status Solidi C **2**, 2424 (2005).

[18]M. Drakopoulos, M. Laügt, T. Riemann, B. Beaumont, and P. Gibart, Phys. Status Solidi B **243**, 1545 (2006).

[19]H. M. Ng, D. Doppalapudi, T. D. Moustakas, N. G. Weimann, and L. F. Eastman, Appl. Phys. Lett. **73**, 821 (1998).

[20]D. C. Look and J. R. Sizelove, Phys. Rev. Lett. **82**, 1237 (1999).

[21]M. McLaurin, T. E. Mates, F. Wu, and J. S. Speck, J. Appl. Phys. **100**, 063707 (2006).

[22]A. R. Smith, R. M. Feenstra, D. W. Greve, M.-S. Shin, M. Skowronski, J. Neugebauer, and J. E. Northrup, Appl. Phys. Lett. **72**, 2114 (1998).

[23]G. Koblmüller, S. Fernandez-Garrido, E. Calleja, and J. S. Speck, Appl. Phys. Lett. **91**, 161904 (2007).

[24]B. Heying, E. J. Tarsa, C. R. Elsass, P. Fini, S. P. DenBaars, and J. S. Speck, J. Appl. Phys. **85**, 6470 (1999).

[25]C. R. Elsass, T. Mates, B. Heying, C. Poblenz, P. Fini, P. M. Petroff, S. P. DenBaars, and J. S. Speck, Appl. Phys. Lett. **77**, 3167 (2000).

In-polar InN grown by plasma-assisted molecular beam epitaxy

Chad S. Gallinat,[a] Gregor Koblmüller, Jay S. Brown,
Sarah Bernardis, and James S. Speck
Materials Department, University of California, Santa Barbara, California 93106-5050

Grace D. Chern, Eric D. Readinger, Hongen Shen, and Michael Wraback
*U.S. Army Research Laboratory, Sensors and Electron Devices Directorate, 2800 Powder Mill Road,
Adelphi, Maryland 20783*

We study the effect of different deposition conditions on the properties of In-polar InN grown by plasma-assisted molecular beam epitaxy. GaN buffer layers grown in the Ga-droplet regime prior to the InN deposition significantly improved the surface morphology of InN films grown with excess In flux. Using this approach, In-polar InN films have been realized with room temperature electron mobilities as high as 2250 cm^2/V s. We correlate electron concentrations in our InN films with the unintentionally incorporated impurities, oxygen and hydrogen. A surface electron accumulation layer of 5.11×10^{13} cm^{-2} is measured for In-polar InN. Analysis of optical absorption data provides a band gap energy of $\sim$0.65 eV for the thickest InN films. © *2006 American Institute of Physics.*
[DOI: 10.1063/1.2234274]

Recent advances in III-nitride deposition techniques have facilitated the growth of high quality InN films and established an updated band gap value of 0.67–0.8 eV.[1–4] This smaller band gap value has opened the III-nitride system to unique possible electronic and optoelectronic applications. However, the electrical properties of InN are still a source of dispute due to the high unintentionally doped electron concentrations.[5–8] Recent theoretical calculations predict an ultimate room temperature electron mobility for InN to reach 14 000 cm^2/V s.[9] Based on this prediction and the flurry of recent activity, there appears to be room for improvement in the growth of InN.

In this letter, we present optimized In-polar InN grown by plasma-assisted molecular beam epitaxy (PA-MBE). Our approach for this study was to create a growth diagram for In-polar InN similar to what has been developed for the PA-MBE growth of Ga-polar GaN,[10,11] understand the effect of a GaN buffer layer, and begin to explore the origin of InN's electrical properties. The samples presented here were grown in a Varian/EPI 620 chamber with conventional Knudsen cells for group III sources and an EPI Unibulb radio frequency plasma source for the active nitrogen species. We document all fluxes in terms of growth rate (nm/min) as calibrated by thickness measurements of In-rich and N-rich InN samples. An Ircon Modline 3 pyrometer was employed to measure the growth temperature. All of the samples presented here were grown on semi-insulating (Fe-doped) Ga-polar GaN templates provided by Lumilog. Reflection high energy electron diffraction (RHEED) was used to monitor the growth mode and metal coverage *in situ*. The samples were characterized *ex situ* by optical microscopy, atomic force microscopy (AFM), room temperature Hall effect measurements, and high-resolution x-ray diffraction (HRXRD). To analyze unintentionally incorporated impurities, secondary ion mass spectrometry (SIMS) measurements were performed using implant standards for the quantification of hydrogen and oxygen.

The initial approach in developing an In-polar InN growth diagram was to identify a temperature window necessary for growth. Figure 1(a) shows the relatively simple InN growth diagram—the details of the construction of this diagram will be published elsewhere. It was observed that at temperatures above 500 °C there was no InN growth and only In metal was deposited onto the substrate, regardless of the In flux/active nitrogen ratio. Growth of In-polar InN should be possible beyond 500 °C, however, with an appropriate increase in active nitrogen to offset InN dissociation. At growth temperatures between 420 and 490 °C fully coalesced InN layers were realized.

Based on this growth temperature window, a series of samples were grown, varying only the In flux (from as high as $\sim$17 nm/min to as low as $\sim$3 nm/min)—keeping the substrate temperature and the active nitrogen constant (450 °C and 12 nm/min, respectively). Two growth regimes were identified, as characterized by surface morphology (by AFM): the N-rich regime [Fig. 1(c)] and the In-droplet regime [Fig. 1(b)]. This observation is different from GaN in which three growth regimes are identified for the PA-MBE growth in the metal-polar orientation.[10,11] This two-regime growth behavior persists for all substrate temperatures at which InN films were realized.

Upon completion of the growth diagram, we turned our attention to optimizing a buffer layer to precede InN growth. Reports of using an AlN buffer layer on sapphire,[12] a low-temperature InN buffer layer on sapphire,[13] a double buffer
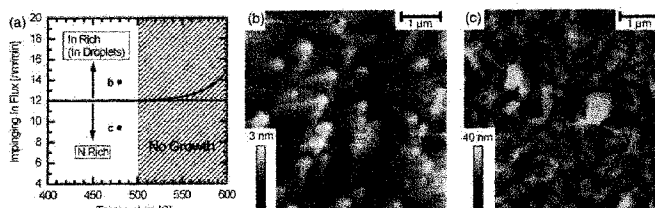

FIG. 1. (a) In-polar InN PA-MBE growth diagram and AFM micrographs of (b) a 1.5 μm thick InN layer grown in the In-droplet regime and (c) a 1 μm thick InN layer grown in the N-rich regime.

[a]Electronic mail: chadsg@engineering.ucsb.edu

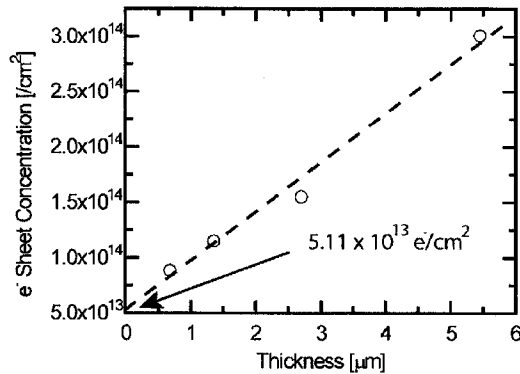FIG. 2. Dependence of the electron sheet concentration on InN film thickness.
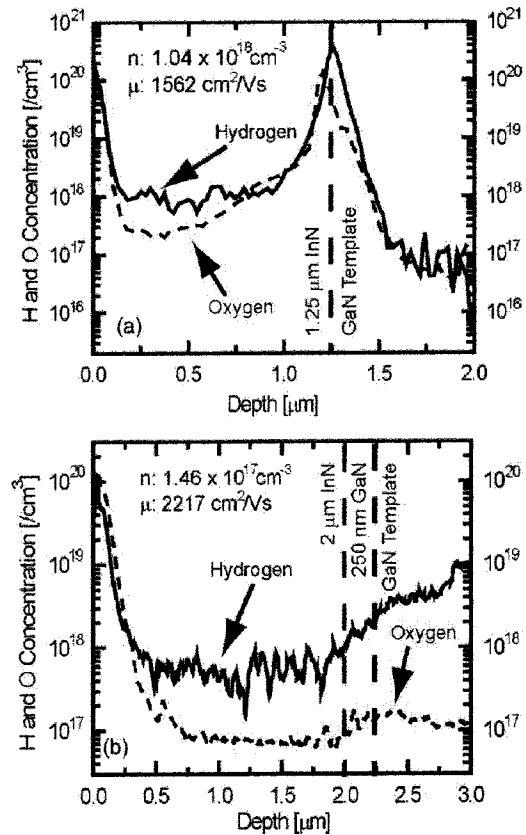

FIG. 3. (Color online) SIMS profiles quantifying the unintentionally incorporated impurities, hydrogen (solid line) and oxygen (dashed line), in (a) a 1.25 μm thick InN sample grown directly on a GaN template and (b) a 2 μm InN sample grown on a 250 nm thick Ga-droplet GaN buffer layer.

utilizing Si_3N_4/AlN on Si,[14] and a GaN buffer on sapphire[15] have all improved the structural and electrical properties of InN. Growth on GaN templates provide yet another substrate for the PA-MBE growth of InN, and optimization of a GaN buffer layer is a necessary step for improving the quality of InN.

Initial In-polar InN epilayers were grown directly on the GaN templates. This resulted in InN layers that were not fully coalesced and exhibited many surface pits as observed by AFM; therefore, it was necessary to optimize the buffer layer to precede InN growth. According to the GaN growth diagram,[10,11] we grew GaN buffer layers in the three different GaN growth regimes (N-rich, intermediate Ga-rich, and Ga-droplet Ga-rich). It was found that In-rich InN layers grown on 100 nm thick N-rich and intermediate grown GaN buffer layers were delaminated from the underlying buffer layer. GaN buffer layers were grown in the Ga-droplet growth regime required complete desorption of excess Ga from the surface before starting InN growth. This was achieved by choosing a high enough substrate temperature (700 °C) and monitoring the increase in RHEED intensity to the pregrowth value. RHEED intensities of low contrast are typically associated with the presence of metallic droplets, while increased RHEED intensity indicates metal desorption.[16] After complete Ga desorption, subsequent InN layers were grown at varying growth temperatures, In fluxes, and plasma conditions. InN layers grown on GaN buffer layers grown in the Ga-droplet regime adhered entirely to the underlying layer with no blistering or delamination. InN layers grown on this optimized buffer layer [Fig. 1(b)] had smoother surface morphologies and less surface pitting as compared to layers grown directly on the GaN template or to those grown in the N-rich regime [Fig. 1(c)].

It has been reported that there exists a large density of electrons at the InN surface (2.5×10^{13} cm^{-2}).[17,18] To evaluate the surface electron accumulation in our optimized In-polar InN, we grew a series of samples at differing thicknesses, measured the Hall sheet carrier concentration, and extrapolated the fitted curve to zero film thickness (Fig. 2). The surface electron density determined from the fit was 5.11×10^{13} cm^{-2}, while the bulk electron density was 4.46×10^{17} cm^{-3}. Throughout this letter, the surface electron density was subtracted from the measured electron concentration to provide a more accurate bulk electron concentration.

The origin of the high electron concentrations in InN was explored using SIMS. Electronic structure calculations predict that both hydrogen and oxygen are shallow donors in InN.[19,20] Using these predictions as a guide, both oxygen and hydrogen levels were quantified in representative samples. Figure 3 shows SIMS profiles for two different samples grown at a substrate temperature of 450 °C in the In-droplet regime: (a) a 1.25 μm InN film grown directly on a GaN template and (b) a 2 μm InN film grown on a 250 nm thick Ga-droplet GaN buffer. For the sample shown in Fig. 3(a), the average hydrogen concentration in the InN layer was 1.11×10^{18} cm^{-3} and the average oxygen concentration was 7.69×10^{17} cm^{-3}. Hall measurements on the same sample yielded a bulk electron concentration of 1.04×10^{18} cm^{-3} and a mobility of 1562 cm^2/V s. The InN layer in Fig. 3(b) exhibited a smaller average hydrogen concentration (5.72×10^{17} cm^{-3}) and a smaller oxygen concentration (8.75×10^{16} cm^{-3}) through the bulk of the InN layer. This layer also had a lower measured electron concentration (1.46×10^{17} cm^{-3}) and a higher mobility (2217 cm^2/V s) than the sample grown directly on the GaN template. In both samples the hydrogen levels in the InN layer were comparable to the free electron concentrations—suggesting that hydrogen was the dominant unintentional impurity donor in these films.

Overall, samples grown directly on the GaN templates had on average higher electron carrier concentrations (4.71×10^{17}–1.04×10^{19} cm^{-3}) and lower electron mobilities (1575–1290 cm^2/V s) as compared to samples grown using a Ga-droplet GaN buffer layer (3.5×10^{17}–7.75×10^{17} cm^{-3} and 2250–1606 cm^2/V s).
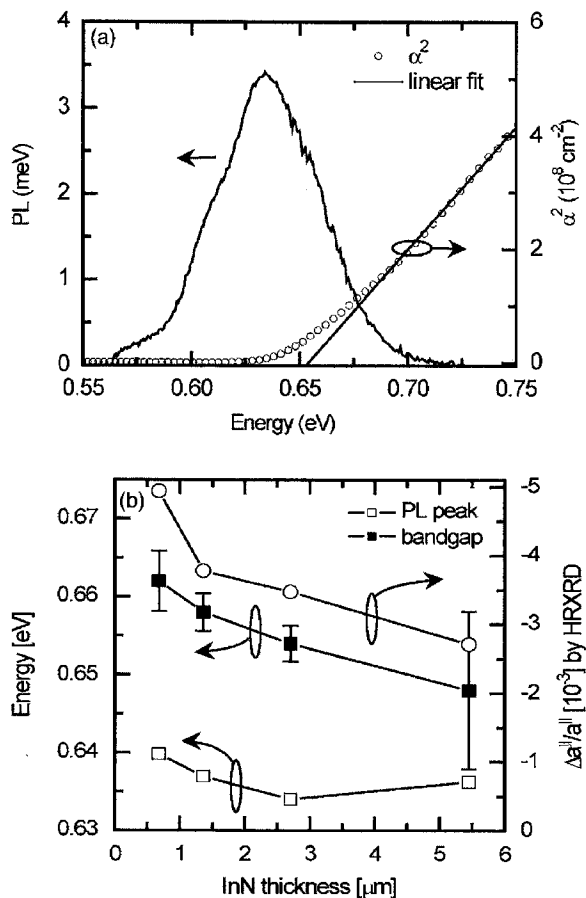
FIG. 4. (a) Band gap obtained from absorption data and PL spectrum from the 2.7 μm InN sample; (b) comparison of band gap energy, peak PL emission energy, and residual compressive strain as a function of InN thickness.

With a value of 2250 cm^2/V s, we report one of the highest measured RT electron mobilities for In-polar InN.

The optical properties of the InN thickness series were evaluated at room temperature by cw reflectance, transmission, and photoluminescence (PL) measurements. The absorption coefficient was calculated from the reflectance and transmission data, and its square is plotted versus photon energy to determine the direct band gap of the InN. Figure 4(a) shows representative results for the 2.7 μm thick sample. The intercept of the linear fit with the energy axis provides a band gap of 0.654±0.002 eV. The PL peak was Stokes shifted from 20 meV to 0.634 eV, implying that the emission emanates substantially from the bandtail states. Figure 4(b) compares the band gap obtained from the fit described above, the PL peak energy, and the residual compressive strain (as measured by HRXRD) for the InN film thickness series. The band gap decreased from 0.662±0.004 to 0.648±0.01 eV as the film thickness increased from 0.68 to 5.45 μm, most likely due to the reduction in residual compressive strain. Comparison of the shift in band gap with variation in compressive strain allows us to estimate the deformation potential for wurtzite InN to be 5.0 eV, a higher value than what was expected according to theoretical calculations (4.2 eV).[21] Extrapolation to zero

strain using the experimentally determined deformation potential (5.0 eV) yields a band gap value of 0.63±0.007 eV. A similar shift in PL peak energy, from 0.64 to ~0.635 eV, was observed with increasing film thickness. This wavelength shift may be less pronounced because the absorption depth of the 900 nm excitation laser is much smaller (~200–300 nm) than the thickness of most of the InN films.

In summary, the presence of a GaN buffer layer grown in the Ga-droplet regime was necessary for the highest quality InN films. We have measured amongst the highest RT electron mobility for In-polar InN (2250 cm^2/V s) and found a direct correlation between the free electron concentration in InN and the incorporation of hydrogen and oxygen. We measured an electron accumulation layer of 5.11 × 10^{13} cm^{-2} at the surface of In-polar InN films and presented optical data that indicate that the band gap of thick, partially strain-relaxed InN films may be below 0.65 eV.

[1] M. Higashiwaki and T. Matsui, J. Cryst. Growth **269**, 162 (2004).
[2] T. Araki, Y. Saito, T. Yamaguchi, M. Kurouchi, Y. Nanishi, and H. Naoi, J. Vac. Sci. Technol. B **22**, 2139 (2004).
[3] K. M. Yu, Z. Liliental-Weber, W. Walukiewicz, W. Shan, J. W. Ager III, S. X. Li, R. E. Jones, E. E. Haller, H. Lu, and W. J. Schaff, Appl. Phys. Lett. **86**, 071910 (2005).
[4] J. Wu, W. Walukiewicz, K. M. Yu, J. W. Ager III, E. E. Haller, H. Lu, W. J. Schaff, Y. Saito, and Y. Nanishi, Appl. Phys. Lett. **80**, 3967 (2002).
[5] H. Lu, W. J. Schaff, J. Hwang, H. Wu, W. Yeo, A. Pharkya, and L. F. Eastman, Appl. Phys. Lett. **77**, 2548 (2000).
[6] C.-F. S. Chin-An Chang, Nai-Chuan Chen, Pen-Hsiu Chang, and Kuo-Shiun Liu, Phys. Status Solidi C **1**, 2559 (2004).
[7] R. P. T. Craig, H. Swartz, Thomas H. Myers, Hai Lu, and William J. Schaff, Phys. Status Solidi C **2**, 2250 (2005).
[8] F. Chen, A. N. Cartwright, H. Lu, and W. J. Schaff, J. Cryst. Growth **269**, 10 (2004).
[9] V. M. Polyakov and F. Schwierz, Appl. Phys. Lett. **88**, 032101 (2006).
[10] B. Heying, R. Averbeck, L. F. Chen, E. Haus, H. Riechert, and J. S. Speck, J. Appl. Phys. **88**, 1855 (2000).
[11] B. Heying, I. Smorchkova, C. Poblenz, C. Elsass, P. Fini, S. D. Baars, U. Mishra, and J. S. Speck, Appl. Phys. Lett. **77**, 2885 (2000).
[12] H. Lu, W. J. Schaff, J. Hwang, H. Wu, G. Koley, and L. F. Eastman, Appl. Phys. Lett. **79**, 1489 (2001).
[13] Y. Saito, N. Teraguchi, A. Suzuki, T. Araki, and Y. Nanishi, Jpn. J. Appl. Phys., Part 2 **40**, L91 (2001).
[14] H. Ahn, C.-H. Shen, C.-L. Wu, and S. Gwo, Appl. Phys. Lett. **86**, 201905 (2005).
[15] C. J. Lu, L. A. Bendersky, H. Lu, and W. J. Schaff, Appl. Phys. Lett. **83**, 2817 (2003).
[16] C. Adelmann, J. Brault, D. Jalabert, P. Gentile, H. Mariette, G. Mula, and B. Daudin, J. Appl. Phys. **91**, 9638 (2002).
[17] H. Lu, W. J. Schaff, L. F. Eastman, and C. E. Stutz, Appl. Phys. Lett. **82**, 1736 (2003).
[18] T. D. Veal, I. Mahboob, L. F. J. Piper, C. F. McConville, H. Lu, and W. J. Schaff, J. Vac. Sci. Technol. B **22**, 2175 (2004).
[19] C. G. Van de Walle, Phys. Status Solidi B **235**, 89 (2003).
[20] C. Stampfl, C. G. Van de Walle, D. Vogel, P. Kruger, and J. Pollmann, Phys. Rev. B **61**, R7846 (2000).
[21] S.-H. Wei, X. Nie, I. G. Batyrev, and S. B. Zhang, Phys. Rev. B **67**, 165209 (2003).

Optimization of the surface and structural quality of N-face InN grown by molecular beam epitaxy

G. Koblmüller,[a] C. S. Gallinat, S. Bernardis, and J. S. Speck
Materials Department, University of California, Santa Barbara, California 93106-5050

G. D. Chern, E. D. Readinger, H. Shen, and M. Wraback
U.S. Army Research Laboratory, Sensors and Electron Devices Directorate, 2800 Powder Mill Road, Adelphi, Maryland 20783

The authors demonstrate the impact of growth kinetics on the surface and structural properties of N-face InN grown by molecular beam epitaxy. Superior surface morphology with step-flow growth features is achieved consistently under In-rich conditions in a low-temperature region of 500–540 °C. Remarkably, off-axis x-ray rocking curve (ω scans) widths are found to be independent of the growth conditions. The band gap determined from optical absorption measurements of optimized InN is 0.651 eV, while photoluminescence peak emission occurs at even lower energies of $\sim$0.626 eV. Hall measurements show room temperature peak electron mobilities as high as 2370 cm^2/V s at a carrier concentration in the low 10^{17} cm^{-3} region. Analysis of the thickness dependence of the carrier concentration demonstrates a n-type surface accumulation layer with a sheet carrier concentration of $\sim$3 $\times$ 10^{13} cm^{-2}. © 2006 American Institute of Physics. [DOI: 10.1063/1.2335685]

Over the past few years, InN has fueled tremendous interest because the fundamental band gap energy has been revised to approximately 0.7 eV.[1–3] Consequently, InN is becoming increasingly attractive not only as a near-infrared (IR) material for optoelectronic applications, including its possible performance as a terahertz emitter,[4] but also for extending the emission of light emitting diodes from deep ultraviolet to near IR, if alloyed with GaN or AlN.[5] Beyond this, superior electronic transport properties, i.e., high electron peak velocities[6] and mobilities, are expected due to its small electron effective mass of $\approx$0.04m_0.[6,7] Indeed, a few experimental studies of undoped InN point to room temperature electron mobilities exceeding 2000 cm^2/V s.[8,9]

For the In-face orientation, numerous attempts, using mainly plasma-assisted molecular beam epitaxy (MBE), have been undertaken to generate good crystal and surface quality for improved optical and transport properties. The implementation of various buffer layers, such as AlN,[10] low-temperature InN,[11] and GaN,[9,12] has helped especially to reduce free electron carrier concentration and sharpen the optical absorption edge, partly overcoming the lack of a near-lattice-matched substrate. However, the low InN decomposition temperature presents significant growth challenges, limiting the growth temperature to $\approx$500 °C.[13,14]

Most recently, the challenges of InN deposition have been addressed by growing films along the thermally more stable N-face orientation,[15,16] where growth temperatures up to 600 °C seem feasible. Higher structural quality InN films with sharp step-flow surface features may be achieved, even under N-rich growth conditions. This appears contradictory to the established knowledge of high adatom diffusion under purely metal-rich conditions, as in GaN (Ref. 17) or AlN (Ref. 18) growth. In this letter, we investigate these important aspects of N-face InN growth, with special emphasis on the effect of growth kinetics on the advancement of the physical properties.

As substrates for N-face growth, we used high-quality freestanding N-face GaN templates provided by Lumilog with threading dislocation densities specified to be less than 1×10^8 cm^{-2}. To produce a surface free of contamination and of good interface quality we have grown an $\approx$40 nm thick GaN buffer layer under Ga-rich conditions at a temperature of 700 °C. Both the GaN buffer and InN layer growths were performed in an Epi 620 MBE system using standard effusion cells for Ga and In, and an Epi Unibulb radio frequency plasma source for supplying active nitrogen. A pyrometer was used to measure the substrate temperature *in situ*. We give all molecular fluxes in terms of potential growth rate in units of nm/min, as calibrated from thickness measurements of InN films grown under In-rich and N-rich conditions at temperatures for which thermal decomposition was negligible. High-resolution x-ray rocking curves (ω scans) and ω-2θ scans were performed using a triple-axis diffractometer with a resolution limit of $\sim$10 arc sec. The structural quality of the InN films was correlated with the surface morphology by employing atomic force microscopy (AFM). In addition, we have selected optimized InN films on N-face GaN layers (200 nm thick) grown on NOVASiC polished C-face 6H–SiC substrates[19,20] for optical spectroscopy, using a combination of photoluminescence (PL) and optical absorption obtained from reflectance and transmission measurements. To identify transport properties, we performed Hall measurements in the van der Pauw geometry on as-grown InN layers on the buffered, semi-insulating C-face 6H–SiC substrates.

Reflection high energy electron diffraction (RHEED) was used to confirm the N-face growth direction prior to each InN growth. By cooling the GaN buffer layer to temperatures below $\sim$620 °C we observed a distinct 3$\times$3 RHEED reconstruction, which is a well known characteristic of a N-face GaN growth surface.[21] The N-face InN layers presented here were grown at different temperatures and
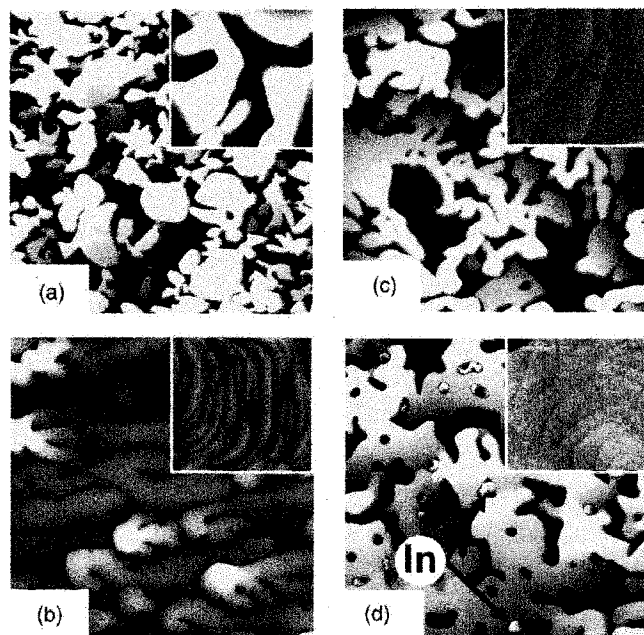
[a]Electronic mail: gregor@engineering.ucsb.edu

FIG. 1. AFM micrographs [10×10 μm^2 and 1×1 μm^2 (insets)] of InN layers grown on freestanding GaN; growth temperatures and In/N flux ratios are (a) 530 °C and 0.9, (b) 530 °C and 1.4, (c) 595 °C and 0.9, and (d) 595 °C and 1.4. The height scale of the inset images is 2 nm for all samples, but for the larger images it is 50 nm for (a) and (c) and 20 nm for (b) and (d).

In/N flux ratios. To achieve different flux ratios, we kept the N flux constant at 7.5 nm/min and varied only the In flux, from N-rich (In/N=0.9) to In-rich droplet conditions (In/N=1.4). The designation of these growth regimes and their intricate relationship with thermal decomposition have been elaborated in detail and will be published elsewhere.[22] In Fig. 1, typical AFM surface morphologies are shown for nominally ~0.9 μm thick InN layers grown at two temperatures (530 and 595 °C) and In/N ratios of 0.9 and 1.4, respectively. The measured InN thicknesses from cross-sectional scanning electron microscopy coincided with the nominal thickness for layers grown at 530 °C (~0.87 μm), but were slightly reduced due to thermal decomposition for layers grown at 595 °C (~0.67 μm). InN layers grown under N-rich growth conditions exhibit the roughest surfaces with root-mean-square (rms) values of 54.1 nm [Fig. 1(a)] and 29.6 nm [Fig. 1(c)] over a 10×10 μm^2 area. In contrast, when the growth was performed under In-rich droplet conditions and low temperature (T=530 °C) significantly improved surface quality was achieved (rms roughness =6.6 nm) [Fig. 1(b)]. Imaging the areas in between the few and randomly distributed In droplets displays large atomically flat terraces with clear step-flow growth features that are separated by occasional pits and coalescence boundaries. These step-flow features are characterized by arrays of curved terraces (as part of spiral growth hillocks) with step heights of ~3 Å corresponding to the monolayer height of $c/2$=2.88 Å for bulk InN. Increasing the growth temperature to 595 °C [Fig. 1(d)] resulted in much rougher surface (rms=18.7 nm). In this case, a higher density of metallic In droplets was observed on the surface (including small nuclei of droplets indicated by the arrows), as a result of increased In accumulation due to significant thermal dissociation of InN and limited In desorption at these temperatures.[22] Note that the step-flow surface morphologies generated under In-

rich conditions are similar to those commonly observed for GaN growth under metal-rich conditions.[17] Recent experiments have demonstrated that the GaN growth front is stabilized by a metallic Ga adlayer,[23] which promotes quite high N-adatom surface diffusion. Analogously, we have found an In adlayer on the N-face InN surface under In-rich conditions with a saturation coverage of 1 ML (as determined by In adsorption experiments using RHEED Bragg spot intensity variations).[22] High-temperature InN growth under N-rich conditions, however, is remarkably different from what is known for GaN growth. As shown in Fig. 1(c), the terrace-like surface structure exhibits step-flow features, as also observed by Xu and Yoshikawa.[15] These smooth surfaces indicate that high surface diffusion of In and N adatoms must be prevalent even in N-rich growth. We assume that the diffusion barrier for In adatoms on a bare InN surface is likely to be smaller than the barrier for Ga migration on a GaN surface.

To correlate the AFM surface morphologies with the structural quality, we have systematically determined the x-ray rocking curve (ω scans) widths [full width at half maximum (FWHM)] of on-axis and off-axis reflections (the latter measured in a skew-symmetric geometry) of several InN layers grown in the temperature range between 500 and 595 °C. For the more important off-axis scans we observe no dependence between FWHM values and growth conditions (both temperature and In/N flux ratio), with values scattered randomly between 1020 and 1200 arc sec for the ($10\bar{2}2$) reflection and between 1320 and 1550 arc sec for the ($20\bar{2}1$) reflection. These results indicate that the twist about the c axis is negligibly impacted by the growth conditions. In accordance with investigations of GaN by Heying *et al.*,[24] this means that the majority of pure edge-type threading dislocations (TDs) are essentially invariant with growth conditions. In contrast, we observe a slight dependence of the on-axis (0002) FWHM values [i.e., representing minority pure screw and mixed TDs (Ref. 24)] on the growth conditions, giving the lowest FWHM (~320 arc sec) for layers grown under In-rich conditions in a moderately low temperature range (500–540 °C). These values are comparable with the best values reported for N-face InN (Ref. 15) and are in general slightly better than those realized for In-face InN.[14,25]

The significance of choosing optimum conditions of low growth temperature and In-rich conditions for the optical properties of N-face InN is illustrated in Fig. 2. Room-temperature PL, reflectance, and transmission data were obtained on optimized InN layers grown on N-face GaN buffer layers on C-face SiC substrates. The absorption coefficient was determined from both the reflectance and transmission data, and its square is plotted versus photon energy to determine the direct band gap of the InN. The intercept of the linear fit with the energy axis provides a band gap of 0.651 eV. The PL peak emission from a thick sample was determined using a Lorentzian fit to the data to occur at ~0.626 eV, with a FWHM of 54 meV. The slight redshift with respect to the band gap implies that the emission emanates primarily from the bandtail states. The band gap and PL peak emission energy are among the lowest reported values for wurtzite InN.[1–3,14,15,26]

Finally, the transport properties were evaluated using an InN series with different thicknesses under identical and optimized conditions (T=535 °C, In/N=1.4) on a 200 nm
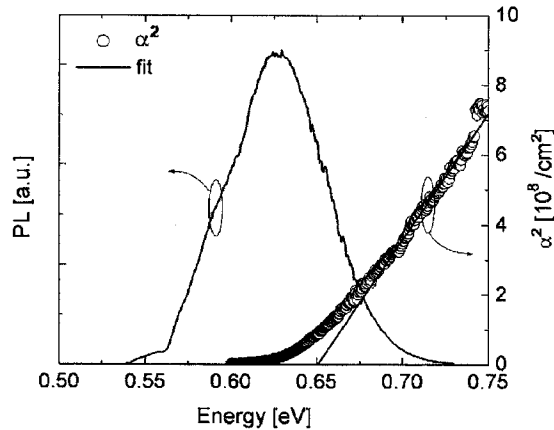
FIG. 2. Band gap obtained from absorption data and PL spectrum from optimized N-face InN samples.

thick N-face GaN buffer layer grown on semi-insulating C-face 6H–SiC substrates. To facilitate this we performed Hall measurements at 300 K on the as-grown InN layers (containing a small density of In droplets), with their results shown in Fig. 3. The Hall electron mobility increases continually with increasing layer thickness, reaching a maximum mobility of 2370 cm^2/V s for a layer thickness of 4.4 μm. These electron mobilities are almost a factor of 2 higher, and the corresponding bulk carrier concentration of 2.8×10^{17} cm^{-3} is nearly one order of magnitude lower than those reported for the best MBE grown N-face InN.[15] By linear extrapolation of the sheet carrier concentration of the InN layers to zero thickness (for a series of samples grown to different InN thickness), a surface electron accumulation layer density of $\sim 3 \times 10^{13}$ cm^{-2} was determined. The surface carrier concentration is in close agreement with the $\sim 2.5 \times 10^{13}$ cm^{-2} density determined independently by energy electron loss spectroscopy and theoretical calculations.[27] Despite this consistency, we suggest that a more detailed analysis is needed for differentiating between bulk conduction and surface or interface conduction.

In summary, systematic growth kinetics studies were conducted to optimize the surface and structural properties of N-face InN grown on freestanding GaN. InN films with high
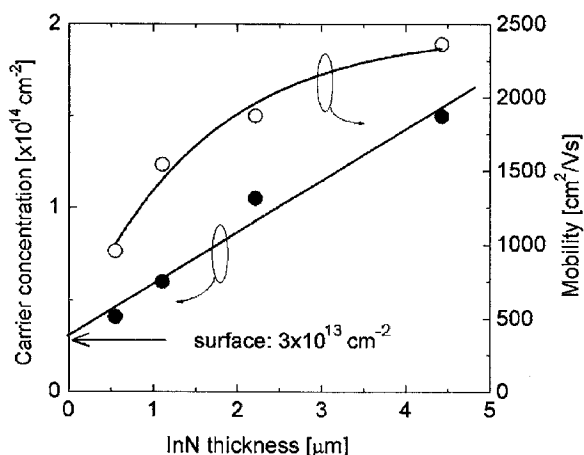
structural quality and smooth step-flow-like surface morphologies were achieved in a rather low-temperature region of 500–540 °C under In-rich conditions. The structural quality of InN was facilitated by the multiple effect of negligible thermal decomposition at these temperatures and the autosurfactant action of a 1 ML thick In adlayer on the surface. The band gap of 0.651 eV and room-temperature PL peak emission at 0.626 eV of our optimized InN are among the lowest reported values. In addition, Hall mobilities reached 2370 cm^2/V s at bulk carrier concentrations in the low 10^{17} cm^{-3}, and a surface accumulation layer with an electron density of $\sim 3 \times 10^{13}$ cm^{-2} was determined.

[1]V. Yu. Davydov, A. A. Klochikhin, R. P. Seisyan, V. V. Emtsev, S. V. Ivanov, F. Bechstedt, J. Furthmüller, H. Harima, A. V. Mudryi, J. Aderhold, O. Semchinova, and J. Graul, Phys. Status Solidi B **229**, R1 (2002).
[2]J. Wu, W. Walukiewicz, K. M. Yu, J. W. Ager, E. E. Haller, H. Lu, W. J. Schaff, Y. Saito, and Y. Nanishi, Appl. Phys. Lett. **80**, 3967 (2002).
[3]T. Matsuoka, H. Okamoto, M. Nakao, H. Harima, and E. Kurimoto, Appl. Phys. Lett. **81**, 1246 (2002).
[4]R. Ascazubi, I. Wilke, K. Denniston, H. Lu, and W. J. Schaff, Appl. Phys. Lett. **84**, 4810 (2004).
[5]M. Higashiwaki and T. Matsui, Jpn. J. Appl. Phys., Part 2 **41**, L540 (2002).
[6]V. M. Polyakov and F. Schwierz, Appl. Phys. Lett. **88**, 032101 (2006).
[7]S. K. O'Leary, B. E. Foutz, M. S. Shur, and L. F. Eastman, Appl. Phys. Lett. **87**, 222103 (2005).
[8]J. Wu, W. Walukiewicz, W. Shan, K. M. Yu, J. W. Ager, S. X. Li, E. E. Haller, H. Lu, and W. J. Schaff, J. Appl. Phys. **94**, 4457 (2003).
[9]C. S. Gallinat, G. Koblmüller, S. Bernardis, J. S. Brown, J. S. Speck, G. D. Chern, E. D. Readinger, H. Shen, and M. Wraback, Appl. Phys. Lett. **89**, 032109 (2006).
[10]H. Lu, W. J. Schaff, J. Hwang, H. Wu, G. Koley, and L. F. Eastman, Appl. Phys. Lett. **79**, 1489 (2001).
[11]Y. Saito, N. Teraguchi, A. Suzuki, T. Araki, and Y. Nanishi, Jpn. J. Appl. Phys., Part 2 **40**, L91 (2001).
[12]C. J. Lu, L. A. Bendersky, H. Lu, and W. J. Schaff, Appl. Phys. Lett. **83**, 2817 (2003).
[13]E. Dimakis, E. Iliopoulos, K. Tsagaraki, and A. Georgakilas, Appl. Phys. Lett. **86**, 133104 (2005).
[14]T. Ive, O. Brandt, M. Ramsteiner, M. Giehler, H. Kostial, and K. H. Ploog, Appl. Phys. Lett. **84**, 1671 (2004).
[15]K. Xu and A. Yoshikawa, Appl. Phys. Lett. **83**, 251 (2003).
[16]H. Naoi, F. Matsuda, T. Araki, A. Suzuki, and Y. Nanishi, J. Cryst. Growth **269**, 155 (2004).
[17]B. Heying, R. Averbeck, L. F. Chen, E. Haus, H. Riechert, and J. S. Speck, J. Appl. Phys. **88**, 1855 (2000).
[18]G. Koblmüller, R. Averbeck, L. Geelhaar, H. Riechert, W. Hoesler, and P. Pongratz, J. Appl. Phys. **93**, 9591 (2003).
[19]S. Rajan, M. Wong, Y. Fu, F. Wu, J. S. Speck, and U. K. Mishra, Jpn. J. Appl. Phys., Part 2 **44**, L1478 (2005).
[20]E. Monroy, E. Sarigiannidou, F. Fossard, N. Gogneau, E. Bellet-Amalric, J.-L. Rouviere, S. Monnoye, H. Mank, and B. Daudin, Appl. Phys. Lett. **84**, 3684 (2004).
[21]A. R. Smith, R. M. Feenstra, D. W. Greve, M. S. Shin, M. Skowronski, J. Neugebauer, and J. E. Northrup, Appl. Phys. Lett. **72**, 2114 (1998).
[22]G. Koblmüller, C. S. Gallinat, and J. S. Speck (unpublished).
[23]G. Koblmüller, R. Averbeck, H. Riechert, and P. Pongratz, Phys. Rev. B **69**, 035325 (2004).
[24]B. Heying, X. H. Wu, S. Keller, Y. Li, D. Kapolnek, B. P. Keller, S. P. DenBaars, and J. S. Speck, Appl. Phys. Lett. **68**, 643 (1996).
[25]V. V. Mamutin, V. A. Vekshin, V. Y. Davydov, V. V. Ratnikov, T. V. Shubina, S. V. Ivanov, P. S. Kopev, M. Karlsteen, U. Södervall, and M. Willander, Phys. Status Solidi A **176**, 247 (1999).
[26]M. Higashiwaki and T. Matsui, J. Cryst. Growth **269**, 162 (2004).
[27]I. Mahboob, T. D. Veal, C. F. McConville, H. Lu, and W. J. Schaff, Phys. Rev. Lett. **92**, 036804 (2004).

FIG. 3. Dependence of room-temperature Hall mobility and sheet carrier concentration on layer thickness for InN grown on N-face GaN on C-face 6H–SiC templates. A linear extrapolation of the carrier concentration to zero thickness yields an estimate of $\sim 3 \times 10^{13}$ cm^{-2} for the surface electron density.

Characterisation of Multiple Carrier Transport in Indium Nitride Grown by Molecular Beam Epitaxy

Tamara B. Fehlberg*, Gilberto A. Umana-Membreno, Brett D. Nener, Giacinta Parish, Chad S. Gallinat[1], Gregor Koblmüller[1], Siddharth Rajan[1], Sarah Bernardis[1] and James S. Speck[1]

School of Electrical, Electronic and Computer Engineering, The University of Western Australia, Crawley WA 6009, Australia
[1]*Materials Department, University of California, Santa Barbara, California 93106-5050, U.S.A.*

Transport properties of two distinct electron species in indium nitride grown by molecular beam epitaxy (MBE) have been measured. Variable field Hall and resistivity voltages were used in a quantitative mobility spectrum analysis (QMSA) to extract the concentrations and mobilities of the two electron species, attributed to the bulk electrons and a surface accumulation layer. Single magnetic field data corresponds to neither electron species. The bulk electron distribution has an extracted average mobility of $3570\,cm^2/(V\,s)$ at 300 K, which rises to over $5100\,cm^2/(V\,s)$ at 150 K. Bulk electron concentration in the sample is $1.5 \times 10^{17}\,cm^{-3}$. The surface electrons have a higher sheet charge density and an order of magnitude lower average mobility than those in the bulk. [DOI: 10.1143/JJAP.45.L1090]

KEYWORDS: indium nitride, MBE, QMSA, transport, characterisation

Recent improvements in indium nitride (InN) growth techniques have lead to the successful growth[1–3] of high quality crystalline InN layers. The focus now lies on characterisation and improvement of electrical properties. As with all III–nitrides the material is unintentionally doped highly n-type. In addition, it has been well established that in InN a surface electron accumulation layer exists.[2–6] Capacitance–voltage (C–V) measurements[4,6] and transport properties of layers grown with decreasing thickness[2–5] have indicated that the concentration of electrons is very much higher at the surface than in the underlying bulk material, while the mobility is significantly lower.

Conventionally, determination of transport properties is performed via a Hall measurement at a single magnetic field, which only presents an averaged contribution of all carriers in the sample. If more than one carrier exists, the calculated result may not necessarily represent any individual carrier species. As such, results reported for InN calculated from transport measurements performed at single magnetic fields are not likely to accurately represent the bulk electron properties when an accumulation layer of electrons exists at the surface.

A multivariate measurement over temperature and a large magnetic field range, together with quantitative mobility spectrum analysis (QMSA),[7] is a method of determining the transport characteristics of each carrier species present. The power of this method lies in the fact that the bulk properties can be extracted regardless of surface or interface contributions. Previous multi-field measurements on InN have only been performed with magnetic fields up to 4.5 T.[5,8] In this work, measurements were taken using magnetic fields of up to 12 T. The large magnetic fields enable the extraction of low mobility carriers, less than $1000\,cm^2/(V\,s)$, with much greater confidence. This work reveals the high electrical quality of the InN material under study.

The 2.7-µm InN layer was grown by plasma-assisted molecular beam epitaxy (MBE) on a semi-insulating (Fe-doped) Ga-polar gallium nitride (GaN) template at the University of California, Santa Barbara. InN was deposited at a substrate temperature of 450 °C under In-droplet conditions on an optimized GaN buffer layer.[2,3]

The sample was processed into eight-contact Hall bars, defined by hydrogen/methane reactive ion etching. Contacts were thermally evaporated. Variable field resistivity and Hall measurements were performed between 0 and 12 T on an Oxford Instruments superconducting magnet. A continuous flow liquid helium cryostat was used to provide measurement temperatures between 77 and 300 K. At a given temperature, measurements were made at 30 values of magnetic field, for each magnetic field polarity.

QMSA was performed using the Lakeshore iQMSA software package, based on the improved algorithm outlined by Vurgaftman et al.[7] The QMSA algorithm takes multi-field Hall and resistivity data and produces a spectrum showing the conductivity contributions of electrons and holes in the mobility domain. Unlike traditional multi-carrier fitting techniques, QMSA makes no *a priori* assumptions about the carriers present in the material.

The results from measurement of the Hall bar structure show clear signs of multi-carrier contributions to transport in both Hall coefficient, R_H, and the conductivity tensor, σ_{xy}. R_H, which for a single carrier would be constant as a function of magnetic field, varies significantly over the 0 to 12 T range. σ_{xy}, given in Fig. 1, shows a distinct "flattening" of the curve at high magnetic field values, indicating the presence of at least a second carrier with lower mobility.

The electron mobility spectrum generated by iQMSA for the Hall bar sample is given in Fig. 2 for 300 K. Very similar spectra were obtained for 77, 100, 150, 200, and 250 K. All mobility spectra clearly show two electron peaks. There is a low mobility electron carrier with significant conduction contributions at mobilities ranging from approximately 300 to $1000\,cm^2/(V\,s)$, and a high mobility electron distributed between 3000 and $7000\,cm^2/(V\,s)$, depending on the measurement temperature. The low mobility carrier is assigned to the surface electron, as the mobility corresponds to that in the literature found via Hall measurements on InN layers of decreasing thickness,[4,5] while the high mobility electron is assigned to the electrons throughout the bulk of the InN layer. Similar distinction is made by Swartz *et al.* in refs. 5 and 8.

The extracted transport properties for the two electron

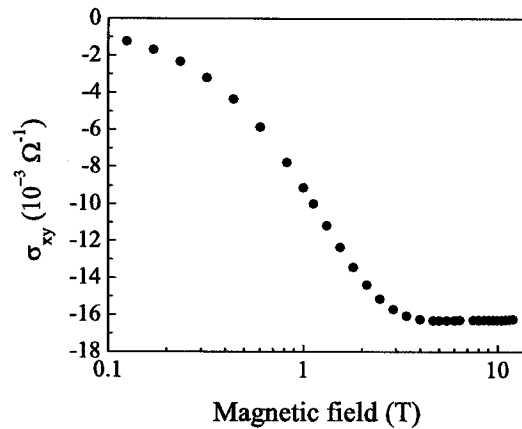*E-mail address: tamara@ee.uwa.edu.au

Fig. 1.   Conductivity tensor, σ_{xy}, as a function of magnetic field at 300 K.
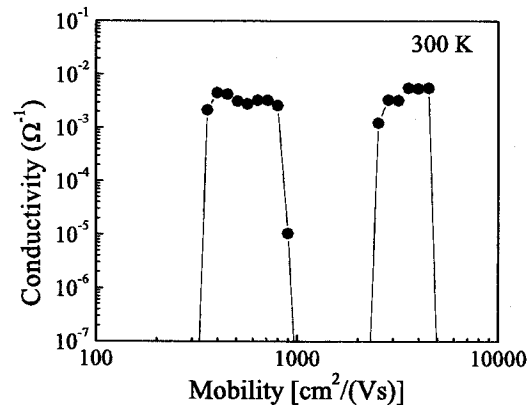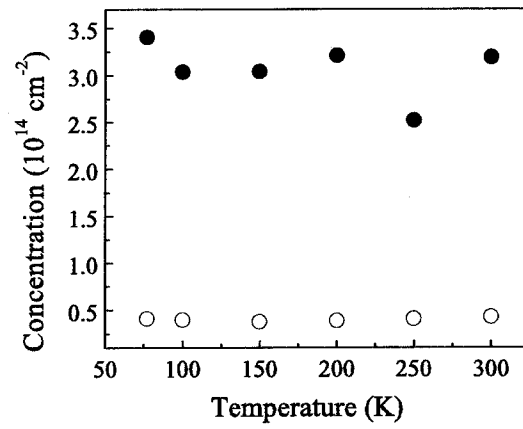

Fig. 2.   InN mobility spectrum 300 K determined from Hall bar measurements using the iQMSA algorithm.

Fig. 3.   The extracted sheet carrier density (a) and mobility (b) of bulk electron (open symbols) and surface electron (closed symbols) species in MBE grown InN as a function of temperature. Hall measurements were taken at variable magnetic fields using a Hall bar configuration.

species are given in Fig. 3. The mobility of each electron species is a weighted average over the entire peak in the mobility spectrum, and represents the mobility of the electron species as a whole.
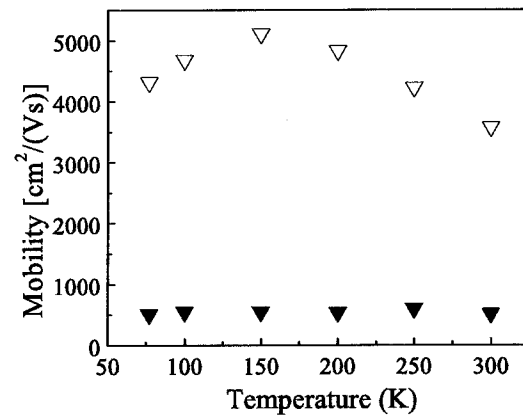
The largely temperature independent sheet density of around 4×10^{13} cm^{-2} for the higher mobility bulk electrons equates to a bulk density of approximately 1.5×10^{17} cm^{-3} over the 2.7 μm thickness of the layer. For comparison, single field Hall results for this sample (at 1 T) give a bulk concentration of 6×10^{17} cm^{-3} at 300 K. Clearly, the surface electron layer has a significant influence on the results; the electron concentration, when determined from a single magnetic field, is four times the actual bulk electron concentration.

The extracted mobility of the bulk electrons is 3570 cm^2/(V s) at 300 K, which is to our knowledge the highest ever reported for InN. Over the temperature range between 77 and 250 K the bulk mobility ranges from 4300 to over 5100 cm^2/(V s), as shown in Fig. 3. The variation of the mobility with temperature suggests that the bulk electron species is non-degenerate.

The theoretically calculated maximum mobility in InN with electron concentration around 10^{17} cm^{-3} at 300 K is approximately 4000 cm^2/(V s).[9,10] This suggests that the 300 K mobility of this film is approaching the theoretical limit, and thus the InN grown is of high crystal and electrical quality. The theoretical limit calculated at 77 K for 10^{17}

cm^{-3} InN, however, is 12000 cm^2/(V s)[9] which is more than twice the mobility measured. This indicates that a large number of defect, ion and impurity related scattering centres exist and are severely limiting the low temperature mobility of this material.

For the low mobility carrier attributed to surface accumulation electrons, the sheet charge density of around 3×10^{14} cm^{-2} (Fig. 3) is an order of magnitude higher than that reported by Lu et al. from C–V and variable thickness Hall measurements.[4] Lu et al. estimate the thickness of the surface accumulation to be on the order of 6 nm. A depth of 6 nm would give a volume concentration of 5×10^{20} electrons per cm^{-3} near the surface. The origin of the very high density surface charge seen in this particular sample remains under investigation.

The surface electron has a largely temperature independent mobility of about 500 cm^2/(V s), comparable with reported values.[4,5] While we have assigned the low mobility peak to the surface accumulation region, the peak would also contain any other low mobility carriers with similar mobilities in the device that have a significant contribution to conduction. Theory suggests that a GaN/ InN interface charge may exist.[4] If such an accumulation of carriers does exist and contributes to conduction at similar mobility values to the surface electrons it is unlikely to be resolved, since Hall measurements cannot differentiate between

Jpn. J. Appl. Phys., Vol. 45, No. 41 (2006)

I. B. FEHLBERG et al.

similar mobility carriers located in different regions of the material.

In summary, from variable magnetic field resistivity and Hall measurements we have extracted the transport properties of two electron species present in a 2.7-μm InN layer grown by MBE at temperatures between 77 and 300 K. QMSA has enabled the bulk electron properties to be separated from raw measurement data which contains significant contributions from the large accumulation of electrons at the surface. The high mobility of the bulk electrons in the InN sample, 3570 cm^2/(V s) at 300 K, signifies the high quality of the material.

Acknowledgements

1) H. Lu, W. J. Schaff, J. Hwang, H. Wu, G. Koley and L. F. Eastman: Appl. Phys. Lett. **79** (2001) 1489.
2) C. S. Gallinat, G. Koblmuller, J. S. Brown, S. Bernardis, J. S. Speck, G. D. Chern, E. D. Readinger, H. Shen and M. Wraback: Appl. Phys. Lett. **89** (2006) 032109.
3) G. Koblmuller, C. S. Gallinat, S. Bernardis, J. S. Speck, G. D. Chern, E. D. Readinger, H. Shen and M. Wraback: Appl. Phys. Lett. **89** (2006) 071902.
4) H. Lu, W. J. Schaff, L. F. Eastman and C. E. Stutz: Appl. Phys. Lett. **82** (2003) 1736.
5) C. H. Swartz, R. P. Tompkins, N. C. Giles, T. H. Myers, H. Lu, W. J. Schaff and L. F. Eastman: J. Cryst. Growth **269** (2004) 29.
6) R. E. Jones, K. M. Yu, S. X. Li, W. Walukiewicz, J. W. Ager, E. E. Haller, H. Lu and W. J. Schaff: Phys. Rev. Lett. **96** (2006) 125505.
7) I. Vurgaftman, J. R. Meyer, C. A. Hoffman, D. Redfern, J. Antoszewski, L. Faraone and J. R. Lindemuth: J. Appl. Phys. **84** (1998) 4966.
8) C. H. Swartz, R. P. Tomkins, T. H. Myers, H. Lu and W. J. Schaff: Phys. Status Solidi C **2** (2005) 2250.
9) V. W. L. Chin, T. L. Tansley and T. Osotchan: J. Appl. Phys. **75** (1994) 7365.
10) V. M. Polyakov and F. Schwierz: Appl. Phys. Lett. **88** (2006) 032101.

Excitation wavelength dependence of terahertz emission from InN and InAs

Grace D. Chern,[a] Eric D. Readinger, Hongen Shen, and Michael Wraback
U.S. Army Research Laboratory, Sensors and Electron Devices Directorate, AMSRD-ARL-SE-EM,
2800 Powder Mill Road, Adelphi, Maryland 20783

Chad S. Gallinat, Gregor Koblmüller, and James S. Speck
Materials Department, University of California, Santa Barbara, California 93106-5050

The authors report on the excitation wavelength dependence of terahertz emission from n-InN and bulk p-InAs pumped with femtosecond pulses tunable from 800 to 1500 nm. The terahertz amplitude, normalized to pump and probe power, from both narrow band gap semiconductors remains relatively constant over the excitation wavelength range. In addition, terahertz radiation from In- and N-face InN samples with bulk carrier concentrations ranging from 10^{17} to 10^{19} cm^{-3} is also investigated, showing a strong dependence of terahertz emission on bulk carrier concentration. The experimental results agree well with calculations based on drift-diffusion equations incorporating momentum conservation and relaxation. © *2006 American Institute of Physics.* [DOI: 10.1063/1.2358938]

The terahertz region of the electromagnetic spectrum, lying between microwave frequencies (100 GHz) and photonic frequencies (30 THz), is a potentially important region for a wide variety of applications, including imaging, time-domain spectroscopy, and material identification and characterization.[1–3] Traditionally, optically generated terahertz systems utilize femtosecond mode-locked Ti: sapphire lasers or continuous-wave (cw) lasers with a wavelength centered near 800 nm. Significant advantages associated with the use of telecommunications grade optoelectronics and compact fiber lasers could be gained in cost, size, weight, and efficiency by shifting the wavelength to 1550 nm if an appropriate narrow band gap semiconductor terahertz source were available. In addition, for cw terahertz generation obtained by photomixing (or optical heterodyne conversion), 1550 nm operation is advantageous because the photomixing conversion efficiency, which increases as λ^2, is about four times higher than for conventional terahertz systems using 800 nm. Terahertz generation using compact fiber laser systems has already been demonstrated with InAs, InSb, and GaAs.[4–6]

High quality InN thin films exhibit a band gap E_g below[7] 0.7 eV, a much smaller value than what was previously accepted ($E_g = 1.9$ eV or $\lambda = 650$ nm).[8] Recently, we have measured using absorption data an InN band gap below 0.65 eV in compressively strained InN films on GaN templates.[9] Estimates of the deformation potential point to an unstrained band gap of ~0.63 eV. By constructing InN/GaInN quantum well structures, it should be possible to engineer a material with a band gap close to 1550 nm for use with low-cost, 1550 nm lasers. Unlike conventional III-V semiconductor compounds, wurtzite III-nitride semiconductors possess a significant spontaneous polarization, leading to an internal electric field in quantum wells about an order of magnitude larger than that found in conventional III-V materials.[10] This phenomenon combined with a high saturation velocity ($>1.5 \times 10^7$ cm/s),[11] large intervalley spacing to confine carriers within the high mobility Γ valley, short

carrier lifetime, and potentially high breakdown voltage in InN may lead to up to an order of magnitude higher efficiency InN-based terahertz sources compared with the commonly employed arsenides.

Recently, Adomavicius *et al.*[12] have measured the spectral dependence of terahertz emission from (111) InAs at high carrier densities, where nonlinear effects are the dominant terahertz generation mechanism. Such high optical fluences, however, are not suitable for compact fiber lasers. Additionally, at lower carrier densities, the optical rectification contribution is no longer the main terahertz generation mechanism in (111) InAs, but becomes comparable to effects due to the difference of the electron and hole diffusion coefficients (photo-Dember effect).[13]

The possibility of terahertz emission from InN has been demonstrated by Ascazubi *et al.*,[14] who attributed the terahertz generation mechanism to transient photocurrents but did not specify the exact mechanism. Similar to InAs, InN has a surface accumulation layer, which has a width that is more than an order of magnitude shorter than the optical absorption length.[15] The high surface state density leads to a high field near the surface but virtually no field in the bulk of the crystal. The optically induced transient photocurrents in InN should therefore be similar to InAs, that is, due to the photo-Dember effect.

In this letter, we present a comparison of terahertz emission from n-InN and bulk p-InAs, one of the best known terahertz semiconductor surface emitters, excited with ultrafast laser pulses tuned between 800 and 1500 nm. The terahertz radiation generated from InAs and InN exhibits similar dependence on the excitation wavelength. The terahertz amplitude from both narrow band gap semiconductors remains on the same order of magnitude, while the pump wavelength is tuned from 800 to 1500 nm. At a fixed pump wavelength, the terahertz amplitude from n-InN is about an order of magnitude smaller than for p-InAs due to larger screening from n type as compared to p-type carriers, as well as larger screening due to a larger density of background electrons in the n-InN than background holes in the p-InAs. Terahertz radiation from In-

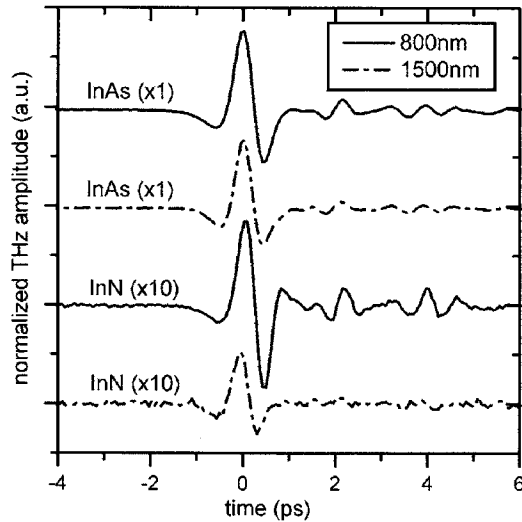[a]Electronic mail: grace.chern@arl.army.mil

FIG. 1. Time-domain wave forms of terahertz emission, normalized to pump and probe power, from bulk *p*-type InAs and In-face *n*-InN excited with 800 nm (solid line) and 1500 nm (dashed line) femtosecond pulses.
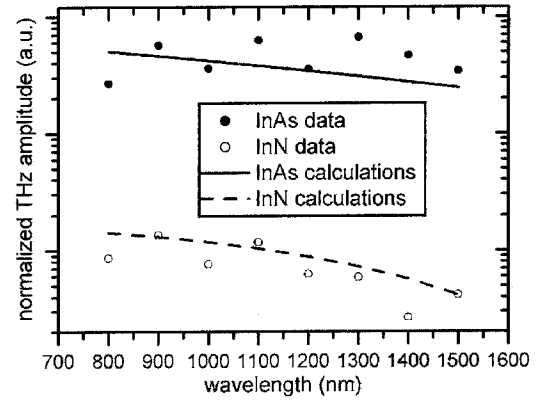

FIG. 2. Excitation wavelength dependence of terahertz amplitude, normalized to pump and probe power, from InN and InAs. The points indicate experimental data (solid circles: InAs and empty circles: InN) and lines indicate calculated results (solid: InAs and dashed: InN).

(Ref. 9) and N-face[16] *n*-InN samples with a bulk carrier concentration n_{bulk} ranging from 10^{17} to 10^{19} cm^{-3} is examined and shows a significant decrease as n_{bulk} increases. These results are consistent with the dominant mechanism for terahertz generation in InN and InAs being the current associated with the diffusion of the photogenerated electrons at elevated electron temperature (photo-Dember effect) and the redistribution of the background electrons under drift.

Our measurements are performed using a Coherent regenerative amplifier (RegA) system, which operates at 800 nm and has a repetition rate of 250 kHz. The output of the RegA is split into two beams. The stronger beam is frequency doubled to serve as the pump source for an optical parametric amplifier, which generates an infrared idler pulse tunable from 0.9 to 2.6 μm. The infrared beam, after compression with a prism pair to typical pulse widths of $\sim$150 fs, is then focused onto the semiconductor sample at a 45° incidence angle with a beam diameter of $\sim$1 mm. The pump power is $\sim$4 mW for all excitation wavelengths. The subsequent terahertz emission from the semiconductor surface is collected with a pair of parabolic mirrors onto a ZnTe crystal for electro-optic sampling. The weaker RegA split-off beam is used to probe the terahertz emission for all excitation wavelengths, as well as to irradiate the samples at 800 nm.

The *n*-InN sample used for the excitation wavelength dependence measurements is a 1-μm-thick In-face film grown by molecular beam epitaxy on an Fe-doped GaN template with a GaN buffer layer. Details of the growth technique are described elsewhere.[9] The unintentionally doped *n*-InN sample has a bulk carrier concentration of 2.25 $\times 10^{17}$ e/cm^3, a Hall mobility of 2098 cm^2/V s, and a threading dislocation density of $\sim$3 $\times 10^{10}$ cm^{-2} (as determined by x-ray diffraction and transmission electron microscopy measurements). A description of the growth technique for the N-face InN samples can be found in Ref. 16. The *p*-type (111) InAs sample is 450 μm thick with a doping level of $\sim$10^{16} cm^{-3}.

Figure 1 shows the time-domain wave forms of the terahertz emission, normalized to pump and probe power, from bulk *p*-type InAs and *n*-InN optically excited with 800 nm

(solid line) and 1500 nm (dashed line) femtosecond pulses. For both semiconductors, the terahertz amplitude at 800 nm is comparable to the signal amplitude at 1500 nm. This result is reflected in the systematic measurements of the terahertz emission from InAs and InN at excitation wavelengths varying from 800 to 1500 nm displayed in Fig. 2. Measurements of terahertz emission as a function of azimuthal angle (about the surface normal) indicate that the optical rectification component is small ($<10\%$) for InAs and negligible for InN.

A one-dimensional momentum conservation and relaxation equation,

$$\frac{\partial J_n}{\partial t} = e\left(n\frac{eE}{m^*} + \frac{kT}{m^*}\frac{\partial n}{\partial x}\right) - \frac{J_n}{\tau}, \tag{1}$$

with a *k*-dependent effective mass[17] m^* is used to simulate the subpicosecond electron current density J_n. The parameters e, n, E, T, and τ are the elementary electric charge, carrier concentration, electric field, carrier temperature, and momentum relaxation time, respectively. Photogenerated and background electron currents are calculated separately due to their different carrier temperatures. Both the photogenerated and background hole currents are calculated using drift-diffusion equations assuming that their temperatures are invariant at room temperature. These equations with carrier conservation equations are solved using a modified Scharfetter-Gummel scheme.[18] The emitted terahertz signal is then calculated as the volume integration of the time derivative of the total current density.

Modeling shows that the dominant currents are the diffusion of the photogenerated electrons at elevated electron temperature [the second term on the right hand side of Eq. (1)] and the redistribution of the background electrons under drift effect [the first term on the right hand side of Eq. (1)]. As the excitation wavelength increases, the photoexcited electron temperature decreases, thereby lowering the terahertz amplitude. However, the photon number increases as the excitation wavelength increases, enhancing the terahertz amplitude. As the excitation wavelength goes from 800 to 1500 nm for InN, the photoexcited electron temperature decreases by a factor of 5 while the photon number increases by a factor of $\sim$1.9, producing an overall decrease of less than four times. The decrease in terahertz signal for InN is only slightly larger than for *p*-InAs (E_g=0.36 eV),
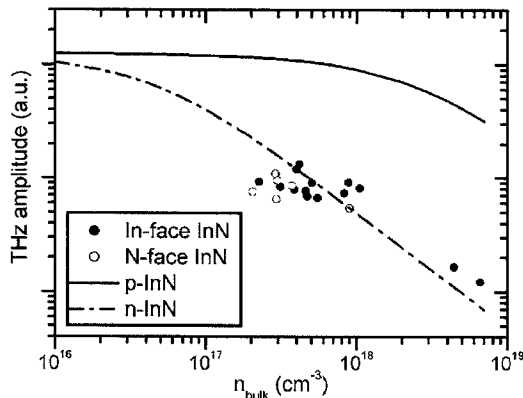
FIG. 3. Terahertz amplitude dependence on bulk carrier density n_{bulk} for In-(solid circles) and N-face (empty circles) InN samples optically excited with 800 nm femtosecond pulses. Calculated results for p-type and n-type InN are shown with solid and dashed lines, respectively.

where the photoexcited electron temperature decreases by a factor of 2.5, giving an overall decrease in signal amplitude of less than two times from 800 to 1500 nm. The experimental results agree well with calculations (solid and dashed lines in Fig. 2).

The measured terahertz amplitude from n-InN is about an order of magnitude smaller than from p-InAs due to larger screening from the higher mobility electrons as compared to holes. For example, at the fixed bulk carrier concentration of 10^{18} cm^{-3}, the calculations in Fig. 3 show that the terahertz amplitude from p-InN would be more than an order of magnitude larger than from n-InN. The higher density of background carriers in the InN sample, as compared to InAs, also contributes to the larger screening effect. As seen in Fig. 3, the measured normalized terahertz amplitude from InN decreases by about one order of magnitude as the bulk carrier concentration n_{bulk} increases by one order of magnitude. Although there are several other effects which contribute to the terahertz amplitude, including photoexcited electron temperature, mobility, absorption, and carrier lifetime, screening from carriers appears to be the dominant effect. There is no discernable difference between the In- and N-face InN samples, as expected for the improved crystalline quality and concomitant low background electron density and high mobility for both polarities.[9,16] Liu *et al.*[13] have shown a similar dependence on carrier concentration for the terahertz radiation from InAs.

In summary, we have demonstrated a similar excitation wavelength dependence of terahertz emission from n-InN and bulk p-InAs excited with femtosecond laser pulses. When the excitation wavelength is tuned from 800 to 1500 nm, the terahertz amplitude from both narrow band gap semiconductors remains on the same order of magnitude. The terahertz amplitude from n-InN is about an order of magnitude smaller than for p-InAs due to larger screening from n-type as compared to p-type carriers, as well as a higher density of background electrons in InN than background holes in p-InAs. It is expected that the terahertz power from InN will improve with lower n-type bulk carrier concentration or p-type doping, as well as with manipulation of the large built-in electric fields associated with the spontaneous and piezoelectric polarizations in this material.

[1] D. Grischkowsky, S. Keiding, M. van Exter, and C. Fattinger, J. Opt. Soc. Am. B **7**, 2006 (1990).
[2] B. B. Hu and M. C. Nuss, Opt. Lett. **20**, 1716 (1995).
[3] D. M. Mittleman, R. H. Jacobsen, and M. C. Nuss, IEEE J. Sel. Top. Quantum Electron. **2**, 679 (1996).
[4] H. Ohtake, Y. Suzuki, N. Sarukura, S. Ono, T. Tsukamoto, A. Nakanishi, S. Nishizawa, M. L. Stock, M. Yoshida, and H. Endert, Jpn. J. Appl. Phys., Part 2 **40**, L1223 (2001).
[5] H. Takahashi, Y. Suzuki, M. Sakai, S. Ono, N. Sarukura, T. Sugiura, T. Hirosumi, and M. Yoshida, Appl. Phys. Lett. **82**, 2005 (2003).
[6] M. Nagai, K. Tanaka, H. Ohtake, T. Bessho, and T. Sugiura, Appl. Phys. Lett. **85**, 3974 (2004).
[7] J. Wu, W. Walukiewicz, K. M. Yu, J. W. Ager III, E. E. Haller, H. Lu, W. J. Schaff, Y. Saito, and Y. Nanishi, Appl. Phys. Lett. **80**, 3967 (2002).
[8] T. Tansley and C. P. Foley, J. Appl. Phys. **59**, 3241 (1986).
[9] C. S. Gallinat, G. Koblmüller, J. S. Brown, S. Bernardis, J. S. Speck, G. D. Chern, E. D. Readinger, H. Shen, and M. Wraback, Appl. Phys. Lett. **89**, 032109 (2006).
[10] F. Bernardini, V. Fiorentini, and D. Vanderbilt, Phys. Rev. B **56**, R10024 (1997).
[11] S. K. O'Leary, B. E. Foutz, M. S. Shur, and L. F. Eastman, Appl. Phys. Lett. **87**, 222103 (2005).
[12] R. Adomavicius, G. Molis, A. Krotkus, and V. Sirukaitis, Appl. Phys. Lett. **87**, 261101 (2005).
[13] K. Liu, J. Xu, T. Yuan, and X.-C. Zhang, Phys. Rev. B **73**, 155330 (2006).
[14] R. Ascazubi, I. Wilke, K. Dennison, H. Lu, and W. J. Schaff, Appl. Phys. Lett. **84**, 4810 (2004).
[15] I. Mahboob, T. D. Veal, C. F. McConville, H. Lu, and W. J. Schaff, Phys. Rev. Lett. **92**, 036804 (2004).
[16] G. Koblmüller, C. S. Gallinat, S. Bernardis, J. S. Speck, G. D. Chern, E. D. Readinger, H. Shen, and M. Wraback, Appl. Phys. Lett. **89**, 071902 (2006).
[17] E. O. Kane, J. Phys. Chem. Solids **1**, 249 (1957).
[18] D. L. Scharfetter and H. K. Gummel, IEEE Trans. Electron Devices **16**, 63 (1969).

Surface kinetics and thermal instability of N-face InN grown by plasma-assisted molecular beam epitaxy

G. Koblmüller,[a] C. S. Gallinat, and J. S. Speck
Materials Department, University of California, Santa Barbara, California 93106-5050

The role of thermal instability and In surface coverages on the growth kinetics has been investigated for N-face InN films grown by plasma-assisted molecular beam epitaxy. Film thickness analysis using scanning electron microscopy combined with In desorption measurements by quadrupole mass spectrometry demonstrated significant thermal decomposition starting at ~560 °C and inhibiting growth completely beyond ~635 °C. Within this temperature region two decomposition pathways were identified: a low-temperature regime characterized by In droplet accumulation and a high-temperature regime with direct desorption from bulk InN. A growth diagram has been constructed, exhibiting three characteristic growth structures for different In/N flux ratios and growth temperatures: a dry no-adlayer terminated surface under N-rich conditions, an In adlayer terminated surface, and a surface, consisting of an In adlayer and droplets under In-rich conditions. Smooth step-flow growth terraces were observed in films grown under In-rich and surprisingly also under N-rich conditions at temperatures of thermal decomposition. Such high adatom diffusivity resulted from the autosurfactant action of the In adlayer, with a saturated coverage of 1 ML as determined from the reflection high energy electron diffraction patterns during the consumption of adsorbed In by active nitrogen. © *2007 American Institute of Physics.* [DOI: 10.1063/1.2718884]

I. INTRODUCTION

With the recent re-evaluation of the InN band gap energy of close to 0.7 eV,[1,2] this material has become one of the core subjects in group-III nitride research. Because of its narrow gap, many promising applications have been proposed, from photonic devices at optical communication wavelengths[3] to the fabrication of light emitters operating from near-infrared to deep ultraviolet if alloyed with other group-III nitrides.[4] InN has recently been also demonstrated as a potential candidate for terahertz emission.[5] Moreover, the outstanding transport properties, especially high peak drift velocities[6] and Hall mobilities exceeding 3500 cm²/Vs at room temperature,[7] call for the implementation of InN into high-speed microelectronic devices.

The growth of InN, however, has remained quite challenging, due to its inherent thermal instability and high dissociation rates. The resulting necessity for low growth temperatures, along with the large lattice mismatch with common substrates (e.g., sapphire or silicon carbide), generate often unsatisfactory three-dimensional surfaces.[8,9] Unlike the surfactant-mediated growth of GaN (Ref. 10) or AlN (Ref. 11) by plasma-assisted molecular beam epitaxy (PAMBE), where sufficiently high growth temperatures and metal-rich conditions produce smooth surfaces, adatom diffusion remains an unresolved issue in InN growth. In GaN growth, for instance, it is well established that a steady-state metallic Ga adlayer increases the adatom diffusion and seems necessary to achieve superior material quality.[12] Recent InGaN growth studies also point to the existence of a stable In adlayer on the surface,[13,14] but for binary InN

growth very limited experimental knowledge exists about adatom mobility and its correlation to surfactants. So far, the only effective increase of adatom diffusion in InN growth has been reported for migration-enhanced MBE, where growth was achieved with alternating indium flux and nitrogen plasma.[15] In this case, two-dimensional (2D) step-flow growth features were observed, which still appear inferior to common growth morphologies for GaN. As an additional limitation in the PAMBE growth of In-face InN, it has been shown that InN dissociates at temperatures lower than those required for the desorption of metallic In.[16] Thus, the formation of detrimental In droplets under In-rich conditions cannot be inhibited.[17] Recent attempts, however, to grow InN along the N-face orientation allowed growth temperatures of 100 °C higher than the thermal dissociation limit of In-face InN, and which also seemed to facilitate the growth of smooth step-flow-like morphologies without any droplets.[18,19]

In this work, we report growth of InN along the N-face [i.e., $(000\bar{1})$] orientation where we study both the growth kinetics and thermal stability. From these results, we develop a consistent N-face InN growth diagram that allows accurate determination of the PAMBE growth conditions to achieve optimum surface morphology. Additionally, the In adlayer coverage, which is essential for controlling the surfactant-mediated growth of InN, is quantified.

II. EXPERIMENTS

All InN layers were grown in an Epi 620 MBE system with standard effusion cells for the group-III elements and an EPI Unibulb radio frequency plasma source for active nitrogen. The substrate temperature was measured with a pyrom-

[a]Electronic mail: gregor@engineering.ucsb.edu

eter with maximum sensitivity at 940 nm. The templates used were freestanding N-face GaN substrates provided by Lumilog with threading dislocation densities specified to less than 1×10^8 cm^{-2}. To produce a homogenous InN/GaN interface and eliminate the effects of surface contamination, the substrates were overgrown with ~40 nm of GaN under Ga-rich conditions at a temperature of 700 °C. The Ga flux was chosen such that Ga droplets would form on the surface, which typically yields very smooth surfaces without any surface pitting.[12] Before initiating the InN growth, the substrate temperature was increased to 730 °C to desorb all Ga droplets. All fluxes are expressed in $(000\bar{1})$ InN growth rate units, as measured by cross-sectional scanning electron microscopy (SEM) of In-limited and N-limited InN films at temperatures of negligible thermal decomposition. For conversion to a.u., we note that in wurtzite InN one-half of the c lattice constant ($c/2 = 0.288$ nm) or 9.17×10^{14} InN/cm^{-2} areal density refer to 1 ML (monolayer) along the $(000\bar{1})$ direction.

Cross-section SEM was used to determine the thermal decomposition rates by the growth rate reduction for InN layers grown at increased temperatures. To also quantify the decomposition behavior and surface kinetics of InN *in situ*, we employed a quadrupole mass spectrometer (QMS) in direct line of sight to the sample surface to monitor the desorbing In atoms. A description of the experimental setup and the data acquisition was presented in detail in our earlier work.[20] To express the In desorption rate in units of InN equivalent growth rate, we calibrated the QMS detector response by exposing a sapphire wafer at 750 °C to a series of known In fluxes well below the critical flux for In droplet formation. These experiments provided a direct proportionality constant of 2.87×10^{-12} Torr nm/min between the measured ^{115}In partial pressure and the total desorbing In flux in equivalent growth rate units of nm/min. To assess the In adlayer coverage during InN growth, we monitored the integrated intensity of the reflection high energy electron diffraction (RHEED) specular spot (00) along the $[11\bar{2}0]$ azimuth in real time, as has been routinely shown for Ga surface coverages during GaN growth.[21,22] This method employs the oscillatory transients in RHEED intensity, which are observed during adsorption, desorption, or nitridation of metallic adlayers. Additionally, atomic force microscopy (AFM) in tapping mode was used to determine the characteristic surface morphologies.

III. RESULTS

A. Thermal decomposition

The temperature dependence of the N-face InN growth rate, as measured by cross-section SEM, is shown in Fig. 1(a). All InN layers were grown for 2 h under identical In-rich flux conditions ($\Phi_{In} = 10$ nm/min) with a slightly lower N flux ($\Phi_N = 7.3$ nm/min). Up to temperatures of ~560 °C the growth rate equaled the supplied N flux, which resembled the typical metal-rich growth behavior of GaN (Ref. 10) and AlN,[11] where the growth rate was limited by the active N flux. With increasing temperature though, the InN
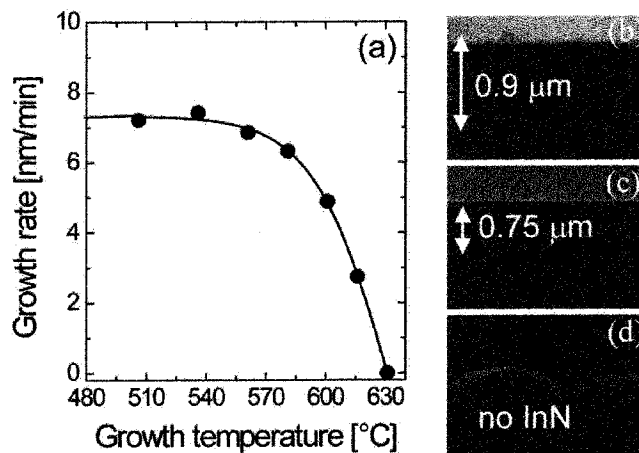

FIG. 1. (a) Growth rate of N-face InN as a function of growth temperature for N-limited growth (N flux=7.3 nm/min). The data points were determined from thickness measurements by cross-section SEM, exemplified for three different temperatures: (b) 560 °C, (c) 580 °C, and (d) 635 °C. Note the decrease in InN thickness with increasing temperature and the accumulation of In droplets in (d).

growth rate decreased substantially, yielding no growth beyond 635 °C. Instead, and as found by other groups,[9,18] macroscopic In droplets formed on the surface [Fig. 1(d)], suggesting that the sum of excess In supply and rate of In accumulation by InN decomposition was higher than the desorption of the saturated In adlayer from the surface.[16] To quantify the decomposition of N-face InN, we determined its effective activation energy. Arrhenius fits of the temperature dependence of the growth rate reduction (in the range of 590–635 °C) yielded an activation energy of about 1.2 eV.

To further investigate the temperature dependence of the In/N flux ratio on the growth rate, we have also grown a series of InN layers under slightly N-rich conditions (In/N=0.82). Both onset temperature for decomposition and the decrease in growth rate were similar to the In-rich growth case, indicating the InN decomposition rate has little dependence on the incident In flux.

More detailed analysis of the decomposition process was conducted using the QMS technique, which facilitated monitoring the In desorption in direct proportionality of the InN decomposition rate. For these studies, the InN films were grown at fairly low temperature (i.e., 540 °C) under slightly N-rich conditions (to prevent the formation of In droplets on the surface) and then incrementally heated to a final temperature of 650 °C. It is important to note that during this experiment neither nitrogen nor indium were supplied to the surface. The monitored In desorption into vacuum is shown in Fig. 2(a) and has three characteristic regimes, as follows.

The low-temperature regime (I) illustrates the In desorption for temperature increments between 560 and 595 °C. In this regime, we observed low In desorption, concurrent with quite low intensity RHEED diffraction streaks (see inset). RHEED intensities of low contrast are typically associated with a surface structure consisting of a metallic adlayer and droplets on top, where the latter cause severe shadowing effects of the diffracted electron beam.[21] Thus, this regime can be referred to strong *metal In accumulation* due to thermally limited desorption of the metallic In adlayer and droplets
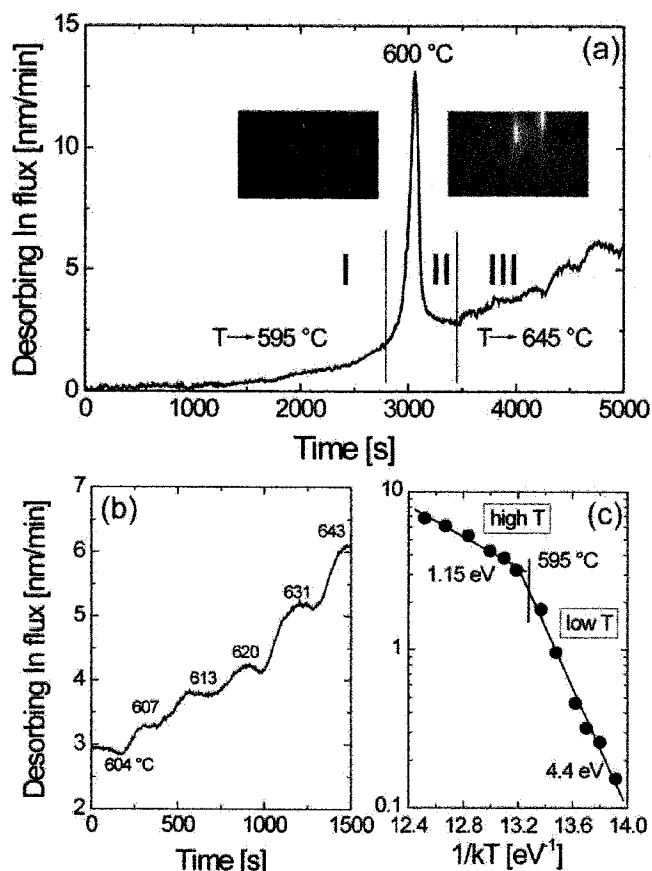
FIG. 2. (a) In desorption measured by QMS during InN decomposition in a temperature range between 560 and 645 °C (insets show typical RHEED patterns on each side of the desorption maximum); (b) closeup view of the In desorption in the high-temperature region III: (c) Arrhenius presentation of In desorption over $1/kT$ yielding two activation energies of 4.4 eV (low T) and 1.15 eV (high T).

FIG. 3. (a) In desorption of $\approx$40 ML In adsorbed on a N-face GaN surface at different temperatures. The steady-state desorption (after closure of the In shutter) represents the maximum desorption of In (i.e., droplet boundary), yielding (b) an activation energy of 2.5 eV when plotted as a function of $1/kT$.

terminating the decomposing InN surface structure.

When the temperature was increased from 595 to 605 °C (regime II), the desorption signal increased rapidly to a sharp maximum at ~600 °C, before it stabilized at a rate of ~2.8 nm/min at 605 °C. The concurrent transition in RHEED pattern from a low intensity to a high intensity streaked pattern indicates a significant change on the InN surface where the majority of accumulated droplets have desorbed.

Further temperature increase caused no change in RHEED pattern but a stepwise increase in the In desorption rate, exceeding a rate of 6 nm/min at 643 °C [also shown in a closeup view in Fig. 2(b)]. We refer this region (III) to a regime of "dry" *InN decomposition*, because the progressively constant high intensity RHEED pattern suggests no further metallic In accumulation on the surface.

Investigating the temperature dependence of the In desorption over the entire temperature region yielded two different Arrhenius dependencies: (i) at low temperatures the desorption process underlies a high activation energy (E^A=4.4 eV) and (ii) at high temperatures above 595 °C the activation energy was much lower (E^A=1.15 eV). The latter describes more the true energy barrier for decomposition, matching favorably with the value determined independently
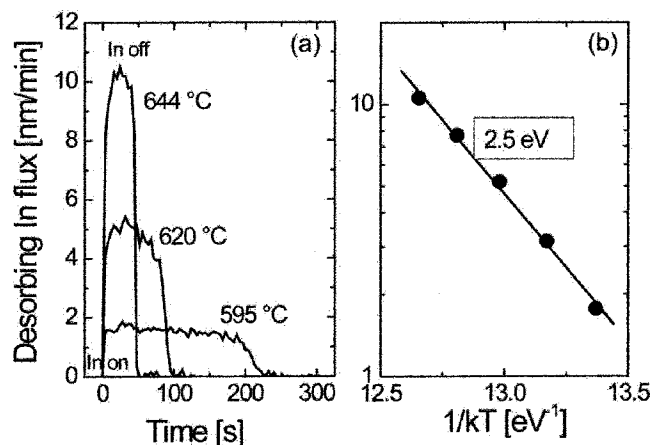
from the growth rate reduction by *ex situ* cross-section SEM (E^A=1.2 eV).

Further comparison of the In desorption rate (by QMS) with the growth rate reduction (by SEM) demonstrates that our assumption of direct proportionality between In desorption flux and InN decomposition rate holds true. In addition, these results show that the decomposition rates are the same for vacuum conditions (no active nitrogen) and typical growth conditions (under active nitrogen), which will be discussed more in detail later.

B. Metallic In accumulation and desorption

To develop a MBE growth diagram as recently established for GaN (Ref. 10) and AlN,[11] it is important to determine the boundary flux for metallic droplet formation. Precise knowledge of this droplet boundary flux has proven as the most critical measure for controlling and optimizing the PAMBE growth of nitrides.[10–12,14,20,23] Assessing this boundary flux for the metallic In droplets, we conducted a temperature dependent In wetting experiment on a N-face GaN substrate. Selection of a substrate different from InN was necessary, to avoid measuring contributions in In desorption caused by InN decomposition at elevated temperatures.

These In wetting experiments were performed by adsorbing the equivalent of ~40 ML of In onto the GaN surface and measuring its subsequent desorption into vacuum by QMS. The results are shown in Fig. 3(a) and demonstrate evidence for two distinct desorption regimes at a given temperature: first, upon closing the In shutter, a steady-state desorption regime was observed, followed by a monotonic decrease to zero desorption—this mimics the behavior we have previously identified for the desorption of adsorbed Ga from GaN and AlN surfaces.[24,25] In these cases, the steady-state desorption was attributed to the desorption of droplets (by maintaining the adlayer in its equilibrium), while the final monotonic decrease was associated with the decay of the remaining adlayer.

According to these observations, the steady-state In desorption represents thus the maximum desorbing In flux as the limit of In droplet accumulation. From the plot over inverse temperature [Fig. 3(b)] this boundary flux can be expressed by

$$\Phi^{\text{In(droplets)}} = (6.2 \times 10^{14} \text{ nm/min}) \exp\left(\frac{-2.5 \text{ eV}}{kT}\right), \quad (1)$$

where k is the Boltzmann constant and T is the substrate temperature in Kelvin. The Arrhenius-type fit to the data resulted in an activation energy of 2.5 eV, which agrees well with the evaporation energy of In over liquid In ($E^A = 2.49$ eV), as derived from equilibrium In vapor pressure data.[26] The prefactor of 6.2×10^{14} nm/min corresponds to a desorption attempt frequency of 3.95×10^{13} Hz.

The effect of substrate material on the In desorption boundary has been elucidated, in particular, also for Ga-polar GaN and Al-polar AlN substrates. We have observed similar steady-state In desorption levels and nearly identical activation energies ($E^A = 2.5 \pm 0.2$ eV). Hence, we state that the desorption boundary for metallic In is independent of the underlying substrate and should also hold for InN as the host surface.

C. Growth diagram for N-face InN

Constructing a growth diagram for N-face InN, the most challenging part is determining the temperature dependence of the net In accumulation rate on the surface. The net In accumulation rate can be defined as the difference of two competitive processes: (i) InN decomposition and its effective In flux from bulk InN *to* the surface, and (ii) the rate of maximum In desorption *from* the surface (i.e., droplet boundary).

For the case where no impinging In or N fluxes were supplied to the surface (i.e., stationary, no growth case), these competitive rates were both evaluated in Figs. 2 and 3 and illustrated again in Fig. 4, showing the maximum In desorption rate $\Phi^{\text{In(droplets)}}$ (black curve) and the InN decomposition rate $\Phi^{\text{In,dec}}$ (blue curve). Up to ~610 °C, In generated on the surface from decomposing InN is apparently limited by the maximum In desorption rate, inevitably resulting in the accumulation of metallic In (a saturated adlayer and droplets). In contrast, at higher temperatures $\Phi^{\text{In(droplets)}}$ exceeded $\Phi^{\text{In,dec}}$, confirming the earlier conclusion that InN decomposes at high temperature without the accumulation of In droplets. The net In accumulation rate on the surface can therefore be determined by the difference between the two curves, $\Phi^{\text{In(droplets)}} - \Phi^{\text{In,dec}}$. As demonstrated in Fig. 4(b), this gives an In adsorption diagram for the case that additional In is impinging on the surface.

Depending on the substrate temperature and impinging In flux two InN surface structures can be depicted—(i) at low temperature, any incident In flux yields a surface terminated by In droplets on top of an adlayer (the nature of the adlayer is determined in detail in Sec. III E). (ii) At temperatures ≥ 610 °C, In droplets can form only for In fluxes greater than the difference $\Phi^{\text{In(droplets)}} - \Phi^{\text{In,dec}}$. In the limit of lower In fluxes, all impinging In can desorb, and the surface is
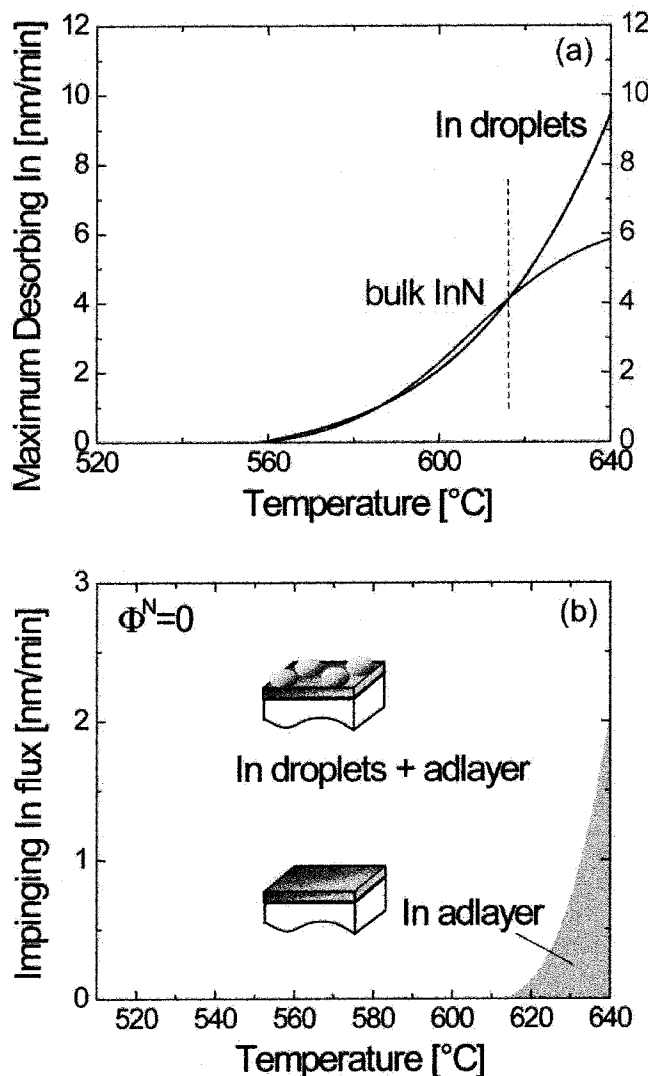

FIG. 4. (Color online) (a) Evaluation of the net In accumulation rate on the surface by balancing (1) the rate of thermal decomposition from bulk InN "to" the surface (blue curve) with (2) the rate of maximum In desorption "from" the surface (black curve). The difference between the two curves yields (b) a surface structure diagram for impinging In flux vs substrate temperature (In adsorption), showing a small region where an In adlayer can be formed on the surface and a large region of In droplet formation.

suggested to be terminated merely by the In adlayer, similar to the Ga adlayer stabilized GaN surface found in previous Ga adsorption studies.[20,24]

Picturing the more complex growth case, we identified the role of active N flux (i.e., In/N ratio) on the growth surface. For the results presented here, we used a constant N flux of $\Phi_N = 7.3$ nm/min under variable incident In fluxes. Considering the conservation of a 1:1 film stoichiometry of In:N atoms, InN decomposition limits the N-limited growth rate to g.r. $= \Phi_N - \Phi^{\text{In,dec}}$, where $\Phi^{\text{In,dec}}$ represents again the effective In flux from bulk to surface due to decomposition. In the growth case, we defined $\Phi^{\text{In,dec}}$ as the In loss, which could be directly assessed from the growth rate reduction determined by SEM [Fig. 1(a)], and which in first order approximation is independent of the incident In flux.

The combined curves for the In loss $\Phi^{\text{In,dec}}$ and the maximum In desorption $\Phi^{\text{In(droplets)}}$ (i.e., droplet boundary)
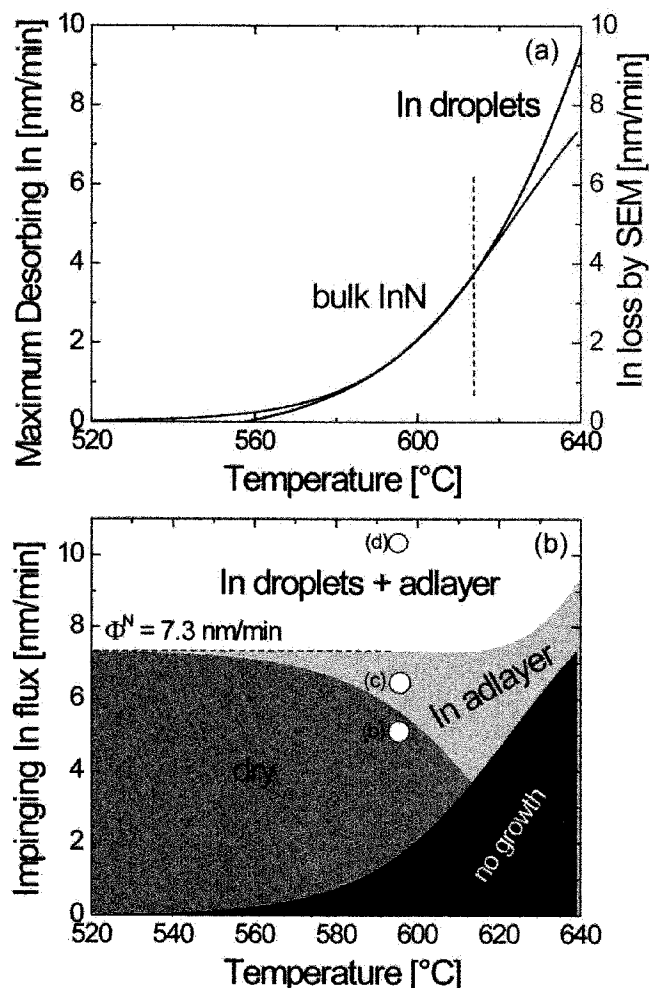
FIG. 5. (Color online) (a) Determination of the net In accumulation rate on the surface for the growth case showing (1) the rate of thermal decomposition from bulk InN, i.e., the In loss from the SEM growth rate analysis (blue curve) and (2) the rate of maximum In desorption "from" the surface (black curve). Similar to Fig. 4, the difference between the two curves allows to construct (b) a growth structure diagram for actual growth conditions (i.e., impinging In flux at constant N flux versus growth temperature). Three characteristic growth surface structures can be achieved: one dry no-adlayer terminated surface, one In adlayer stabilized surface, and one consisting of In droplets on top of the adlayer. Growth is found unsustainable at temperatures above ~635 °C.

are illustrated in Fig. 5(a). Essentially, both curves follow the same trend as in the stationary (no growth) case. Calculation of the net In accumulation rate for In-rich conditions yielded again the boundary line between the In adlayer terminated surface and the surface consisting of In droplets and adlayer as shown in the growth diagram of Fig. 5(b). Since the growth diagram underlies also the temperature dependence of the growth rate, additional surface structures can be realized. We classified in total three different growth surfaces, in accordance with the possible surface structures on the GaN growth front:[10,12,20] (i) In droplet-on top of adlayer-structure under In-rich growth conditions; (ii) In adlayer structure under slightly In-rich and also slightly N-rich growth conditions at high temperatures; and (iii) a dry no-adlayer terminated surface under more N-rich growth conditions.

The second important boundary, the boundary between the In adlayer terminated surface and dry no-adlayer termi-nated surface under N-rich conditions, is given by the ratio between In loss due to decomposition and excess N flux at a given temperature. If the excess N flux is larger than the effective In loss, then all In on the surface is consumed by the excess N leaving a dry surface. In contrast, if the excess N flux is smaller than the effective In loss, then part of the In on the surface is consumed by the excess N, while the other part is in an adsorption/desorption equilibrium with the surface, thus generating an incomplete In adlayer.

D. InN surface morphologies

The surface morphologies for the different growth re-gimes have been investigated by growing nominally 1 μm thick InN layers on freestanding N-face GaN templates under variable In/N flux ratios and temperatures. Despite InN growth was sustainable up to temperatures of 635 °C, InN layers grown between 610 and 635 °C directly on GaN did not exhibit the single-crystalline wurtzite phase, as deter-mined from Ω-2Θ scans using high-resolution x-ray diffrac-tion (HRXRD). This result was also independent of the cho-sen In/N flux ratio and further agrees with the current temperature limit of ~600 °C for N-face InN growth deter-mined by Xu et al. under similar growth rate (i.e., N flux) conditions.[18] Therefore, we present InN layers grown at a slightly lower temperature of 595 °C with In fluxes ranging from 5 nm/min (N-rich growth) to 10 nm/min (In-rich growth) at fixed N flux of 7.3 nm/min [illustrated by the open symbols in Fig. 5(b)].

Prior to the InN growth we investigated the ≈40 nm GaN buffer layer grown under Ga-rich droplet conditions. Recently, we demonstrated that the growth of a homoepi-taxial GaN buffer layer was necessary to significantly im-prove both structural and electrical properties in InN films, by also effectively suppressing the impurity incorporation at the substrate interface.[17] The respective surface morphology of this GaN buffer is shown in the AFM image of Fig. 6(a), which consists of an array of narrow terraces separated by ~2–3 Å high steps [equivalent to one (0001) GaN mono-layer] and occasional surface pits.

The InN layers grown under the different In fluxes ex-hibited a wide variety in surface morphology, as illustrated in the AFM images in Fig. 6. InN grown under very N-rich conditions (Φ_{In}=5 nm/min) yielded a very rough surface morphology characterized by a high density of pits and fac-ets and a root mean square (rms) larger than 100 nm over a 10×10 μm^2 area [Fig. 6(b)]. Analysis of several layers grown under N-rich conditions in a temperature range of 500–600 °C showed similarly rough surface structures.

A slightly smoother and more coalesced morphology with larger flat areas was observed for InN growth performed under less N-rich conditions (Φ_{In}=6.5 nm/min), where we proposed the In adlayer (or at least fractions of it) to termi-nate the surface. The rms roughness decreased substantially to below 30 nm over a 10×10 μm^2 and 0.15 nm over a 1×1 μm^2 area, as compared to the more N-rich growth stated above. Analysis of the atomically flat plateaus re-
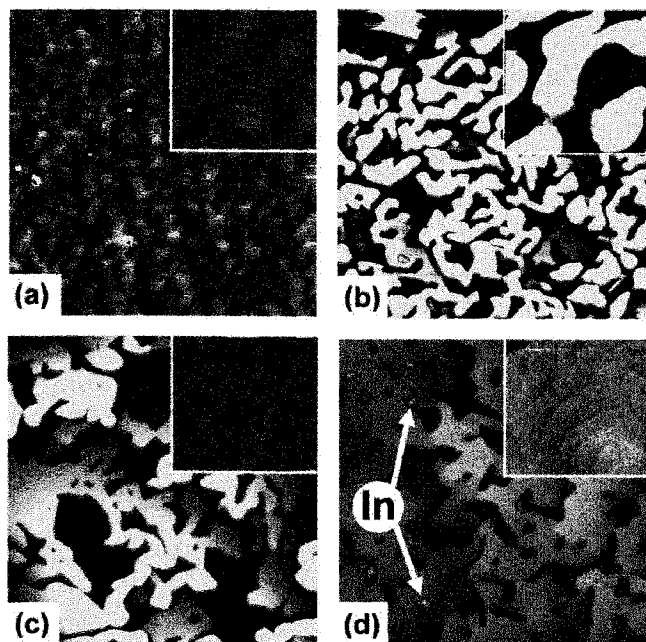
FIG. 6. 10×10 and 1×1 μm^2 (insets) AFM micrographs of 1 μm thick InN layers grown on N-face freestanding GaN templates with (a) $a \approx 40$ nm GaN buffer layer, under conditions of constant temperature ($T = 595$ °C) but variable In fluxes of (b) 5 nm/min (dry N-rich regime), (c) 6.5 nm/min (In-adlayer N-rich regime), and (d) 10 nm/min (In-droplet regime). The height scale of the 10×10 μm^2 images is 50 nm and for the 1×1 μm^2 images is 2 nm.

vealed typical characteristics of step-flow growth with characteristic parallel ~ 3 Å high monolayer steps (monolayer height=$c/2$=2.88 Å for bulk InN).

As expected, step-flow morphologies persisted when growth was performed under In-rich droplet conditions [$\Phi_{In} = 10$ nm/min, Fig. 6(d)], where the surface is covered by In droplets on top of the adlayer. Here, the step terraces were arranged with a distinct curvature, characteristic of spiral growth hillock formation around screw-component threading dislocations.[27] The surface exhibits more coalesced and larger flat areas with fewer surface pits. The high density of metallic In droplets (highlighted by the arrows) resulted from the increased In accumulation under the In-rich conditions, but also from significant InN decomposition and limited In desorption at the given temperature. Excluding areas of larger In droplets, the rms roughness was reduced to less than 10 nm over a 10×10 μm^2 and 0.1 nm over a 1×1 μm^2 area. Similar surface morphologies and rms roughness values have been found even for much lower growth temperatures.[19]

E. In adlayer coverage

The apparent improvements in surface morphology by the In adlayer require a more detailed analysis of its equilibrium coverage and the crossover to droplet formation. For this purpose, we performed a set of In wetting experiments by depositing well defined amounts of In onto the surface, followed by subsequent consumption (i.e., growth of InN) by exposure to active nitrogen. The substrate temperature for these experiments was 530 °C, low enough to prevent ther-
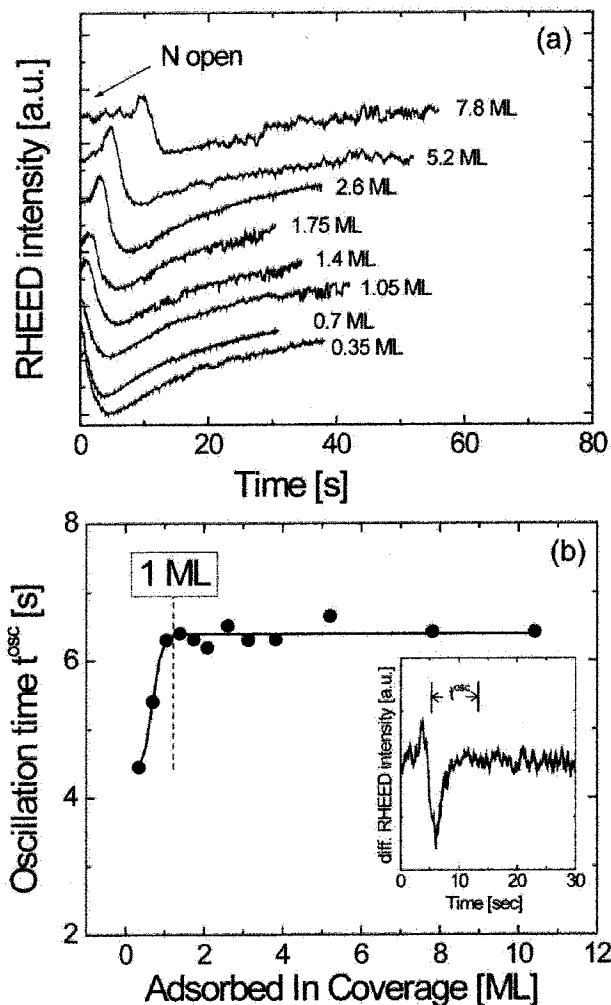

FIG. 7. (a) Variation of the RHEED specular intensity during the nitrogen consumption of various different In surface coverages at 530 °C. (b) Time period of RHEED intensity oscillation as a function of adsorbed In coverage pointing to a saturated In adlayer coverage of 1 ML. The oscillation time t^{osc} is defined by the time span between onset of oscillation and last inflection point in the differentiated RHEED intensity.

mal decomposition. After shuttering the In flux off, we recorded the RHEED specular spot intensity during the complete consumption by nitrogen.

The measured RHEED intensity profiles during this nitridation step are shown in Fig. 7(a) for different In coverages (0.35–7.8 ML). As expected, for sub-monolayer (i.e., <1 ML) In coverages no full intensity oscillation was observed. In contrast, one complete intensity oscillation was observed for In coverages exceeding 1 ML, consistent with the idea that full intensity oscillations can be attributed to the layer-by-layer consumption of metallic adlayer coverages.[28] Also, a distinct delay was observed for the onset of the oscillation with increasing adsorbed In coverage. Delays in RHEED oscillation transients and the absence of additional oscillations are commonly associated with the accumulation or consumption of droplets on the surface, which do not obey a layer-by-layer-like consumption behavior.[21,23] We therefore suggest that adsorbed In coverages in excess of 1 ML accumulated as droplets which acted as an In reservoir that sustained a full 1 ML In adlayer coverage until the In droplets were depleted by growth of InN.

To give a measure for the oscillation period, we defined t^{osc} as the time between the onset of the oscillation and the last inflection point where the differentiated RHEED intensity signal stabilized. Figure 7(b) shows the dependence of the full oscillation periods t^{osc} on the adsorbed In coverage. We found a monotonic increase in the oscillation time period for In coverages approaching 1 ML. Above 1 ML coverage, t^{osc} saturated at a constant value of ~6.3 s, which corresponds to an average rate of ~0.16 ML/s for the consumption of 1 ML of In (in terms of InN equivalent growth rate units) and is the same as the supplied N flux (N-limited growth rate) with an experimental error of less than 20%.

IV. DISCUSSION

The results presented here demonstrate that the PAMBE growth of N-face InN is governed by two major processes, thermal decomposition and In adlayer mediated growth. InN's limited thermal stability is mainly a consequence due to the low binding energy of the group-III atom-N bond in InN (1.93 eV), which is much weaker than in the case for the other binaries GaN or AlN (2.2 and 2.88 eV, respectively).[29]

The thermal stability of InN, however, does depend strongly on the ambient species and pressure, leading to large variations in experimentally observed decomposition rates.[30–32] For the less studied N-face InN, our results demonstrated a certain invariance of the decomposition rates between MBE vacuum conditions (no active nitrogen) and decomposition under typical growth conditions (with active nitrogen). Nearly identical decomposition rates were also observed when the InN growth was performed between slightly N-rich and slightly In-rich growth conditions ($0.82 < In/N < 1.3$).

To understand this invariance, it is necessary to view the metastable InN growth process as the competition between the forward reaction, which depends on the arrival of the active nitrogen species at the growth surface and the reverse reaction, whose rate is limited by a kinetic barrier to decomposition. As elaborated in detail for metastable GaN growth by Newman et al.,[33] this means that decomposition can be significantly suppressed if the arrival rate of active nitrogen is larger than the sublimation rate. This indicates also that (at least for GaN) the decomposition rate is expected to depend strongly on the excess nitrogen flux (or metal/N flux ratio in general).[34]

Since the flux ratio dependence of the InN decomposition was investigated in a narrow range close to stoichiometry ($0.82 < In/N < 1.3$), our experiments give only a limited range of the decomposition rates. The proximity to flux stoichiometry (In/N ~ 1) thus represents a metastable equilibrium between the forward and reverse reactions, explaining the nearly identical InN decomposition rates between the growth case and the case where no active nitrogen was supplied to the surface. Either large deviations from stoichiometric fluxes or a significant increase in the active nitrogen flux may be more effective in suppressing the InN decomposition.

Comparison with decomposition studies of In-face InN demonstrates a much stronger influence of the In/N flux ra-

tio on the decomposition rate, with even complete growth interruption for In/N $>$ 1.[35] Such unsustainable growth of In-face InN under In-rich conditions resulted from substantial In accumulation, which may even catalytically enhance the decomposition.[36] In contrast, N-face InN growth was found completely sustainable under In-rich conditions, most likely due to the feasibility of much higher growth temperatures (up to ~100 °C) and the remarkably higher In desorption, preventing the accumulation of metallic In on the surface.

Regarding the InN decomposition mode, the morphological observation of a consistently streaky RHEED pattern during the incremental temperature increases supports the interpretation of a two-dimensional decomposition process (Fig. 2). However, it is still unclear if the decomposition proceeds by a layer-by-layer or a step-flow process. Additional support of the two-dimensional decomposition mode comes from recent studies of off-axis x-ray rocking curve (ω scans) widths of InN layers grown in nondecomposition ($T=530$ °C) and intermediate-decomposition ($T=595$ °C) regimes. They have indicated a clear invariance of the crystal quality with growth temperature,[19] as opposed to deteriorated surface and structural quality if decomposition proceeded by three-dimensional (3D) faceting. Significant crystal degradation yielding nonsingle crystalline InN layers was observed, indeed, when growth temperatures exceeded ~610 °C (high-decomposition regime), which marks an upper boundary for successful InN growth at the given flux conditions.

This study demonstrates further that the InN growth by PAMBE is very sensitive to the In/N flux ratio, which generated the three characteristic growth regimes shown in Fig. 6. Within each regime, the surface morphology was found independent of film thickness, as demonstrated for InN layers grown to different thicknesses (0.4–5 μm). Therefore, the boundaries among the different growth regimes can delineate optimum growth "windows," similar to the growth diagrams recently established for GaN (Ref. 10) and AlN.[11] Systematic comparison with these evidences, however, some distinct differences.

First, the growth window for the In adlayer terminated regime (analogous to the intermediate growth regime in GaN and AlN growth) undergoes a characteristic transition with varying temperature: initially, the growth window widens with increasing temperature, but as thermal decomposition becomes predominant it diminishes significantly above ~610 °C. Thus, higher In fluxes are required to sustain growth and to provide for an In adlayer terminated surface, to allow the self-regulating growth behavior. In contrast to GaN growth, the In adlayer intermediate growth regime is feasible also under slightly N-rich growth conditions, while the Ga-stabilized growth front during GaN growth can be achieved only under metal-rich conditions.[12,20] This is a consequence of the strong decomposition at typical InN growth temperatures, compared to the negligible decomposition at standard GaN growth temperatures. Also, In-rich InN growth allows only infinitesimally small excess of the incident In fluxes with respect to active nitrogen (i.e., ~0.65 nm/min at 630 °C) to prevent the formation of In droplets.

Further studies of the temperature dependence of the InN surface morphologies verified that the surface structure

within a growth regime is reproducible and independent of the growth temperature,[19] unlike reports by other groups.[37] In particular, all InN layers grown between 500 and 600 °C resulted in a heavily pitted surface when grown under very N-rich conditions, while In-rich growth conditions yielded less pitted, step-flow-like morphologies with spiral growth hillocks in the same temperature region. Similar to GaN growth, this points to the well known autosurfactant action of the metallic adlayer,[12] i.e., providing substantial increases in adatom surface diffusion during InN growth by the In adlayer. Under very N-rich conditions and low temperatures, the absence of the In adlayer (i.e., dry N-rich surface) can be viewed as the main reason for the limited adatom mobility. Contrary to this, InN growth with an In adlayer (under slightly N-rich and In-rich conditions) is subjected to enhanced surface diffusion mediated step-flow growth behavior.

The influence of the In adlayer on the adatom diffusion is also reflected in the evolution of the surface pit density (the predominant morphological feature observed in our InN layers) from a high density (under very N-rich conditions) to a low density (under In droplet conditions). Consistent with theoretical calculations for the In adlayer on GaN surfaces,[38] adatom mobilities under In-rich conditions are so high that the growth morphology can planarize and reduce the surface free energy. Under N-rich growth conditions, where no or only a fractional In adlayer exists, the surface pit defects (associated with threading dislocations) cannot be filled in and propagate to the surface due to much lower adatom mobilities. Complete suppression of surface pit defects under highly metal-rich growth conditions as recently observed for the In-face InN (Ref. 17) or Ga-face GaN (Refs. 10 and 12) polar surfaces could not be realized so far for N-face InN, most likely due to the significantly lower surface diffusion on N-face nitride surfaces as compared to metal-face surfaces.[38,39] Additionally, differences in adatom diffusivities are also governed by the different equilibrium metallic adlayer structures on the two polar nitride surfaces, the laterally contracted bilayer (>2 ML) on the metal-face surface opposed to the only 1 ML thick adlayer on the N-face surface.[40]

V. CONCLUSIONS

In conclusion, we have systematically studied the thermal stability and surface kinetics during the PAMBE growth of N-face InN. Under typical growth conditions (with the In/N flux ratio close to unity) the decomposition rates were similar to those determined without the supply of active nitrogen, owing to the large metastability of InN growth. Employing *in situ* quadrupole mass spectrometry, two different InN decomposition regimes were identified: one with In droplet accumulation at low temperatures (560—600 °C) and one with direct desorption from bulk InN at higher temperatures (>600 °C). Due to the high vapor pressure of liquid In, the growth of N-face InN was hampered by the propensity for In accumulation on the surface. Balancing the decomposition and desorption rates from metallic In yielded a growth diagram, which depicts impinging In flux to available N flux and growth temperatures to classify different

growth surfaces. We have found three characteristic surface structures: a dry no-adlayer terminated surface under N-rich conditions, an In adlayer stable surface, and another where In droplets on top of the adlayer formed under In-rich conditions. In contrast to the typical GaN or AlN growth, the metallic In adlayer (or at least fractions) also existed on N-face InN under slightly N-rich conditions due to the significant In loss during decomposition. The saturated In adlayer coverage is 1 ML on N-face InN. Finally, surface pit defects and surface roughnesses decreased with increasing In/N flux ratio during growth.

[1]V. Yu. Davydov *et al.*, Phys. Status Solidi B **229**, R1 (2002).
[2]J. Wu *et al.*, Appl. Phys. Lett. **80**, 3967 (2002).
[3]S. B. Che, W. Terashima, Y. Ishitani, A. Yoshikawa, T. Matsuda, H. Ishii, and S. Yoshida, Appl. Phys. Lett. **86**, 261903 (2005).
[4]M. Higashiwaki and T. Matsui, Jpn. J. Appl. Phys., Part 2 **41**, L540 (2002).
[5]R. Ascazubi, I. Wilke, K. Denniston, H. Lu, and W. J. Schaff, Appl. Phys. Lett. **84**, 4810 (2004).
[6]B. E. Foutz, S. K. O'Leary, M. S. Shur, and L. F. Eastman, J. Appl. Phys. **85**, 7727 (1999).
[7]T. B. Fehlberg *et al.*, Jpn. J. Appl. Phys., Part 2 **45**, L1090 (2006).
[8]B. Liu, T. Kitajima, D. Chen, and S. R. Leone, J. Vac. Sci. Technol. A **23**, 304 (2005).
[9]E. Dimakis, E. Iliopoulos, K. Tsagaraki, and A. Georgakilas, Appl. Phys. Lett. **86**, 133104 (2005).
[10]B. Heying, R. Averbeck, L. F. Chen, E. Haus, H. Riechert, and J. S. Speck, J. Appl. Phys. **88**, 1855 (2000).
[11]G. Koblmüller, R. Averbeck, L. Geelhaar, H. Riechert, W. Hoesler, and P. Pongratz, J. Appl. Phys. **93**, 9591 (2003).
[12]G. Koblmüller, J. Brown, R. Averbeck, H. Riechert, P. Pongratz, and J. S. Speck, Jpn. J. Appl. Phys., Part 1 **44**, L906 (2005).
[13]J. E. Northrup and J. Neugebauer, Phys. Rev. B **60**, R8473 (1999).
[14]H. Chen, R. M. Feenstra, J. E. Northrup, T. Zywietz, and J. Neugebauer, Phys. Rev. Lett. **85**, 1902 (2000).
[15]H. Lu, W. J. Schaff, J. Hwang, H. Wu, W. Yeo, A. Pharkya, and L. F. Eastman, Appl. Phys. Lett. **77**, 2548 (2000).
[16]T. Ive, O. Brandt, M. Ramsteiner, M. Giehler, H. Kostial, and K. H. Ploog, Appl. Phys. Lett. **84**, 1671 (2004).
[17]C. S. Gallinat *et al.*, Appl. Phys. Lett. **89**, 032109 (2006).
[18]K. Xu and A. Yoshikawa, Appl. Phys. Lett. **83**, 251 (2003).
[19]G. Koblmüller, C. S. Gallinat, S. Bernardis, J. S. Speck, G. D. Chern, E. D. Readinger, H. Shen, and M. Wraback, Appl. Phys. Lett. **89**, 071902 (2006).
[20]G. Koblmüller, J. Brown, R. Aberbeck, H. Riechert, P. Pongratz, and J. S. Speck, Appl. Phys. Lett. **86**, 041908 (2005).
[21]G. Mula, C. Adelmann, S. Moehl, J. Oullier, and B. Daudin, Phys. Rev. B **64**, 195406 (2001).
[22]O. Brandt, Y. J. Sun, L. Däweritz, and K. H. Ploog, Phys. Rev. B **69**, 165326 (2004).
[23]C. Adelmann, J. Brault, D. Jalabert, P. Gentile, H. Mariette, G. Mula, and B. Daudin, J. Appl. Phys. **91**, 9638 (2002).
[24]G. Koblmüller, R. Averbeck, H. Riechert, and P. Pongratz, Phys. Rev. B **69**, 035325 (2004).
[25]J. Brown, G. Koblmüller, R. Averbeck, H. Riechert, and J. S. Speck, J. Vac. Sci. Technol. A **24**, 1979 (2006).
[26]I. Barin, *Thermodynamical Data of Pure Substances* (VCH, Weinheim, 1993).
[27]B. Heying, E. J. Tarsa, C. R. Elsass, P. Fini, S. P. DenBaars, and J. S.

Speck, J. Appl. Phys. **85**, 6470 (1999).

[28]J. S. Brown, G. Koblmüller, F. Wu, R. Averbeck, H. Riechert, and J. S. Speck, J. Appl. Phys. **99**, 074902 (2006).

[29]J. H. Edgar, *Group-III Nitrides* (INSPEC, London, 1994).

[30]Y. Huang, H. Wang, Q. Sun, J. Chen, J. F. Wang, Y. T. Wang, and H. Yang, J. Cryst. Growth **281**, 310 (2005).

[31]Q. Guo and O. Kato, J. Appl. Phys. **73**, 7969 (1993).

[32]M. Drago, T. Schmidtling, C. Werner, M. Pristovsek, U. W. Pohl, and W. Richter, J. Cryst. Growth **272**, 87 (2004).

[33]N. Newman, J. Ross, and M. Rubin, Appl. Phys. Lett. **62**, 1242 (1993).

[34]S. Fernandez, G. Koblmüller, J. S. Speck, and E. Calleja (unpublished).

[35]E. Dimakis, E. Iliopoulos, K. Tsagaraki, Th. Kehagias, Ph. Komninou, and G. Georgakilas, J. Appl. Phys. **97**, 113520 (2005).

[36]R. C. Schoonmaker, A. Buhl, and J. Lemley, J. Phys. Chem. **69**, 3455 (1969).

[37]X. Wang, S. B. Che, Y. Ishitani, and A. Yoshikawa, J. Appl. Phys. **99**, 073512 (2006).

[38]J. Neugebauer, T. K. Zywietz, M. Scheffler, J. E. Northrup, H. Chen, and R. M. Feenstra, Phys. Rev. Lett. **90**, 056101 (2003).

[39]T. Zywietz, J. Neugebauer, and M. Scheffler, Appl. Phys. Lett. **73**, 487 (1998).

[40]A. R. Smith, R. M. Feenstra, D. W. Greve, M. S. Shin, M. Skowronski, and J. Neugebauer, J. Vac. Sci. Technol. B **16**, 2242 (1998).

A growth diagram for plasma-assisted molecular beam epitaxy of In-face InN

C. S. Gallinat,[a)] G. Koblmüller, J. S. Brown, and J. S. Speck

Materials Department, University of California, Santa Barbara, California 93106-5050, USA

We investigated the role of temperature and In/N flux ratios to determine suitable growth windows for the plasma-assisted molecular beam epitaxy of In-face (0001) InN. Under vacuum, InN starts decomposing at 435 °C as defined by the release of N_2 from the InN crystal and a buildup of an In adlayer and liquid In droplets on the sample surface. At temperatures greater than 470 °C, InN decomposition was characterized by a release of both In vapor and N_2 in the absence of a significant accumulation of an In adlayer. No growth was observed at substrate temperatures above 500 °C or at temperatures in which the decomposition rates were higher than the growth rates. A growth diagram was then constructed consisting of two growth regimes: the "In-droplet regime" characterized by step-flow growth and relatively flat surfaces and the "N-rich regime" characterized by rough, three-dimensional surfaces. The growth diagram can then be used to predict the surface structure of films grown at varying substrate temperatures and In fluxes. A 2.5 monolayer In adlayer was observed during In-droplet growth, suggesting that an In wetting layer was necessary for step-flow growth. © *2007 American Institute of Physics.* [DOI: 10.1063/1.2781319]

I. INTRODUCTION

The recent resurgence in InN research can be attributed to the updated band gap value of ~0.65 eV.[1–4] This narrow band gap material opens the III-nitride system to a host of potential optoelectronic devices such as emitters spanning a wider wavelength range and high-efficiency photovoltaics.[5] InN's electrical properties are somewhat anomalous due to the high unintentionally doped electron concentration all InN films exhibit while maintaining relatively high electron mobilities[6–10]—room temperature mobilities up to 3500 cm^2/V s have been measured.[9,10] Recent calculations predict an ultimate room temperature electron mobility for InN to reach 14 000 cm^2/V s.[11] These promising transport properties are optimal for high speed electronic devices and InN could be an ideal channel material for high electron mobility transistors. The presence of a large density of electrons at the InN surface (on the order of 10^{13}–10^{14} e^-/cm^2)[3,4,12,13] provides an additional arena for possible applications ranging from sensors[14] to low resistance contacts and terahertz emitters.[15,16]

Unfortunately, integration of InN into device applications has been limited by a number of growth difficulties—particularly InN's thermal instability, high dissociation rates, and inconsistent surface morphologies. InN is the least thermally stable of the group III-nitrides[17–19] due to the relatively weak In–N bond (1.93 eV).[20] This inherent instability is responsible for the relatively low temperatures necessary to grow InN films. Further complicating deposition conditions is the growth temperature dependence on crystal polarity—In-face (0001) InN is limited to growth temperatures below ~540 °C,[3,21–24] while N-face (000$\bar{1}$) InN can be grown almost 100 °C hotter.[4,25–27] Similar to the other

III-nitrides,[28,29] InN has a clear surface morphology dependence on substrate temperature and III/V ratio during plasma-assisted molecular beam epitaxy (PAMBE) growth.[3,4,27] Films grown with excess In exhibit step-flow growth characteristic spiral hillocks, while those grown under N-rich conditions have rough, facetted surfaces.[3] For both GaN (Ref. 29) and AlN,[29] an intermediate metal-rich growth regime is characterized by a pitted surface with step-flow growth features between pits. This morphology is in contrast with our observations for In-face InN in which In-rich grown films always results in In-droplet coverage and step-flow growth features without pitting.[3]

In this work, we present a PAMBE growth diagram for In-face InN and identify the surface structures expected for differing growth conditions. We present an analysis of the thermal stability of InN during growth and under vacuum. Finally, we quantify the In adlayer coverage of InN during In-rich growth.

II. EXPERIMENTS

The samples presented here were grown in a Varian/EPI 620 growth chamber with conventional Knudsen cells for group III sources and a Veeco Uni-Bulb radio frequency plasma source for the active N species. The In and active N fluxes (Φ_{In} and Φ_N) are reported in terms of growth rate (nm/min) as calibrated by cross-sectional scanning electron microscopy (SEM) measurements of In-rich and N-rich InN samples grown at substrate temperatures in which thermal decomposition is negligible. For conversion of molecular flux to growth rate, we note that in wurtzite InN, $c/2$ = 0.288 nm and 9.17 × 10^{14} InN/cm^2 areal density refer to 1 ML (monolayer) along the (0001) direction. An Ircon Modline 3 pyrometer was employed to measure the growth temperature. All of the samples were grown on semi-insulating

[a)]Electronic mail: chadsg@engineering.ucsb.edu

(Fe-doped) Ga-face GaN templates provided by Lumilog. The optimized GaN buffer layer discussed in Ref. 3 preceded the InN growth.

Cross-sectional SEM was employed to measure InN decomposition by evaluating the thickness of InN samples grown at varying substrate temperatures. Line-of-sight quadrapole mass spectrometry (QMS) was employed *in situ* to monitor InN decomposition and liquid In desorption. The experimental details of this technique can be found in earlier work on the evolution of the Ga adlayer during PAMBE growth of GaN.[30] Quantification of the desorbing In flux (Φ_{In}^{des}) in terms of InN equivalent growth rate (nm/min) required calibration of the QMS response to the ^{115}In signal. This was achieved by dosing the surface of a sapphire wafer at 800 °C with a series of In fluxes lower than what is necessary for droplet accumulation. A proportionality constant of 2.87×10^{-12} Torr (nm/min)$^{-1}$ was determined to convert the measured ^{115}In partial pressure to the total Φ_{In}^{des} in equivalent growth rate units of nm/min. The line-of-sight QMS technique was also employed to monitor the desorbing N_2 (^{28}N) during the decomposition of InN. Quantification of the desorbing N_2 in terms of equivalent growth rate was not possible due to the lack of an appropriate desorbing flux calibration scheme for nitrogen.

Reflection high energy electron diffraction (RHEED) was used to monitor the growth mode and metal coverage *in situ*. RHEED intensity variations of the specular spot along the [11$\bar{2}$0] azimuth were measured to assess the In wetting layer of In-face InN. The RHEED intensity was monitored during In adsorption on a dry InN surface and subsequent exposure of the In coverage to the active nitrogen species (InN growth). InN films were then evaluated *ex situ* by optical microscopy, atomic force microscopy (AFM), SEM, and high-resolution x-ray diffraction (HRXRD).

III. RESULTS

A. Thermal decomposition

The dependence of the InN growth rate, as measured by cross-sectional SEM, on growth temperature is shown in Fig. 1. The films were grown under equivalent In-rich conditions ($\Phi_{In} = 13.5$ nm/min) for 2 h using plasma conditions corresponding to a nitrogen-limited growth rate of 10.5 nm/min. For substrate temperatures up to 480 °C, the growth rate remained relatively constant—approximately maintaining the nitrogen-limited growth rate of 10.5 nm/min. At substrate temperatures above 480 °C, however, the growth rate decreased significantly and for temperatures above 500 °C, there was no InN growth—rather, In droplets accumulated on the GaN buffer layer. The representative SEM image shown in Fig. 1 was recorded from a sample grown at 460 °C. The excess In supplied during growth ($\Phi_{In} - \Phi_N = 3$ nm/min) accumulated into large In droplets on the surface of the sample—similar to what has been observed for excess Ga supplied during GaN growth.[28]

To further measure and quantify the InN decomposition, line-of-sight QMS along with RHEED intensity scans were employed to monitor the desorbing ^{115}In and ^{28}N from a 500 nm thick InN film grown under N-rich conditions
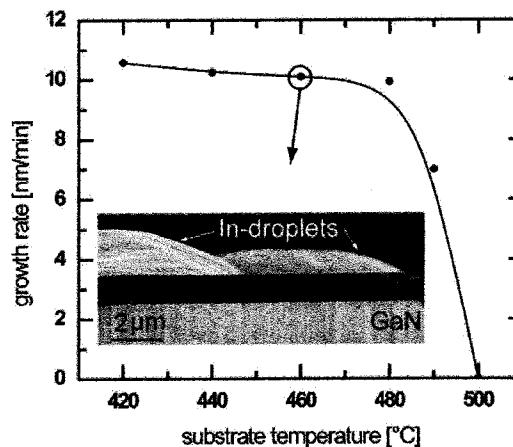

FIG. 1. Dependence of the InN growth rate on the substrate temperature. The growth rate was determined by thickness measurements using cross-sectional SEM. The inset SEM image was recorded from a sample grown at 460 °C and clearly shows the InN and GaN layers with In droplets formed on the InN surface.

($\Phi_{In}/\Phi_N < 1$). The InN layer was grown with excess Φ_N at 420 °C to ensure that In droplets did not accumulate on the surface during growth. This was confirmed by a bright and spotty RHEED pattern (Fig. 2 inset), indicating a surface free of excess metal.[31,32] Subsequent to InN growth, the MBE chamber was pumped to the pregrowth base pressure to remove residual ^{28}N species present in the growth environment. When the optimum background pressure (for ^{28}N and ^{115}In base line signals) was achieved, the sample was heated at constant power intervals corresponding to nonlinear increases in the measured temperature. Starting at 435 °C the ^{28}N signal increased significantly above the background level, while the ^{115}In signal remained at the background level (Fig. 2). The increasing ^{28}N desorption signal was accompanied by a decrease in RHEED intensity, indicating In-droplet formation. RHEED intensities of low contrast indicate excess metal surface coverage during growth, while higher RHEED intensities indicate metal-free surfaces.[31,32] Upon further heating, the ^{28}N signal increased and the RHEED intensity decreased until the sample reached a temperature of
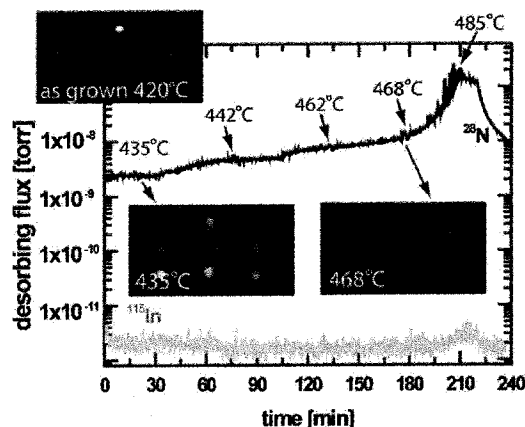

FIG. 2. Line-of-sight QMS data monitoring both desorbing ^{28}N (black curve) and ^{115}In (gray curve) during an InN decomposition experiment. The evolution of the RHEED pattern during annealing is also presented. The desorbing ^{115}In signal remained at its base line level throughout the decomposition experiment, indicating that no In vapor was released.
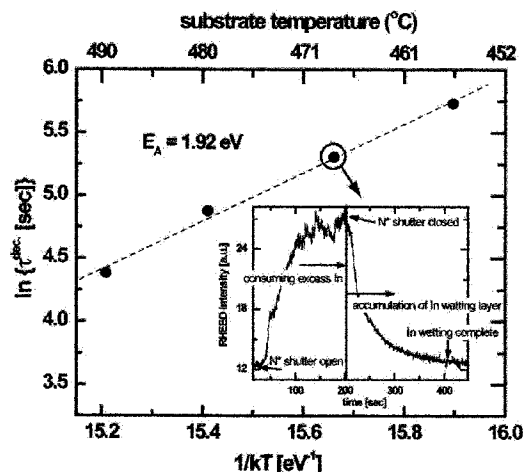
FIG. 3. Temporal evolution of the RHEED intensity during decomposition of InN as shown in an Arrhenius plot of the time necessary for the RHEED intensity to decrease to the steady state value recorded before the consumption of excess In on the surface (τ^{dec}). The resulting Arrhenius relationship provides an activation energy of 1.92 ± 0.11 eV for low temperature decomposition of InN. The inset plot is an example of a typical RHEED intensity measurement used to determine τ^{dec}.

485 °C at which time the ^{28}N signal reached a maximum and quickly dropped to the background level. The ^{115}In signal remained at its base line level throughout this entire process, suggesting negligible In desorption from the InN surface. The abrupt decrease of the ^{28}N level indicated that all nitrogen had left the InN crystal and In droplets remained on the growth surface—this was confirmed by the presence of In droplets visible by optical microscopy and the absence of a single-crystalline film observed by HRXRD.

InN decomposition then proceeds as $2\text{InN(s)} \rightarrow 2\text{In(l)} + \text{N}_2\text{(g)}$ (in agreement with Ref. 17) starting at 435 °C. As gaseous N_2 was released from the InN film, In remained on the surface and accumulated into an In wetting layer (quantified later) plus In droplets. This is in contrast to the thermal decomposition of Ga-polar GaN under vacuum in which a sublimation decomposition process proceeds as $2\text{GaN(s)} \rightarrow 2\text{Ga(v)} + \text{N}_2\text{(g)}$ (Ref. 33).

During InN decomposition, we analyzed the RHEED intensity evolution more systematically. At elevated temperatures the intensity decreased, indicating an accumulation of liquid In on the InN surface. Once the RHEED intensity reached a steady state value, the InN film was exposed to an active N flux to consume the excess In (by growing InN). The consumption of liquid In was accompanied by a corresponding increase in RHEED intensity. Once the intensity increased to a steady state value, the active N flux was shuttered off to the InN surface and the time was then recorded for the RHEED intensity to decrease to the same steady state value prior to the consumption of excess In on the surface (τ^{dec}). The inset of Fig. 3 shows a typical RHEED intensity scan recorded during this experiment. This was performed for different temperatures during thermal decomposition. Figure 3 shows an Arrhenius plot of the natural log of τ^{dec} from which an activation energy of 1.92 ± 0.11 eV for the decomposition of InN can be extracted—in close agreement with the published In–N bond strength of 1.93 eV.[20] At temperatures above 490 °C, the RHEED intensity would not in-
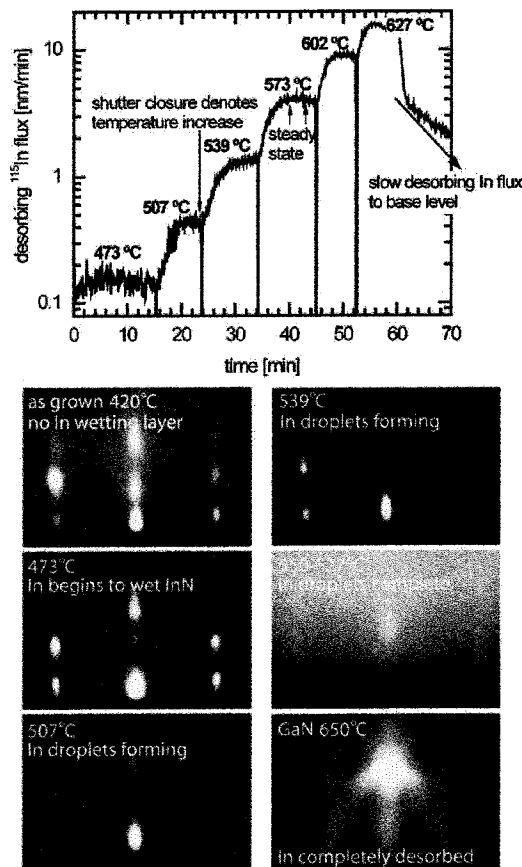

FIG. 4. InN decomposition results showing the desorbing ^{115}In flux as the InN sample decomposes. The representative RHEED images (recorded in a separate experiment) accompanying the decomposition results illustrate the evolution of In wetting of the sample surface as the sample is annealed from growth temperature (420 °C) through complete InN and In desorption (GaN substrate at 650 °C).

crease when exposed to active N, indicating that In remained on the surface during exposure to the active N and the InN surface was never completely free of excess In. At these elevated temperatures, InN was decomposing at a faster rate than the InN could be grown.

To observe decomposition at higher temperatures using the QMS to monitor In desorption from InN, another 500 nm thick InN sample was grown under N-rich conditions at 420 °C to prevent the accumulation of In on the sample surface. The substrate temperature was then rapidly increased to 470 °C and higher temperatures while monitoring both the desorbing ^{115}In atoms (Fig. 4) and RHEED intensity. The quick increase of the substrate temperature (at time zero in Fig. 4) was necessary to suppress significant In-droplet formation on the InN surface as observed in the previous decomposition experiment. By following this procedure, the desorbing ^{115}In signal increased beyond the background level starting at a substrate temperature of ~470 °C. A steady state desorbing signal was recorded at temperature intervals of ~30 °C until the InN layer completely desorbed at 627 °C. An Arrhenius plot of the steady state desorbing flux (Fig. 5, dashed line) is linear with an activation energy of 1.78 ± 0.03 eV for the decomposition of InN.
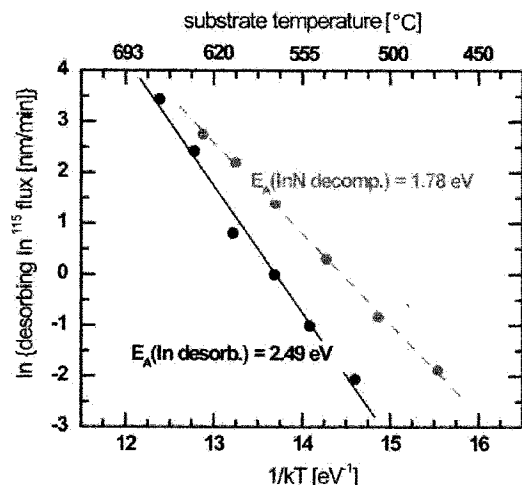
FIG. 5. The Arrhenius relationships for the partial pressures of the desorbing [115]In fluxes over liquid In (solid black curve) and over InN (dashed gray curve) as measured by QMS. The different slopes of the two curves suggest a different mechanism for the desorption of In and the decomposition of InN.

During the initial temperature increase to 470 °C, the RHEED intensity remained constant, thus indicating negligible In accumulation on the surface. Upon further heating, the RHEED intensity decreased until the desorbing [115]In signal peaked at 627 °C and then declined, indicating that the InN film had completely desorbed and only In remained on the GaN. By holding the temperature at 627 °C, the [115]In signal declined toward the base line level and to expedite In desorption the sample was further heated to 650 °C. Once In was completely desorbed from the substrate (as evidenced by the [115]In signal reaching its base line level), the RHEED intensity increased and the typical 1×1 GaN surface reconstruction reappeared, thus indicating that the entire InN layer and liquid In had completely desorbed from the underlying GaN. The observation of an eventual decrease in RHEED intensity during this experiment suggests that In was accumulating on the InN surface during decomposition. For temperatures greater than $\sim$470 °C, InN decomposition thus proceeds as $2InN(s) \rightarrow 2In(1+v)+N_2(g)$.

B. Liquid In desorption

To confirm that the [115]In signal measured during InN decomposition (as in Fig. 4) predominantly originated from the InN surface and not In desorbing from the GaN substrate, another QMS experiment was performed in which pulses of known In flux were deposited on a Ga-face GaN substrate at varying temperatures. The activation energy for the desorption of In atoms from liquid In was determined by both monitoring the RHEED intensity and the [115]In desorption signal during each pulse. In this experiment 20 ML of In was deposited on a MBE grown GaN buffer layer (grown in the Ga-droplet regime and free of excess Ga) at $\sim$25 °C intervals starting at $\sim$675 °C down to $\sim$525 °C. Significant In-droplet formation was observed at these substrate temperatures—indicated by a steady state [115]In desorption signal.[30,34] At temperatures greater than 675 °C, a 20 ML In fluence was insufficient to form droplets.
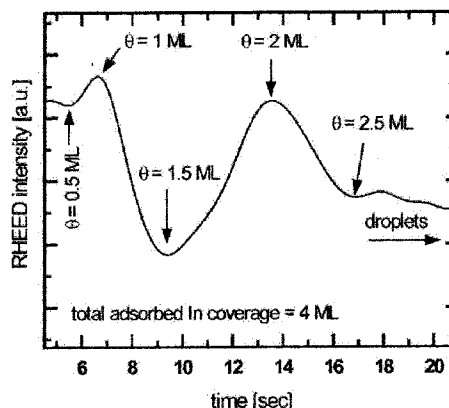

FIG. 6. RHEED intensity oscillations during the adsorption of 4 ML of In onto a dry InN surface. Each $\frac{1}{2}$ oscillation corresponds to $\frac{1}{2}$ ML of In adsorbing onto the surface.

For each temperature at which In droplets were present, the steady state [115]In desorption signal was recorded. Arrhenius plots of the steady state desorption signal (Fig. 5, solid line) yielded an activation energy for the desorption of In from liquid In [E_A (In desorb.)] of 2.49 ± 0.13 eV, which closely agrees with previously published values.[35] This is a significantly higher activation energy than what was observed for the decomposition of InN, indicating that the [115]In signal from the InN decomposition experiment primarily originated from the decomposition of InN and not desorbing liquid In.

C. In adlayer coverage of InN

It is well established that the presence of a metallic adlayer during the PAMBE growth of both GaN (Refs. 36–39) and AlN (Ref. 29) enhances the step-flow growth and allows for smoother surface morphologies due to increased active N surface diffusion. Similar to measurements of the Ga adlayer on GaN,[34,39] line-of-sight QMS would have been the ideal tool to measure the In adlayer during InN growth; however, due to the low decomposition temperature and high In partial pressure over InN, the QMS technique was unsuitable. Instead, the RHEED intensity was measured to evaluate the In surface coverage on InN.

To perform these experiments, a 500 nm InN sample was grown slightly N rich at 420 °C to ensure that the In metal was not accumulating on the surface of the sample. The InN sample was then held at 420 °C (to avoid thermal decomposition) while a series of known In coverages (Φ_{In} = 0.5–5 ML in 0.5 ML steps) were deposited onto the InN surface while monitoring the RHEED intensity. Subsequent to In deposition, the film was exposed to active N to consume the excess In. The RHEED intensity oscillated upon adsorption of In but oscillations were not observed for the active N consumption of In. For In coverages of 2.5 ML and greater, 2.5 RHEED oscillations were observed (Fig. 6), indicating that an In adlayer of up to 2.5 ML was present during In-rich ($\Phi_{In}/\Phi_N > 1$) InN growth. When more than 3 ML of In was deposited, the RHEED intensity would exhibit 2.5 oscillations and then continually decrease until deposition was complete—characteristic of metallic droplets accu-
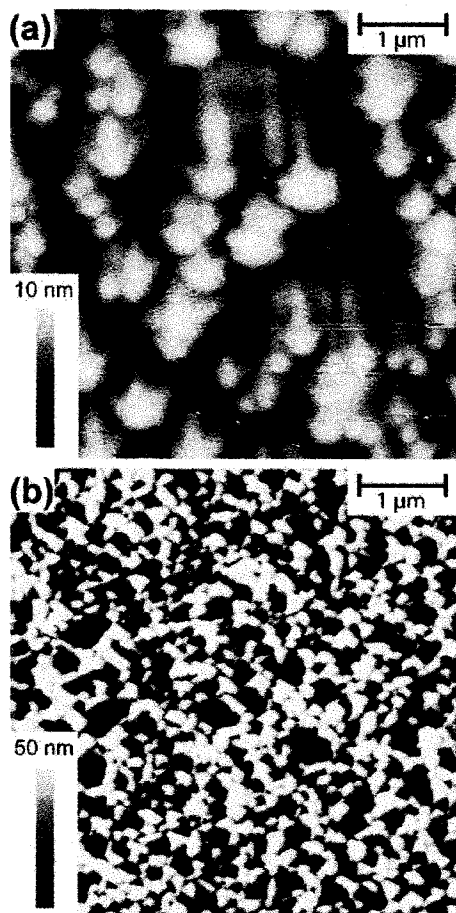
FIG. 7. Representative surface morphologies of two samples grown at substrate temperatures of 450 °C. (a) The surface morphology of a 1 μm InN sample grown in the In-droplet regime (the In droplets have been etched away in HCl). (b) Characteristic surface morphology of a 1 μm InN sample grown in the N-rich regime.
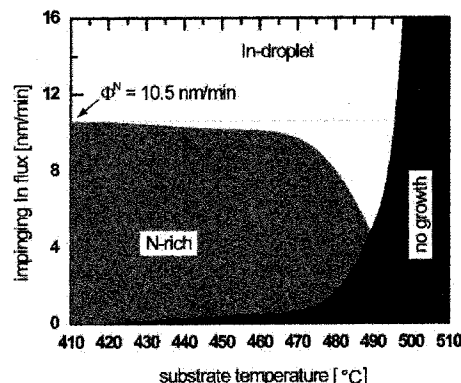

FIG. 8. The PAMBE growth diagram for In-face (0001) InN. Two growth regimes exist: the N-rich regime in which the supplied In flux is less than the active nitrogen flux and the In-droplet regime in which In-droplets accumulate when the In flux is greater than the active nitrogen. No growth is observed for substrate temperatures beyond 500 °C.

mulating on the sample surface.[32] For In coverages less than 3 ML, $\frac{1}{2}$ of an oscillation was observed for every 0.5 ML deposited, suggesting a continuous In adlayer coverage of 0–2.5 ML for In-rich PAMBE growth of In-face InN.

D. Surface morphologies

In contrast to GaN in which three distinct surface morphologies are observed,[28,38] only two characteristic surface morphologies were observed for InN. Figure 7 shows representative 5×5 μm^2 AFM images for the two discernible growth regimes in InN. Figure 7(a) shows the surface morphology of a 1 μm InN sample grown with excess In (Φ_{In} = 13.5 nm/min and Φ_N = 10.5 nm/min). The InN surface of Fig. 7(a) exhibited a relatively smooth, spiral hillock rich morphology typical for the dislocation pinned step-flow growth of GaN.[29,31,40] This is a morphology characteristic of that seen in all InN films grown with excess In. All samples grown with excess In exhibited In-droplet accumulation visible by optical microscopy. Droplets became larger and more dense as increased excess In was supplied during growth. The RHEED patterns (typical 1 × 1 surface reconstructions similar to what is seen during the MBE growth of Ga-face GaN)[31,41,42] observed at the onset of In-rich InN growth were

spotty during the nucleation stage but quickly turned streaky and dim as the InN layer coalesced and In droplets began to accumulate on the surface.

As the impinging In was decreased to a flux less than the active N ($\Phi_{In} < \Phi_N$), the surface morphology roughened and lost the step-flow growth (spiral hillock) features characteristic of In-rich grown samples. A representative AFM image is shown in Fig. 7(b) for a 1 μm InN N-rich grown film (Φ_{In} = 8.5 nm/min and Φ_N = 10.5 nm/min). This N-rich morphology was characterized by a rough, three-dimensional facetted surface similar to the morphologies reported for other N-rich PAMBE grown III-nitrides.[28,29,31] In addition, no In adlayer or droplets were observed *ex situ* in N-rich samples, suggesting a dry surface free of excess In during growth. The rms surface roughness of the N-rich films increased as the Φ_{In}/Φ_N decreased. The RHEED patterns observed during growth of the N-rich InN films were similar to the 1 × 1 surface reconstructions observed during the MBE growth of Ga-face GaN.[31,41,42] At the onset of N-rich InN growth, the smooth initial GaN RHEED patterns transitioned to the InN pattern and began to exhibit spotty features characteristic of a three-dimensional growth mode. The spotty RHEED patterns persisted throughout the N-rich growth, consistent with the rough surface observed by AFM. Further, the RHEED pattern exhibited a roughly constant intensity throughout growth, also suggesting a dry InN surface free of an In wetting layer during growth.

E. In-face InN growth diagram

Figure 8 shows the PAMBE growth diagram for In-face InN as determined using a constant supplied active nitrogen flux (Φ_N = 10.5 nm/min). In contrast to the three distinct regimes of growth observed in similar growth diagrams for GaN (Ref. 28) and AlN,[29] only two regimes were observed for In-face InN: the "N-rich" regime and the "In-rich" ("*In-droplet*") regime. The border between N-rich and In-droplet regime is defined by the N-limited growth rate as determined by cross-sectional SEM (Fig. 1). Since no growth was observed at substrate temperatures beyond 500 °C, a *no growth* regime is defined for temperatures greater than 500 °C. The

no growth regime is also defined by thermal decomposition and extended into the higher temperature N-rich regime (~470–500 °C) where decomposition (Φ_{dec}^{InN}) exceeds Φ_{In}.

InN films grown in the N-rich regime exhibited surface morphologies such as shown in Fig. 7(b). InN films grown in the In-droplet regime exhibited morphologies like that seen in Fig. 7(a) between areas with macroscopic In droplets. Attempts to deposit InN in the no growth regime resulted in the accumulation of In droplets on the underlying GaN with no InN present (as determined by AFM and HRXRD).

IV. DISCUSSION

The purpose of this study was to construct a growth diagram for the PAMBE growth of In-face InN similar to the previously reported growth diagrams for GaN (Ref. 28) and AlN.[29] The application of this diagram (Fig. 8) can be used to predict the surface structure of InN films grown with varying Φ_{In} and substrate temperatures for a set Φ_N. The growth diagram can then be used as a guide for comparing the growth morphologies and physical properties of InN films grown under different conditions.

Significant thermal decomposition of InN at relevant growth temperatures (<500 °C) complicated the growth of InN in the higher temperature range (> ~470 °C). For low growth temperatures (< ~470 °C), however, decomposition had been measured but was insignificant during growth and the InN growth rate could be approximated to be the N-limited growth rate when $\Phi_{In} > \Phi_N$ or the In-limited growth rate for $\Phi_{In} < \Phi_N$. In this low temperature regime, thermal decomposition of InN in vacuum proceeded as $2InN(s) \rightarrow 2In(l) + N_2(g)$, leaving liquid In on the surface of the InN film. Decomposition in this temperature regime was too insignificant to provide an observable In adlayer during N-rich growth and any In on the surface of the sample was reincorporated into the crystal as growth continued since active N was still being applied.

Growing films at these relatively low temperatures allowed predicted surface morphologies to directly reflect the III/V ratio (Φ_{In}/Φ_N). For $\Phi_{In}/\Phi_N > 1$, growth occurred in the In-droplet regime of the growth diagram and the surface morphology exhibited spiral hillocks characteristic of step-flow growth [Fig. 7(a)] in the areas between In droplets. For $\Phi_{In}/\Phi_N < 1$, growth occurred in the N-rich growth regime and the surface morphology showed rough, three-dimensional features such as shown in Fig. 7(b).

At growth temperatures above 470 °C where thermal decomposition was significant, InN growth became complicated by the competition between the forward and reverse reactions, and decomposition rates had to be taken into account when calculating growth rates. In the temperature range from ~470 to 500 °C, decomposition prevailed and no growth occurred if the impinging In flux was less than the decomposition rate ($\Phi_{dec}^{InN} > \Phi_{In}$). When $\Phi_{dec}^{InN} < \Phi_{In}$, InN growth could be sustained but the growth rate was reduced by Φ_{dec}^{InN}. In the In-limited ($\Phi_{In} < \Phi_N$) case, the growth rate became $\Phi_{In} - \Phi_{dec}^{InN}$, and in the N-limited ($\Phi_{In} > \Phi_N$) case, the growth rate became $\Phi_N - \Phi_{dec}^{InN}$. These observations are in

contrast with Dimakis *et al.*,[23] who report that In-limited conditions are necessary for sustainable InN growth at higher temperatures.[23]

It is important to note that a desorbing [115]In signal during InN decomposition was unobservable during the experiments in which we annealed the InN sample slowly to measure the liquid In accumulation. In desorption from InN was only observed at higher temperatures (>470 °C) when In was absent from the sample surface (as determined by RHEED intensity measurements). Maintaining a dry InN surface during these experiments could only be achieved if the sample was annealed quickly to ~470 °C. The accumulation of In on an InN surface thus creates a barrier to the direct sublimation of InN into In vapor and gaseous N_2.

The observation of step-flow growth features for samples grown with excess In and the absence of such features for N-rich grown samples suggests that the In adlayer acts as an autosurfactant and enhances the adatom mobility—as predicted for the In wetting of Ga-face GaN.[37] Our experiments suggest that 2.5 ML of In wets InN under In-rich conditions—similar to the observation of the wetting of Ga-face GaN by a laterally contracted Ga bilayer.[39]

V. CONCLUSIONS

We have observed the thermal decomposition of In-face InN *in situ* (RHEED and QMS) and *ex situ* (SEM). At low growth temperatures (435–470 °C), InN decomposition is negligible and leads to a buildup of an In adlayer on the sample surface. At higher growth temperatures (>470 °C), InN decomposition is significant and the accumulation of an In adlayer can prevent the release of In vapor. Under vacuum, InN decomposition is a complicated process that is a function of annealing temperature and time. At slow annealing rates, nitrogen is released from the crystal and In accumulates on the sample surface, preventing In desorption from the InN. If the InN layer is annealed quickly enough, however, In vapor and gaseous nitrogen are released from the decomposing InN layer. An In adlayer present during growth also allows for higher adatom mobility and a smoother surface morphology.

We have also constructed a growth diagram for the PAMBE growth of In-face InN. Application of this diagram can provide an accurate prediction of the resulting surface structure for samples grown under varying conditions. The growth diagram can provide a guide for comparing the physical properties of InN films grown under different conditions. Proper application of the growth diagram provides a powerful tool for the optimization of InN films and a greater understanding of the properties of InN.

[1] A. A. Klochikhin, V. Y. Davydov, V. V. Emtsev, A. V. Sakharov, V. A. Kapitonov, B. A. Andreev, H. Lu, and W. J. Schaff, Phys. Rev. B **71**, 195207 (2005).
[2] K. M. Yu *et al.*, Appl. Phys. Lett. **86**, 071910 (2005).
[3] C. S. Gallinat *et al.*, Appl. Phys. Lett. **89**, 032109 (2006).

[4] G. Koblmüller, C. S. Gallinat, S. Bernardis, J. S. Speck, G. D. Chern, E. D. Readinger, H. Shen, and M. Wraback, Appl. Phys. Lett. **89**, 071902 (2006).

[5] J. Wu *et al.*, J. Appl. Phys. **94**, 6477 (2003).

[6] H. Lu, W. J. Schaff, J. Hwang, H. Wu, W. Yeo, A. Pharkya, and L. F. Eastman, Appl. Phys. Lett. **77**, 2548 (2000).

[7] C.-A. Chang, C.-F. Shih, N.-C. Chen, P.-H. Chang, and K.-S. Liu, Phys. Status Solidi C **1**, 2559 (2004).

[8] F. Chen, A. N. Cartwright, H. Lu, and W. J. Schaff, J. Cryst. Growth **269**, 10 (2004).

[9] C. H. Swartz, R. P. Tomkins, T. H. Myers, H. Lu, and W. J. Schaff, Phys. Status Solidi C **2**, 2250 (2005).

[10] T. B. Fehlberg *et al.*, Jpn. J. Appl. Phys., Part 2 **45**, L1090 (2006).

[11] V. M. Polyakov and F. Schwierz, Appl. Phys. Lett. **88**, 032101 (2006).

[12] H. Lu, W. J. Schaff, L. F. Eastman, and C. E. Stutz, Appl. Phys. Lett. **82**, 1736 (2003).

[13] T. D. Veal, I. Mahboob, L. F. J. Piper, C. F. McConville, H. Lu, and W. J. Schaff, J. Vac. Sci. Technol. B **22**, 2175 (2004).

[14] H. Lu, W. J. Schaff, and L. F. Eastman, J. Appl. Phys. **96**, 3577 (2004).

[15] R. Ascazubi, I. Wilke, K. Denniston, H. Lu, and W. J. Schaff, Appl. Phys. Lett. **84**, 4810 (2004).

[16] G. D. Chern, E. D. Readinger, H. Shen, M. Wraback, C. S. Gallinat, G. Koblmüller, and J. S. Speck, Appl. Phys. Lett. **89**, 141115 (2006).

[17] R. D. Jones and K. Rose, J. Phys. Chem. Solids **48**, 587 (1987).

[18] Q. Guo, O. Kato, and A. Yoshida, J. Appl. Phys. **73**, 7969 (1993).

[19] W.-L. Chen, R. L. Gunshor, J. Han, K. Higashimine, and N. Otsuka, MRS Internet J. Nitride Semicond. Res. **5S1**, W3.30 (2000).

[20] J. H. Edgar, *Group-III Nitrides* (INSPEC, London, 1994).

[21] Y. Nanishi, Y. Saito, T. Yamaguchi, M. Hori, F. Matsuda, T. Araki, A. Suzuki, and T. Miyajima, Phys. Status Solidi A **200**, 202 (2003).

[22] T. Ive, O. Brandt, M. Ramsteiner, M. Giehler, H. Kostial, and K. H. Ploog, Appl. Phys. Lett. **84**, 1671 (2004).

[23] E. Dimakis, E. Iliopoulos, K. Tsagaraki, T. Kehagias, P. Komninou, and A. Georgakilas, J. Appl. Phys. **97**, 113520 (2005).

[24] X. Q. Wang, S. B. Che, Y. Ishitani, and A. Yoshikawa, Jpn. J. Appl. Phys., Part 2 **45**, L730 (2006).

[25] K. Xu and A. Yoshikawa, Appl. Phys. Lett. **83**, 251 (2003).

[26] X. Wang, S.-B. Che, Y. Ishitani, and A. Yoshikawa, Phys. Status Solidi B **243**, 1456 (2006).

[27] G. Koblmüller, C. S. Gallinat, and J. S. Speck, J. Appl. Phys. **101**, 083516 (2007).

[28] B. Heying, R. Averbeck, L. F. Chen, E. Haus, H. Riechert, and J. S. Speck, J. Appl. Phys. **88**, 1855 (2000).

[29] G. Koblmüller, R. Averbeck, L. Geelhaar, H. Riechert, W. Hosler, and P. Pongratz, J. Appl. Phys. **93**, 9591 (2003).

[30] G. Koblmüller, J. Brown, R. Averbeck, H. Riechert, P. Pongratz, and J. S. Speck, Appl. Phys. Lett. **86**, 041908 (2005).

[31] E. J. Tarsa, B. Heying, X. H. Wu, P. Fini, S. P. DenBaars, and J. S. Speck, J. Appl. Phys. **82**, 5472 (1997).

[32] C. Adelmann, J. Brault, D. Jalabert, P. Gentile, H. Mariette, G. Mula, and B. Daudin, J. Appl. Phys. **91**, 9638 (2002).

[33] R. C. Schoonmaker, A. Buhl, and J. Lemley, J. Phys. Chem. **69**, 3455 (1965).

[34] G. Koblmüller, R. Averbeck, H. Riechert, and P. Pongratz, Phys. Rev. B **69**, 035325 (2004).

[35] I. Barin, *Thermodynamical Data of Pure Substances* (VCH, Weinheim, 1993).

[36] T. Zywietz, J. Neugebauer, and M. Scheffler, Appl. Phys. Lett. **73**, 487 (1998).

[37] J. Neugebauer, T. K. Zywietz, M. Scheffler, J. E. Northrup, H. Chen, and R. M. Feenstra, Phys. Rev. Lett. **90**, 056101 (2003).

[38] G. Koblmüller, J. Brown, R. Averbeck, H. Riechert, P. Pongratz, and J. S. Speck, Jpn. J. Appl. Phys., Part 2 **44**, L906 (2005).

[39] J. S. Brown, G. Koblmüller, F. Wu, R. Averbeck, H. Riechert, and J. S. Speck, J. Appl. Phys. **99**, 074902 (2006).

[40] B. Heying, E. J. Tarsa, C. R. Elsass, P. Fini, S. P. DenBaars, and J. S. Speck, J. Appl. Phys. **85**, 6470 (1999).

[41] M. E. Lin, S. Strite, A. Agarwal, A. Salvador, G. L. Zhou, N. Teraguchi, A. Rockett, and H. Morkoc, Appl. Phys. Lett. **62**, 702 (1993).

[42] W. C. Hughes, W. H. Rowland, Jr., M. A. L. Johnson, S. Fujita, J. W. Cook, Jr., J. F. Schetzina, J. Ren, and J. A. Edmond, J. Vac. Sci. Technol. B **13**, 1571 (1995).